DISSERTATION

zur Erlangung

des naturwissenschaftlichen Doktorgrades

der Bayerischen Julius-Maximilians-Universität

Würzburg

vorgelegt von

Niko Spitznagel

aus Würzburg

ENERGIEÜBERTRAGUNG WÄHREND SCHMELZE-WASSER-INTERAKTION

ENERGY TRANSFER DURING MOLTEN FUEL COOLANT INTERACTION

Lehrstuhl für Physische Geographie

Physikalisch Vulkanologisches Labor

Würzburg, 2016

DISSERTATION

zur Erlangung

des naturwissenschaftlichen Doktorgrades

der Bayerischen Julius-Maximilians-Universität

Würzburg

vorgelegt von

Niko Spitznagel

aus Würzburg

ENERGIEÜBERTRAGUNG WÄHREND SCHMELZE-WASSER-INTERAKTION

ENERGY TRANSFER DURING MOLTEN FUEL COOLANT INTERACTION

Lehrstuhl für Physische Geographie

Physikalisch Vulkanologisches Labor

Würzburg, 2016

Eingereicht am 13.07.2016
bei der Philosophischen Fakultät

1. Gutachter: Prof. Dr. Bernd Zimanowski
2. Gutachter: Prof. Dr. Magnus Gudmundsson
der Dissertation

1. Prüfer: Prof. Dr. Bernd Zimanowski
2. Prüfer: Prof. Dr. Ulrich Schüßler
der mündlichen Prüfung

Tag der mündlichen Prüfung 07.12.2016

Doktorurkunde ausgehändigt am

Magma and water - fascinating and dangerous

Volker Lorenz

Überblick

Das Zusammentreffen von heißer Schmelze mit flüssigem Wasser (Schmelze-Wasser-Interaktion) - auf Englisch Molten-Fuel-Coolant-Interaction (MFCI) - kann zu heftigen Explosionen führen. Diese Explosionen sind in verschiedenen Szenarien möglich: in Stahl- und Kraftwerken, aber auch bei Vulkanen. Wegen der möglichen dramatischen Folgen solcher Explosionen ist eine Erforschung dieser Explosionsvorgänge notwendig.

Wesentliche Grundlagen, unter welchen Voraussetzungen Schmelze-Wasser-Interaktionen zu Explosionen führen können, und der Ablauf dieser Vorgänge wurden weitgehend erforscht. Wie diese Forschungen gezeigt haben, kann die übertragene Energie bei diesen Vorgängen wegen positiver Rückkopplungsprozesse sehr hoch sein.

Bislang wurden aber noch nicht in ausreichendem Maß die Einflussparameter auf die Energieübertragung und damit auf die Explosionsheftigkeit geprüft. Ein wichtiger Parameter ist die Schmelzetemperatur, da von ihr abhängt, wie viel thermische Energie freigesetzt werden kann. Die Untersuchung des Einflusses dieses Parameters ist das Hauptziel der vorliegenden Arbeit. Hierfür wurde bei den meisten Versuchen metallische Zinnschmelze verwendet, da die Materialwerte von Zinn über einen weiten Temperaturbereich annähernd konstant sind, von denen die Wärmeübertragung abhängt. Mit dieser Zinnschmelze war die Untersuchung der Schmelzetemperatur im Bereich von 400 $^{\circ}C$ bis 1000 $^{\circ}C$ möglich.

Ein wesentliches Ergebnis zeigt die Abhängigkeit der Dampffilmstabilität von der Schmelzetemepratur. Bei niedrigen Schmelzetemperaturen bis etwa 600 $^{\circ}C$ ist der Dampffilm so instabil, dass er in den Experimenten bereits vor einer mechanischen Erschütterung zusammenbrach, die zu seiner Zerstörung eingesetzt wurde. Wie erwartet ist zu erkennen, dass mit höherer Schmelzetemperatur grundsätzlich mehr Energie umgesetzt werden kann. Obwohl dieser Effekt von weiteren Einflüssen auf die Explosionsstärke unter bestimmten Umständen überdeckt werden kann, wird dieses Ergebnis nach einer konsequenten Filterung der übrigen Einflüsse bestätigt. Diese Tendenz ist nicht nur an den berechneten übertragenen Gesamtenergiemengen erkennbar, sondern auch an den einzelnen Effekten wie z. B. der Fragmentation oder der Wasserverdampfung. Aber auch die weiteren Einflüsse auf die Energieübertragung wie z. B. die Vorvermischung von Schmelze und Wasser zeigten im Rahmen dieser Arbeit und der durchgeführten

Experimente interessante Ergebnisse. Um diese Versuche durchführen zu können, waren die Einrichtung und Vorbereitung einer Versuchsanlage erforderlich.

Zum Vergleich mit dem Vulkanismus und zur besseren Untersuchung der Feinfragmentation während Wärmeübertagung wurden Versuche mit magmatischer Schmelze durchgeführt. In den Ergebnissen konnten thermische Leistungen während der Schmelze-Wasser-Interaktion bestimmt werden. Außerdem konnte das aufgestellte Modell der “kühlenden Fragmente “ sinnvoll angewendet werden.

Abstract

The contact of hot melt with liquid water - called Molten Fuel Coolant Interaction (MFCI) - can result in vivid explosions. Such explosions can occur in different scenarios: in steel or powerplants but also in volcanoes. Because of the possible dramatic consequences of such explosions an investigation of the explosion process is necessary.

Fundamental basics of this process are already discovered and explained, such as the frame conditions for these explosions. It has been shown that energy transfer during an MFCI-process can be very high because of the transfer of thermal energy caused by positive feedback mechanisms.

Up to now the influence of several varying parameters on the energy transfer and the explosions is not yet investigated sufficiently. An important parameter is the melt temperature, because the amount of possibly transferable energy depends on it. The investigation of this influence is the main aim of this work. Therefor metallic tin melt was used, because of its nearly constant thermal material properties in a wide temperature range. With tin melt research in the temperature range from 400 $^{\circ}C$ up to 1000 $^{\circ}C$ are possible.

One important result is the lower temperature limit for vapor film stability in the experiments. For low melt temperatures up to about 600 $^{\circ}C$ the vapor film is so unstable that it already can collapse before the mechanical trigger. As expected the transferred thermal energy all in all increases with higher temperatures. Although this effect sometimes is superposed by other influences such as the premix of melt and water, the result is confirmed after a consequent filtering of the remaining influences. This trend is not only recognizable in the amount of transferred energy, but also in the fragmentation of melt or the vaporizing water. But also the other influences on MFCI-explosions showed interesting results in the frame of this work. To perform the experiments the installation and preparation of the experimental setup in the laboratory were necessary.

In order to compare the results to volcanism and to get a better investigation of the brittle fragmentation of melt additional runs with magmatic melt were made. In the results the thermal power during energy transfer could be estimated. Furthermore the model of “cooling fragments “ could be usefully applied.

Contents

Chapter 1

Introduction

When a hot melt gets into direct contact with liquid water, denoted molten fuel coolant interaction (MFCI), it can result in vivid explosions. These scenarios occur in accidents, e.g. in metal smelters and power-plants (PURVIS, 1995) or in volcanic eruptions, last famous example Eyafjallajökull 2010 (LORENZ, 1987). Some important events in history were originally caused by big volcanic eruptions.

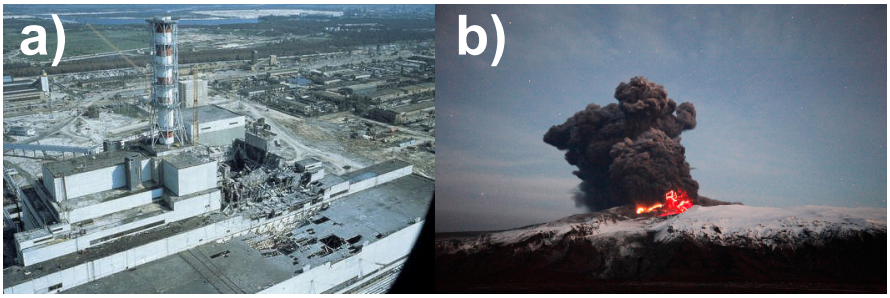

Figure 1.1: a) Block 4 of the Chernobyl nuclear power plant was damaged by MFCI on April 26, 1986. Water from the coolant system got into contact with carbon melt from the moderator (*Arte – Tschernobyl + Europa* 2011). b) MFCI in large scale geometries can cause volcanic eruptions. In these scenarios the amount of produced volcanic ash is very high and can be problematic for civilazation and air traffic (GUDMUNDSSON, 2014).

The Laki eruption on Iceland from 1783 to 1785 caused the death of every fourth Icelander, featuring not only the biggest lava flow in history, but also a huge cloud of "dry fog" over Iceland and Europe consisting of blown-out gas and ash (LYINSKAYA et al., 2016). As a consequence of this darkness the winter 1783/84 was extremely cold and the warm periods in the summers of the years 1783 and 1785 were very short. While the big snow masses melted in spring 1784, flash floods at rivers in Middle Europe occurred. For example the Main river in Würzburg had a water flux of about 2600 $\frac{m^3}{s}$, which is 20 times more than the average value (*Hochwasser, Überschwemmungsgebiete & Anlagen am Gewässer, Historische Hochwasser: 1784 - das 300-jährliche Hochwasser* 2014). Crop failures occurred in Iceland and as well in Europe in the following years caused by acid deposition from the big cloud. A hunger crisis in France was one of the activators for the French revolution in 1789. Because of the in many cases fatal consequences on nature and environment a citerably complete understanding of this process is

Figure 1.2: Main-Hochwasser in Würzburg 1784 (NEBEL, 2016).

desirable with the aim to increase reactor safety and civil defense. For safety arrangements in smelters and power plants most published works on MFCI have been done by applied physics and engineering. The pioneer phase on discovering MFCI was in the 1970s (COLGATE et al., 1973; FRÖHLICH, 1978; PECKOVER et al., 1973). At this time only basic descriptions were made (DULLFORCE et al., 1976; HENRY et al., 1979). After that a period of stagnation occurred caused by the challenge of combining observations in case histories, experimental results and thermodynamic models (BUCHANAN, 1974). Theciteore a first solution was the development of a so called "detonation model" (BOARD et al., 1975; BÜRGER et al., 1985; A. SHARON et al., 1981), which was checked by a series of experiments. It has been used as a standard model for nuclear reactor safety engineering until today (e.g.: CORRADINI, 1981; WORLDWIDESCIENCE.ORG, 2015). For this model strong frame conditions are required that a detonation can occur, but these conditions are not fulfilled under heterogeneous conditions in nature, where detonations occur. But experiences on case histories in industrial accidents and volcanic eruptions show strongly that there must exist a stronger mechanism for such explosions, which is not dependent on strong limited initial frame conditions (BÜTTNER and ZIMANOWSKI, 1998; LORENZ, 1987; K. H. WOHLETZ, 1983). This must be respected in an adequate model of MFCI.

After the Chernobyl disaster in 1986 attention was turned on the investigation of MFCI again (HALL, 1988), but in this new thermodynamic model only boundary conditions for prevention of such explosions in melters and power-plants were studied in a pragmatic way, i.e. the conversion rate of thermal energy into mechanical energy in respect to the initial melt- and coolant temperatures and the melt-water ratio. But this model disclaims on a description of the whole process of MFCI with details of the heat flux from melt to water and the fine fragmentation. Aim of further reasearch in the context of reactor safety was the investigation of critical conditions for MFCI (FREUD et al., 2009). For the influence of the initial temperatures of melt and water only few studies with droplet experiments for critical temperatures have been made so far.

In the Physikalisch Vulkanologisches Labor of the Würzburg University (PVL) and an international cooperation network studies were made in the physics of magma-water interaction in multidisciplinary groups (physicists and geologists) since the late 1980s (BÜTTNER, ZIMANOWSKI, MOHRHOLZ, et al., 2005; ZIMANOWSKI, BÜTTNER, and LORENZ, 1997; ZIMANOWSKI, BÜTTNER, LORENZ, and HÄFELE, 1997; ZIMANOWSKI, BÜTTNER, and NESTLER, 1997; ZIMANOWSKI, FRÖHLICH, et al., 1995; ZIMANOWSKI et al., 1986; ZIMANOWSKI et al., 1991). In the Würzburg laboratory the center of interest has been the interaction of magma or in general of hot melt and water. Theciteore MFCI-explosions were generated under controlled conditions in a small scaled geometry so that the intensity is not too strong to damage an indoor facility, measurements on physical quantities and a high-speed video recording during the process are possible. A comparison of artificial fine fragments from experimental runs with magmatic melt with natural particles from volcanic eruptions (ZIMANOWSKI, K. WOHLETZ, et al., 2002) shows that both groups of particles are very similar in shape and size. So it can be strongly assumed that despite the amounts of melt and water are much lower than in large scale scenarios, the physical mechanisms and normalized amounts (on the involved amount of melt and water) of transferred energy are the same in both cases. This shows that the laboratory is suitable for the investigation of MFCI.

There have already been a lot of studies on the process of MFCI. A major challenge has been and still is to get detailed information of the short time phases of this process. A more detailed investigation of the stage, where energy transfer takes place, is the most difficult part, because this stage is normally shorter than one millisecond. The possibility theciteore is not until the last years existing, since a new acquisition system with a data logger and a high-speed camera with a higher time resolution has been installed in the laboratory. This allows with a special modification to specify the duration and the amount of energy transfer and the influences on it, such as initial conditions like outgoing temperatures and feedback mechanisms during the process. More precise experimental studies will facilitate the description of MFCI-thermodynamics. With the new knowledge it should be possible to predict MFCI-explosions in real scenarios more precisely. This will improve hazard assessment and risk management.

Chapter 2

State of the art

When a hot melt with a temperature higher than the homogeneous nucleation temperature of water (HNT) of 312 $^{\circ}C$ under ambient conditions gets into direct contact with liquid water, a thin vapor film develops between the melt and the liquid water (*Leidenfrost*-phenomena). The heat conduction in vapor is much lower than in liquid water (at the boiling point at ambient conditions at 100 $^{\circ}C$ the heat conduction of liquid water is 0.682 $\frac{W}{m \cdot K}$, this of vapor at the same conditions only 0.0248 $\frac{W}{m \cdot K}$ (WAGNER and KRETZSCHMAR, 2008), the heat transfer from melt to liquid water is very low. After the development of the vapor film the heating of liquid water is low, also the vaporisation of new water is limited, and also the hot melt at the contact surface does not cool down very much. This state is stable as long as the vapor film collapses caused by instabilities in thin regions of the film or it is mechanically destroyed. This premix phase (first phase) is caused by entrance of melt-, ground-, or sea water into the magma chambers in volcanoes. In power plants cooling water can enter molten material as a consequence of technical problems or defects.

During the second phase the isolating vapor film collapses and in some region in the melt-water mixture hot melt gets into direct contact with liquid water. Here the so-called initial contact surface is generated.

The third and most important phase is the so-called phase of direct contact. During this phase the heat transfer from melt to liquid water is increased because of the higher thermal conductivity of liquid water. Although the duration of this phase is shorter than 1 ms, several megajoule of energy per kilogram melt can be transferred. This high energy transfer is the consequence of a positive feedback mechanism: the melt at the surface (so-called interactive melt) cools down quickly at the melt-water surface. The interactive water is heated. During this quasi isochoric process the pressure in the interactive water increases. It can break up the melt surface and enter the cracks in the melt. On the other side a temperature rise of the interactive melt by the hot melt in the background is nearly impossible since the thermal conductivity of melt is low. The thermal gradient in the melt causes thermal stresses, which additionally

support the melt crack propagation. In these cracks new melt water surface is developed and the heat transfer is enhanced. During this process cooling rates of more than $10^6\,K$ can occur. Due to the brittle fragmentation of melt shock waves are emitted. There is hint that these shock waves can trigger a further vapor film collapse (GLAZKOV et al., 2006). To provoke this mechanism a minimal initial direct contact surface in relation to the melt is necessary. Experiences show that this value is about $1\,\frac{m^2}{m^3}$. The reason is the required energy for the creation of new surface by cracks. To fragment a certain mass or volume sufficiently fine, the surface energy therefore has to be provided by the thermal energy in the hot melt. It is converted to pressurize the water for the tension in the melt. After that it can be used for cracks. The amount must be at least as high as surface energy is needed. An analogue is an exploding balloon. In a balloon, that is not or only a little pumped and a small hole (defect) is stinged into its skin, there will be no crack propagation. A crack propagation can only take place if there is enough strain energy in the skin to create a crack. Therefore the balloon must be pumped until the stress energy is high enough and the skin can crack (EDER, 1981). This process is stopped after a short time, when supercritical water vaporizes and aborts the direct contact of melt and liquid water.

During the fourth and last phase supercritical water vaporizes. The system expands and material is blown out. The energy for volume expansion is only a small part of the total amount of converted energy (BÜTTNER, ZIMANOWSKI, MOHRHOLZ, et al., 2005).

In the PVL the main goal is to investigate MFCI-explosion with magmatic melt. For these studies metallic melts are preferred. In the regime of investigation of the melt temperature on such explosions, materials with (nearly) constant material parameters over a wide temperature range (e.g. specific heat capacity and thermal conductivity) are remaining constant. These parameters have large variation in the temperature range of interest (BÜTTNER, ZIMANOWSKI, BLUMM, et al., 1998; FAGENTS et al., 2013), which can not be neglected. During the short time processes it is additionally not clear, how fast materials can change their thermal properties during a rapid cooling. For this work metallic tin melts were used, as its thermal properties are nearly constant in a wide temperature range.

Chapter 3

Experimental setup

The setup in the PVL Würzburg is based in the experience of the TEE-Haus (thermohydraulic explosions experiments) setup (FRÖHLICH et al., 1992). It was advanced from the former TEE-Haus and modified with more modern technique for high speed data and video recording (see also SEEHAUS, 2011). The experimental setup at the PVL consists of four main parts:

- radio frequency generator and induction furnace
- water injection unit
- trigger unit and containment
- controlling system and data acquisition devices

For the MFCI-experiments presented in this thesis the entrapment setup was used, in which a small domain of water is injected into a big volume of melt. A schematic of the setup is shown in Figure 3.1 and photographs in Figure 3.2.

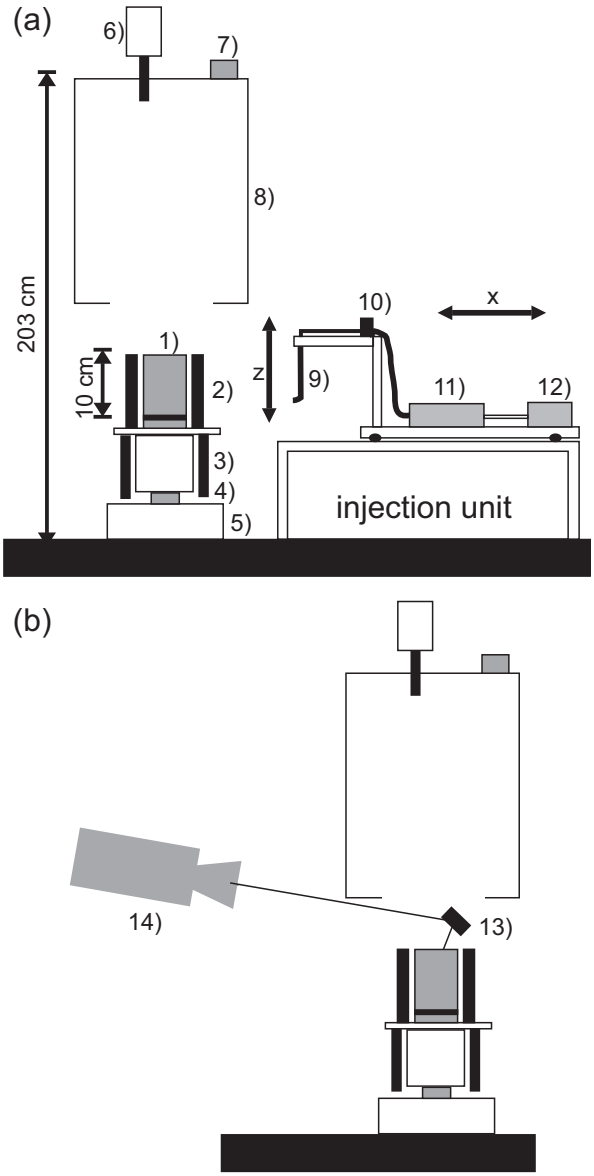

Figure 3.1: a) Schematic of the entrapment setup with its injection unit. 1) Melt crucible within the induction coil 2). The force-sensor 4) is placed under the coolant block 3) on a sandbed 5). The trigger unit 6) is placed on the top. A seismometer 7) is placed on the containment 8). The injection tube 9) can be driven by a linear x-drive and z-drive. The solenoid 10) is placed between the piston pump 11) and the injection tube. The piston pump is driven by a linear drive 12).
b) Side view shows the added mirror 13) for watching the melt surface in the high speed camera 14).

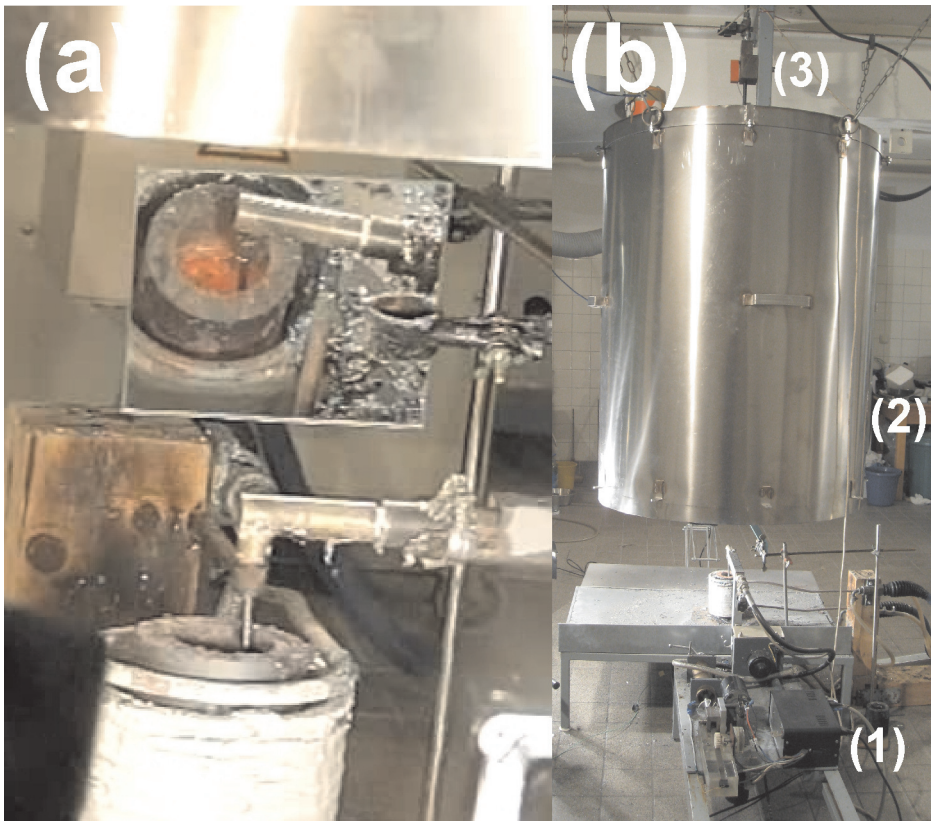

Figure 3.2: a) Melt crucible surrounded by the induction coil. The mirror above allows a direct view onto the melt surface. The injector tube is lowered into the melt for immersed water injection. The containment on the top is for collecting blown out particles.
b) Full experimental setup overview of the setup: (1) water injection unit, (2) containment for particle recovery, (3) solenoid for the trigger gun.

3.1 Radio frequency generator and induction furnace

A radio frequency (RF)-signal is transmitted in a oscillating circuit. The magnetic alternating field induces turbulent electrical flows into the walls of a steel crucible, that is placed inside the heating coil. As the electrical flows have to pass electrical resistance in the crucible, the crucible is heated. The hot crucible transfers heat to the melt material. Beside this the magnetic orientation in the ferromagnetic steel changes continuously. The losses of hysteresis during these changes also produce heat. The melt temperature is measured by a thermocouple. Because of the heterogeneous consistence of the melt the precision of temperature measurement was in the range of $\pm 20 K$. Because there is also a little induction in tin, it is additionally heated to the heat provided by the hot steel crucible, the tin has a temperature of about 50 to $80 K$ over the temperature of the steel in the crucible.

But the crucible transfers heat not only inside but also outside to the heating coil, the other parts of the setup and the environment. The coil and the setup must not get too hot. To avoid this, cooling water flows through the coil and it is wrapped in Al_2O_3-paste. Under the crucible there is an aluminium oxide (Al_2O_3) piece for thermal and electrical isolation of the devices installed under the crucible. A distance slice is placed under the crucible. A second isolating slice is put between the distance slice and the cooling unit. This reduces heat conduction down to the cooling unit and the devices. To prevent overheating of the force sensor, a cooling unit with a cooling coil is installed between the hot crucible and the device. In addition there is a protection plate between the heating and cooling block to isolate the cooling block from electromagnetic radiation.

3.2 Water injection unit

The injection unit is placed on a separate desk. It can be moved in x- and z-direction, so that the injection tube can be dived into the melt short before the water injection. For the movement in z-direction the pipe level for water injection can be set to a certain value in each experimental run so that it is possible to inject water at different positions in the melt crucible. The linear drive for the piston pump pushes through the thin walled steel tube if the solenoid is open and water can be merged into the melt for an entrapment experiment. The injection speed can be adjusted by the voltage for the linear drive. Before opening the solenoid, the injection tube is filled not yet with water to avoid that water can vaporize or flow into the hot melt before the onset of injection.

3.3 Trigger unit and containment

The explosion was triggered by the impact of a low-energy projectile (5 to $6 J$) fired from an airgun onto the surface of the premix. It is shown that he bullet initiates shock waves at its arrival on the melt surface (BÜTTNER and ZIMANOWSKI, 1998). These shock waves propagate through the melt to the water domains and destroy the isolating vapor film. It is not necessary that the bullet itself passes the melt water surface. The time for passing the melt would be much longer than it takes to trigger the explosion.

It is also shown that the layout of the bullet is important. Pointed bullets trigger much weaker explosions than flat bullets under similar conditions (BÜTTNER and ZIMANOWSKI, 1998). The energy provided by the bullet is much lower than the converted thermal energy in the whole process, which is in the range from 10^2 to $10^4 J$. Particles are collected in a cylindrical containment and can be mostly collected for analysis. On the top of the containment there is a seismometer that detects ash particles arriving at the top of containment.

The internal surface of the containment is teflon coated to avoid that hot particles burn at the surface and could not be collected for the later particle analyses. Several teflon sprays were tested. The one with the most useful properties was chosen. It was checked that powder particles and rough peaces of solidified tin can easily be removed.

3.4 Controlling system and data acquisition devices

Because of the high temperatures of the experimental material and danger of damage of devices by the explosions only the devices and sensors, that must be directly installed at the setup, are in the laboratory room. The rest of the system is installed in a separate controlling room.

The experimental procedure is controlled fully computerized. The main reason is that a manual handling of all devices with the exactness of some milliseconds is not possible. The used software is LabView (*M series user manual* 2008). The connection between the computer and the system is realized by the National Instruments DAQ-card NI PCI-6250 (*M series user manual* 2008) and the according break-out box BNC-2110 (*Installation guide bnc-2110* 2007). The digital output from the DAQ-card is reinforced by optocouplers in an additional control box. The maximum current from the DAQ is $5 mA$ and it is too low to switch the relays of the valves. A contributor for incoming signals, ground potential, measurement data and voltage supply is also installed in this control box. The circuit diagrams are shown in Figures 3.3 and 3.4.

3.4.1 Procedure controlling system

The following components are controlled by this system:

- drive for the water injection wagon
- drive for the water injection pump
- valve between the water injection pump and the injection tube
- trigger gun
- trigger for the high-speed camera
- trigger for the data logger

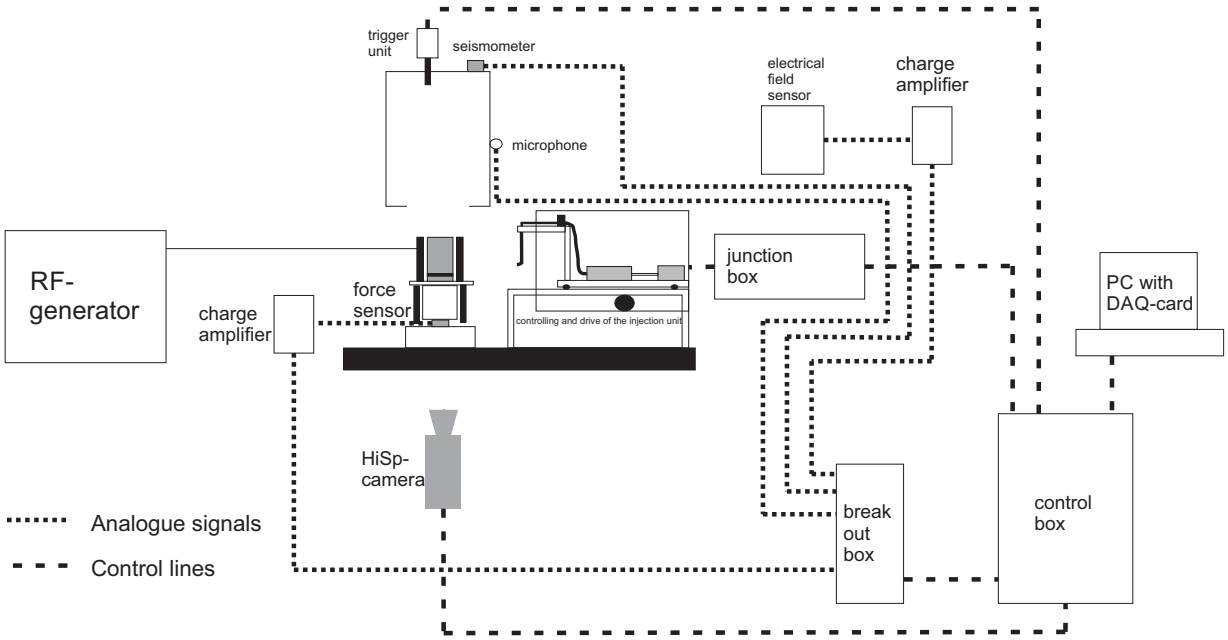

Figure 3.3: Circuit diagram of the experimental setup.

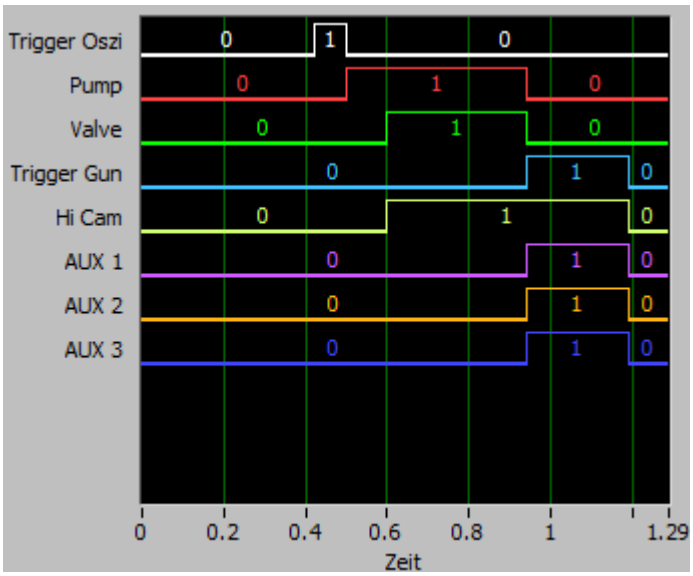

Figure 3.4: Control sequence of an MFCI-explosion. The data logger starts at the falling slope of its trigger signal. All other devices start at the rising slope of their trigger signal. The high-speed camera records after the trigger until its internal memory is full. Time is in seconds.

The LabView program developed for the setup has three modes: configuration mode, main mode and manual mode. In configuration mode you can input the basic parameters, trigger pulse width for the data acquisition system, shutdown delay after which all devices will be set to standby, the total pipe level difference in z-direction and the countdown time before an experimental run. In the main mode the relevant parameters for an automatic experimental run can be adjusted. In manual mode the devices can

be regulated manually. This is necessary for testing and preparing the setup for an experiment.

3.4.2 Data acquisition system

The data acquisition system consists of two main parts: a high-speed data logger and a high speed video-camera.

The data logger records the signals delivered by the sensors 100000 times per second. It is triggered by the falling slope of the trigger signal for the logger (Trigger Oszi). The acquisition time was normally $2\,s$. The data output is saved in a TDMS-file and also in an ASCII-textfile, which can be imported into data analysis software. This system records the following signals:

- trigger for the data logger
- position of the drive for the water injection pump to get a control of the water injection
- repulsion force signal on the crucible, regarding that there is a damping caused by the cooling unit between the crucible and the force sensor
- signal from the electrical field sensor(s)
- signal from the seismometer
- accustic signal from a microphone.

The logger receives all data as a voltage. For the subsequent data analysis the voltage values have to be converted into the values for the unit of each variable. The logger works with the following four steps: First the data recording, second the data conversion for writing the TDMS-file and textfile, third plotting a diagram of the recorded date, and fourth the finished step, when the logger has finished its work.

The high-speed camera NAC ST-751 (*NAC Image Technology. MEMRECAM GX-1 User's Manual ST-751* 2008) can record with a frame rate of 50000 pictures per second. It has to be considered, whether it is necessary to use the maximum frame rate, because of the limited memory of the camera, the size of the recorded pictures has to be reduced or the time span of the recording is too short. Furthermore the pictures are faint. It is advisable to use a framerate which is sufficient to watch the short time process adequately detailed in time and to get good quality pictures, so a framerate from 1000 fps to 20000 fps is normally chosen. The camera is triggered to start recording by the procedure control panel. The recorded sequence is first saved in the internal memory of the camera and can be downloaded from it. The recording format is Multimedia Container Format (mcf), and it can be converted to the most common video format such as avi or mov or in a picture sequence to the TIFF- or JPG-format. There is a lot of software that allows to analyze the video or picture sequences.

3.5 Advanced setup for melt surface observation

Since it is not possible to have a direct view on the melt surface in the crucible (except the crucible is full to the brim), an additional mirror is installed that makes this view possible. It is necessary to obtain more information about the exact bullet impact on the melt surface and the beginning of the break-up of the system.

This additional mirror is installed next to the crucible and adjusted so that it reflects the melt surface into the camera. As the mirror masks up the area of blow-out it is not possible to record the melt surface and the blow-out in one run simultaneously. For further investigation of still unanswered questions of MFCI (e.g. the influence of melt and water temperature) it is important to get more detailed information about the transition from the second to the third phase and the duration of heat transfer, which take place in a very short time of less than $1\,ms$. The technical problem is the investigation of the process during the trigger and heat transfer phase in the crucible since no transparent material for the melt and the crucible can be used. In this work we look for a way of indirect acquisition of the required information, which will help us in further experimental studies. There are data missing regarding the duration of short time phases (duration of vapor film collapse and duration of direct contact between melt and liquid water).

3.6 Calibration of experimental setup

To get useful experimental runs and data, it is necessary to calibrate the components of the setup.

3.6.1 Calibration of data logger and camera

To compare the high speed video recording to the signals recorded by the data logger it is important that both are synchronized in time. As the relays which generate the trigger pulses for the devices have different delay times, also caused by shattering, the time scales of data logger and camera have to be corrected with that delay times.

To get a value of delay time, the trigger signals can be checked by recording with an oscilloscope. This shows that the data logger is triggered about $3.6\,ms$ after the camera if both devices should be triggered at the same moment. Thus the check by oscilloscope does not respect the internal delay of the devices. Therefore some additional tests were made. Some aluminium foil strips were placed on the setup at the position of the crucible and an electrical voltage was installed. These strips were cut through by the trigger bullet. The cutting was filmed by the high speed camera. In the moment of cutting, the voltage signal recorded by the data logger was breaking off. There was also a time difference detected in the range from 3.6 to $4.2\,ms$ and $3.95\,ms$ in average between camera and data logger. A comparison of the video and the force signal, which is the most important signal to be compared with the videos, by the impacting bullet shows a time difference in the range from 3.54 to $4.05\,ms$, in avergage $3.71\,ms$. The difference is shorter, because the force sensor can detect a signal from the air replaced by the flying bullet

and primarily the delay of transducing the force signal through the cooling unit to the force sensor, and during this time the time on the logger goes on and shows a later time value for the force signal. So the difference appears shorter.

To get an estimation for the time difference with a media in the crucible, for these tests a filled crucible was used with only cold water or only hot melt to avoid an explosion. A mirror was installed to see the impact on the liquid surface. These tests show that the time difference now is a little bit shorter, about 3.7 to 3.8 *ms* with hot melt and about 3.6 to 3.7 *ms* with water only. It is shorter, about 3.3 *ms* with a cloth in the crucible. For later MFCI-experiments a time difference of 3.7 *ms* is used, but it is well-known that the signal propagation in a melt-water mixture can be different from pure melt or pure water.

3.7 Calibration of water injection

The quantity of the injected water and the injection velocity affect pre-mixing of melt and water. This has influence on the initial direct contact area and thus on the explosion violence. For this already detailed investigations were made in the laboratory (ZIMANOWSKI, BÜTTNER, and LORENZ, 1997).

3.7.1 Basics of water injection

Around several attempts to be able to compare with one another, the injected quantity of water and the injection velocity must join in with the different attempts as exactly as possible. In addition these values must be selected in such a way, which develops with the melt material and the used melt quantity as favorable premixture. Here above all the viscosity of the melt and the density variation between melt and water plays a dominant role. Therefore you have to make sure that the injected water domain is not too small. In addition it should not become so large that during mixture phase the water in the melt can ascend too fast and be ejected by the melt surface. The water injection should run as plain as possible, as well at its start as at its end. It would be optimal if the injection pipe is filled with water before the onset of injection. The injection tube, that dives into the crucible, cannot be filled with water, because the water would vaporize during the diving procedure and would cause problems. Hence it is filled with air. One risks that first the air is pushed out of the tube before the real water injection starts. The recordings of the test runs show that the air, which ascends quickly to the top of melt, does nearly not disturb the runs.

3.7.2 Test injection for the water volume

To estimate the injected water volume in test runs, a water glass is placed at the position of the crucible in the setup. The water volume can be measured by weighing the glass. Several runs were made to calibrate the injected volume dependent on injection time, pump voltage (which influences the injection velocity), and several delay times for the opening of the solenoid at the injection tube. The values are shown in table B.1.

It is noteworthy that the injection volume first increases linear to the injection time by constant pump voltage. In a time from 420 to 440 ms there is a shift in the volume. A hydrodynamic effect in the injection unit might explain this. Beyond the shift at longer injection times, the increase is linear again. But in the time span during which the shift occurs, the favorised injection volume for the projected tin experiments is located. The calibration runs showed that by a voltage of 6.0 V and an injection time of 440 ms with a valve delay of 100 ms a water volume of (7.2 ± 0.7) ml is injected. A plot of the potentiometer voltage, which controls the drive of the piston pump, is shown in Figure B.1.

3.7.3 Checking of the injection velocity

It is not possible to observe the injection process into liquid tin directly. Therefore injection runs with water were performed, considering that water has similar material values to tin, that are relevant for the injection. To make an injection of water into water visible the injected water is colored. For the run presented in Figure 3.5 the injection time is 440 ms with a valve delay of 100 ms at a voltage of 6.0 V. The video recording is started at the opening of the solenoid. As expected about 30 ms after the opening of the valve the first air bubbles leave the injection tube, that move quickly to the top of the water. After that, about 120 ms later, this means 150 ms after the opening of the valve the jets with colored water start. The first inflowing water has not yet the favorised injection velocity so that a bubble with colored water develops at the end of the tube. About 15 ms later the water flows with its full injection velocity. The now injected water jet passes through the first injected water bubble, which first has formed the top of the water jet. About 200 ms after the opening of the valve the jet strikes on the opposite wall of the glass. The injection velocity is about 1.0 to 1.5 $\frac{m}{s}$. These values are ideal for the premix in the later experiments with entrapped water in tin melt. At the opposite wall a big bubble with colored water grows up. The valve closes 340 ms after its opening. Rest water from the injection unit still flows out. It takes about 30 ms until the water jet becomes weaker. About 200 ms later the influx of water is completely finished. A comparison of several test runs shows that there are oscillations of 5 ms, which are caused by the control system. More oscillations will occur if the injection tube and the connection to the gallow are not carefully discharged of water before an injection run. All in all the injection process is well reproducible. It is to take care that the pump and the injection unit are filled free from air.

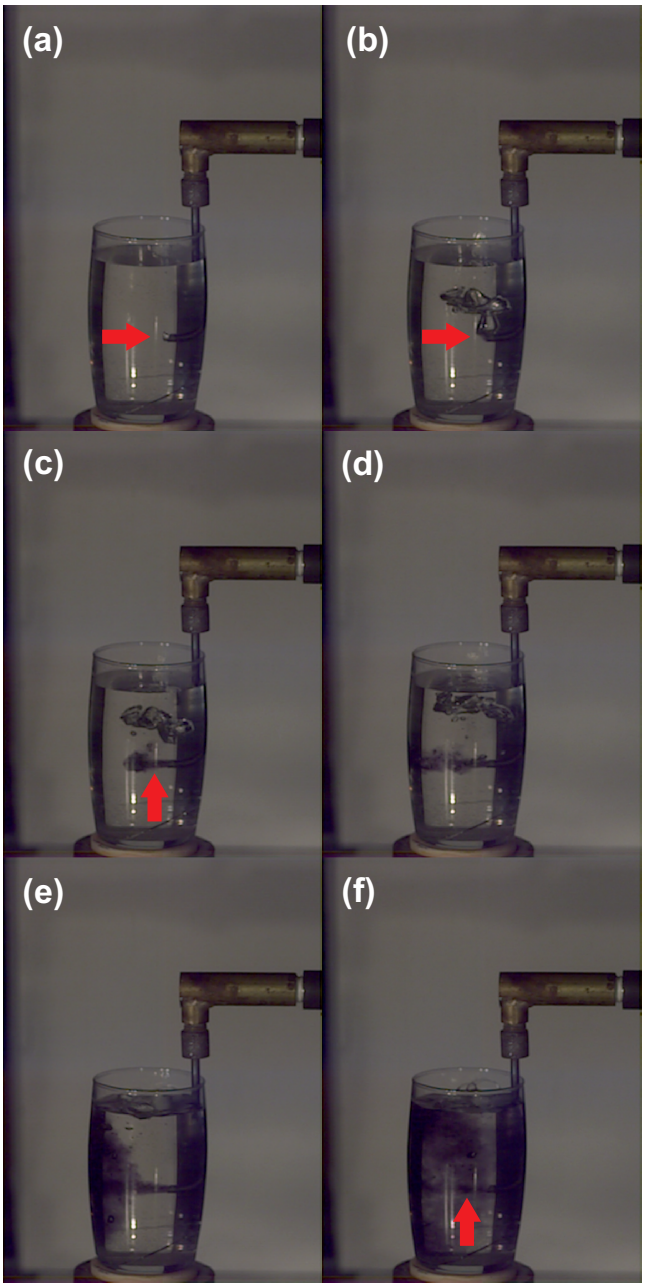

Figure 3.5: Some states during water injection. The valve opens at frame 0, 100 *ms* after the piston pump is started. (a) Onset of the blow-out of rest air in the injection tube about 30 *ms* after the opening of the valve (frame 150). (b) Onset of the water jet after 150 *ms* (frame 750). (c) About 15 *ms* later at about 165 *ms* (frame 825) the jet achieves the requested injection velocity of 1.0 to 1.5 $\frac{m}{s}$. (d) About 200 *ms* at frame 1000 after the opening of the solenoid the injected water reaches the opposite wall of the vessel. (e) The water jet extenuates 30 *ms* after the solenoid is closed at about 370 *ms* (frame 1850). (f) Finish of water injection 200 *ms* later at about 570 *ms* (frame 2850).

Chapter 4

MFCI-experiments with variation of melt temperature

In this chapter tin experiments and the experimental procedure for investigation of the influence of melt temperature in the range from 400 to 1000 $^{\circ}C$ on the melt water interaction are presented. First of all the preparation for such experiments is explained.

4.1 Preparation and selection of appropriate parameters

4.1.1 Melt mass

For the choice of the melt mass for each experimental run several aspects have to be obtained. In the regime of low material costs as much tin as possible should be saved in each run. Therefore rest tin that was not finely fragmented is recycled for the next runs. By this way the pure loss of tin excluding the collected and saved fine fragments is about 5 to 10 g per each run. But otherwise the melt mass has to be sufficient to get a good premix of melt and water so that the initial contact surface can be useful to trigger explosions. For a mostly complete collection of fine fragments and a high recycling rate of rough tin the blowout from the crucible should be vertical. That is also an important aspect for the measurements of particle velocity from the high-speed video recordings. It is useful to fill half of the crucible. In the upper half the blowout can be directed vertically like in a chimney. For a half-full crucible 70 ml of tin are necessary, that is about 420 g.

4.1.2 Water volume and water injection velocity

For this mass of melt a water volume of 7.0 ml is preferable. The injection velocity should be in the range form 1.0 to 1.5 $\frac{m}{s}$. The injection time is 420 ms. But in respect that a certain volume of water flows in the crucible after the valve in the injection unit is closed. It should not be waited for triggering by the bullet impact until all water is flown into the crucible. It was shown that an injection time of 440 ms and 100 ms valve delay is best, when the projectile is launched after 440 ms when the pump stops and the valve at the water injection closes. The bullet impact is about 30 ms later during the influx of rest water. This delay of about 30 ms is to explain by the reaction time of the trigger valve of about 15 ms, which accords to the information of the producer of the valve (HERION, 1994), and the flight time from the

trigger gun at the top of the containment down to the crucible of about $15\,ms$ again. In this delay time there are oscillations of only about $5\,ms$. Water, that arrives after the bullet impact, does not contribute to the explosion. So the total injected water volume is a little bit more than $7.0\,ml$, but the overhang is not used. That the mixed melt can calm after diving in the injection tube, the procedure is delayed for $500\,ms$. The tube is driven into its lowest possible position near to the bottom of the pot so that water is injected near the bottom and can ascend through the melt because of its lower density and the volume for premixture is maximized.

4.1.3 High-speed video recording

The high-speed camera has a limit in its memory for saving recorded pictures. In the performances a compromise between frame rate (pictures recorded per second), picture resolution, and picture size has to be found. For the frame rate there is also the problem that at high frame rates the pictures are only weakly illuminated. For the regular experiments a frame rate of 5000 pictures per second, for the runs with attached mirror a rate of 20000 pictures per second was chosen.

The start of video recording is normally set on the bullet impact on the melt surface in the control panel. But it can make sense to record the injection process. Therefore the camera is triggered earlier at the moment, when the valve for water injection opens.

4.1.4 Temperature range

The aim of the presented investigations is to check the influence of melt temperature on MFCI-explosions. The temperature range with tin melt has a lower and an upper limit. The lower limit is $400\,^{\circ}C$, because the temperature of melt must be higher than the HNT of water at $312\,^{\circ}C$. The upper limit is at $900\,^{\circ}C$. At higher temperatures tin reacts with oxygen from the tin oxide and this can cause darting flames, when fine fragments are blown into the air. Above all it would be interesting to check the temperatures higher than $1000\,^{\circ}C$, because the temperatures of basaltic melt in volcanoes mostly have temperatures below $1000\,^{\circ}C$. The comparison to experiments with magmatic where often a temperature of about $1300\,^{\circ}C$ was chosen would be interesting. For experiments with higher temperatures another metallic melt has to be chosen such as silver or gold. But these materials are more expensive than tin. The steel crucible melts at temperatures below $1500\,^{\circ}C$. For higher temperatures, that are relevant to temperatures in power plants, crucibles made of graphit are necessary. These crucibles are expensive, too.

4.2 Experimental procedure

The procedure for an MFCI-experiment can be divided into the following steps:

- Weighing of melt material and filling it into the crucible
- Switching on of the cooling circulation and the inductive heating
- Putting the trigger bullet into the gun

- Filling of the water pump
- Turning on and adjustment of the cameras
- Setup of the parameters in the control panel
- Test injections of water
- Pressurizing of the trigger gun
- Switching off the furnace after reaching the desired melt temperature
- Starting the measurement and recording system
- **Experiment**
- Saving of the recorded data and videos
- Collection of particles and blow-out after cooling of the setup
- Reset and cleaning of all devices for the next run. Shut down of all devices after the last run of the experimental day

The time for melting and heating of tin melt is about 30 minutes. The full furnace power of $100\,kW$ is not necessary, a heating power of 5 to $10\,kW$ is sufficient. The cooling after an experiment takes about one hour until the temperature is lower than $100\ ^{\circ}C$ and the cleaning can be started. For accurate work two runs per day are possible.

4.3 General remarks for experimental runs

Before starting a detailed analysis of the recorded values, it is necessary to check, whether the experiment was successful or if some of it was unuseful, because some errors occurred. The influence of the geometric arrangement and limitation is to be checked.

4.3.1 Entrapment experiments

For this arrangement and the chosen parameters it could be possible that injected water ascends through the top of the melt before the explosion is triggered and forms a water layer. This would not be a pure entrapment experiment, but a combination of entrapment and layer experiments. It is clearly visible in the recordings of the melt surface with the adjusted mirror that the melt surface is in movement during all injection procedures; this movement is sometimes stronger and sometimes weaker. There are also some bubbles that leave the melt. The recordings with the auxiliary camera show that these bubbles are tin bubbles and not water bubbles. The recording with the mirror shows that the bubbles mix melt from the bottom of the crucible to the top. The mixture starts while the injection tube dives into the melt, and before the onset of the injection, when there cannot be any water in the tube or the crucible yet. A comparison to the recordings of the test injections as in Figure 3.5 for the calibration of the water injection shows that the bubbles in the tin come up at about the same time in the procedure when the air bubbles in the water come up (see Figure 4.2). Sometimes some droplets leave the crucible during the water injection.

These droplets must be tin droplets, because they are too little transparent for water droplets, as shown in Figure 4.1. If there was a water layer over the melt, a vapor film between the hot melt and water layer would exist. This vapor film must collapse during the impact of the trigger bullet. This would be visible in the video records, but it is not visible in any record. The experiment with the maximum filled crucible and deeply dived injection tube shows the mixture of melt as in the other runs. The outcome of water bubbles is less probable because of the longer distance to the top of the melt. All in all the growth of a water layer on the top of the melt during water injection can be excluded. The geometric layout of the premixture depends on the viscosity of melt, which is strongly dependent on temperature (PANCENKOV, 1951). Initially it can be supposed that the premixes would be different at different melting temperatures. A temperature dependence of the explosions would be predicted by different premixes. But this effect is superposed by other probability effects in the water injection and premixture, which are not excludable and already appear at the same temperature and melt viscosity. These probability effects have a higher influence on the premixture than the variation of viscosity at different temperatures.

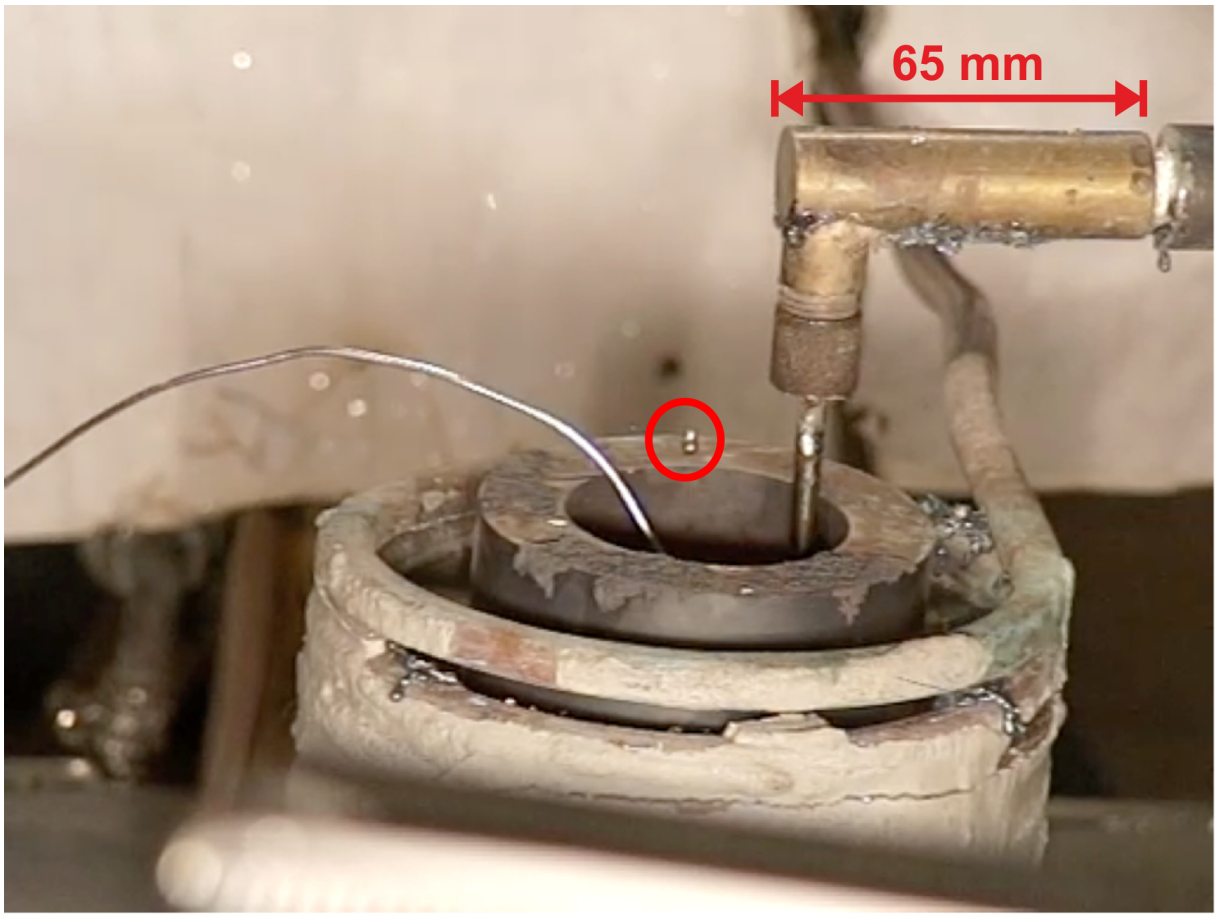

Figure 4.1: Outcoming tin droplets during water injection. The droplets have the typical color of tin and are too little transparent that they could be water droplets.

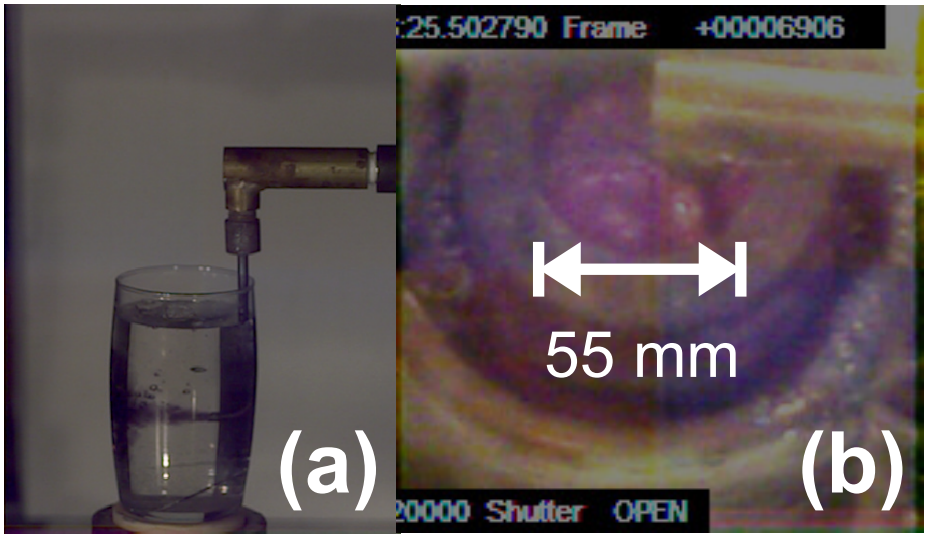

Figure 4.2: Comparison of recordings of a calibration of water injection (a) and a water injection into tin melt (b). The snapshot is recorded at 345 *ms* after the opening of the valve in both cases. It can be seen that the crust on the tin surface is broken by outgoing bubbles in (b). It is demonstrated in picture (a) that these bubbles are air bubbles. The air is pushed out of the injection tube before the real water injection begins.

4.3.2 Influence of the melt mass in the crucible

MFCI-explosions typically take place in larger scenarios than in the crucible in the laboratory. The influence of the limited volume is to check. At least it is possible to check, whether there were differences in the experiment if the crucible is for once filled to its maximum. Additionally it can be checked, whether there is a difference for putting the tube on the bottom or in the middle of the crucible so that the "center of event" is placed at different locations in the melt. One result is that in the run with deep injection the time for elevating the melt is longer until the surface breaks up and ash particles come out. It is to assume that the active domain for melt water interaction is near to the bottom of the crucible and the melt plug which is to break up is higher. In the run where the tube is located in the middle of the crucible there is nearly no difference to the run with half-filled crucible. It can be concluded that the melt plug over the water domain is as high as in the runs with half-filled crucible. Also the recorded force signals are similar in these both cases. All in all there is no significant difference.

4.4 Information from the recorded signals

The recorded values can be qualitatively and/or quantitatively analyzed to get some information about the particular run.

- The most important signal is the **repulsion force** on the crucible. If forces act on melt and water in the crucible, an equivalent repulsion force acts on the crucible. The recorded signal can provide information about the explosion and its intensity. Figure 4.3 (a) displays the typical force signal of an ideal run representing a single triggered explosion. A small peak (1), mostly superposed by a big "main peak" (2). Those pre-cursing small peaks most likely result from the shock waves emitted

during brittle fragmentation. The main peak represents the repulsion force on the crucible by the blown-out material. In some cases a third peak is visible (3), which is caused by expanding steam. The small peaks later on (4) show the oscillation "ringing" of the crucible after the explosion. It has to be noted that deviations from such "ideal" force signals were not rare. In some cases there is more than one "main peak", because multiple explosions occurred. Figure 4.3 (b) shows such a run, where three explosions were triggered in a very quick succession, marked by the numbers (1), (2), and (3). If temperature is lower than 600 $^{\circ}C$ the premature premixes were self-triggered in consequence of the collapse of unstable vapor-film (FRÖHLICH, 1978; LI et al., 2007) before a mechanical collapse could be initialized by the bullet (Figure 4.3 (c), Peak (1)). In cases of higher temperatures, however, the collapse had to be forced mechanically.

By means of the adjusted mirror, it can be observed that the time between trigger (bullet impact) and the opening of the system was shorter than 1 ms in all runs, but with variations between 250 ms and 900 ms. If the premix is in an agitated state, that means that there is a tremor motion during the premix, this period will be significantly shorter, which suggests that in such cases the vapor collapses occur faster or the water droplet is more close to the melt surface. With this information we can conclude that the pure time of direct contact between melt and liquid water (i.e. after the collapse and until the end of fragmentation) is shorter than 0.5 ms.

It is interesting to analyze the state of the melt in the crucible at the moment when the force reaches its peak. It turns out that at this moment the melt surface is breaking up and sometimes first particles leave the system (Figure 4.4). It can be concluded that the acceleration of the blown-out material is at its maximum at this time. Additionally it should be mentioned that at the beginning of the breakup of the melt surface the force signal is on its rising slope in most cases.

If the system is agitated (tremor) during premix, the probability for multiple-triggering was observed to be higher. An explanation for this effect might be that in the agitated system multiple water-domains are established (Figure 4.5). After triggering the first domain, the others are triggered in a chain reaction by the mechanical shock waves generated from exploding pervious ones.

A more detailed comparison between the recorded force signal and the video analysis shows that the transmission time from the center of event in the crucible to the force transducer depends on the individual melt water mix. The transmission time is longer for the first force peak in multiple triggered experiments (Figure 4.6). Additionally in those cases the time until the breakup at the surface is shorter, because of the shorter distance from highly leveled domains to the surface of the melt.

- The records of the **electrical field** during an explosion is also proportional to the intensity of the explosion. The electrical field is mainly generated during the phase of fine fragmentation. Other

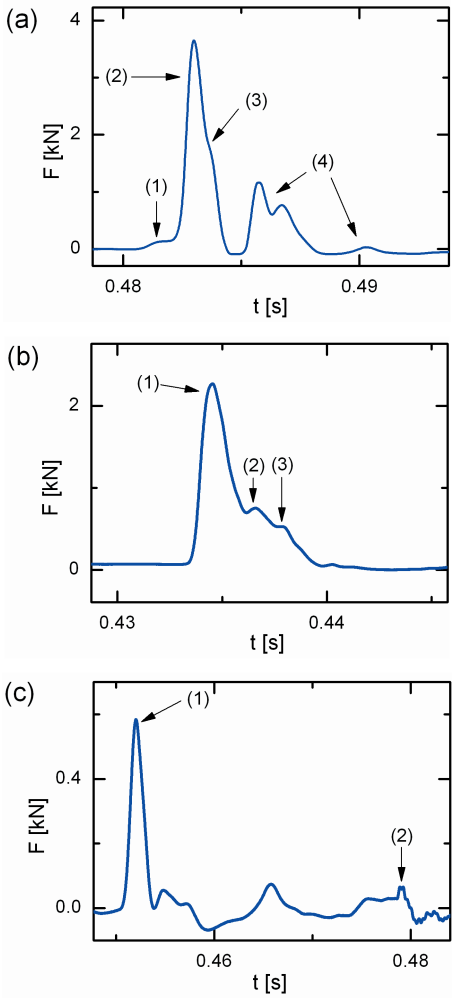

Figure 4.3: Force signals during MFCI-explosions. (a) A signal of a single explosion.This is the force-signal from the explosion presented in Figure and on the video on the attached DVD. (1) shows the transmitted signal from shockwaves, (2) the "main peak" represents the acceleration for blowout, (3) the steam expansion and (4) the "ringing" of the crucible after the explosion. (b) A multiple triggered run, numbers (1 to 3), shows the "main peaks" of the three single explosions in very quick successions. The melt volume was 70 ml, the melt temperature was 900 $^{\circ}C$, and the injected water volume was only about 5 ml with an injection time of 400 ms in this run. (c) A self triggered explosion (1). (2) represents the impact of the projectile after spontaneous self-triggering. The volume was 70 ml, the melt temperature 400 $^{\circ}C$.

effects as friction, hydrodynamic or aerodynamic fragmentation are less important for the generation of the electrical field (BÜTTNER, RÖDER, et al., 1997). The electrical field is directly proportional to generated surface by brittle fragmentation. One has to observe that the containment (*Faraday* cage) shields the field from the sensor. Hence only runs with the same setup in the laboratory are comparable.

- The acoustic recording of the **microphone** did not deliver any useful signal. Only noise could be detected. Shock or sound waves generated by the explosion were almost not detected.
- The seismometer records shock and sound waves and the impact of particles at the top of the

containment.

- The recorded signals of **trigger** and **pump** help to check, whether these devices worked correctly during an experiment. Only the falling slope of the trigger signal is visible in the records, because the record starts during the trigger signal is falling. The voltage at the potentiometer indicates the position of the piston pump. The time, when the pump is moved and the correct movement of the piston, can be checked.

4.4.1 Comparison of explosions produced in the laboratory and other MFCI-explosions

As mentioned the geometry of explosions in the laboratory is much smaller than such in real scenarios as in volcanoes or power plants. It has to be critically verified, to what extent the laboratory explosions accord to real explosions in nature and technique, which are simulated in the laboratory.

A comparison of natural fine fragments and artifical fine fragments produced by explosion in the laboratory shows that form and size of the ash particles are similar in both cases. It can be concluded that the brittle fragmentation is similar in nature and in the laboratory (see BÜTTNER, ZIMANOWSKI, MOHRHOLZ, et al., 2005). It can also be assumed that the energy per mass for fragmentation is similar in both cases. Laboratory experiments allow access to the energy transfer of explosions in other scenarios.

Another difference to real scenarios is the opening of the particular system. The interactive domain is weakly capped by the little melt layer over the active domain. In larger scenarios the cover is thicker and the break-up is not so easy as in the crucible. The last phase for expansion and blow-out can be different. In the small experiment in the crucible it can be that the system is opened and the pressure of the interactive water decreases and water vaporizes after that. In larger scenarios the break-up is not so easy and it is possible that the water has to vaporize first. A larger experimental setup would be helpful to discloud this question.

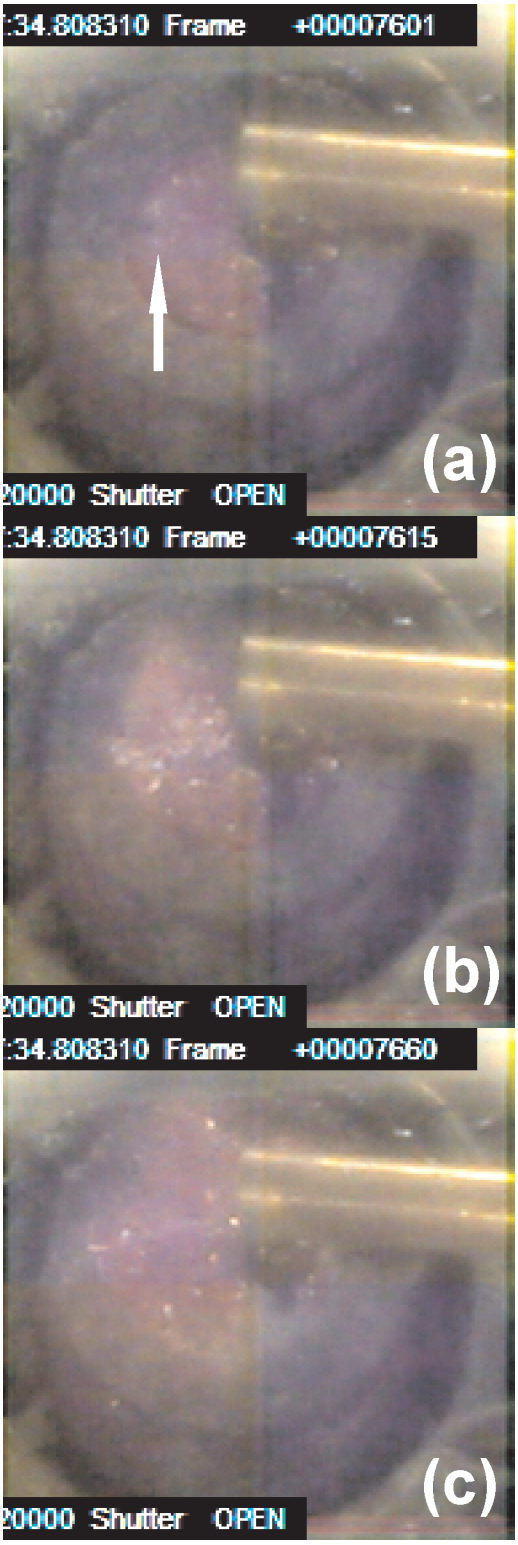

Figure 4.4: Frame of high-speed recording of an MFCI-run. 150 ml of tin melt were heated on 900 $^{\circ}C$. The frame rate was 20000 fps. At $t = 0\,ms$ the water injection pump is started, after 100 ms the solenoid opens and the video recording is started. It ends after $t = 440\,ms$ and the trigger projectile is launched from the gun. 40.05 ms later it arrives at the melt surface ($t = 480.05\,ms$, frame 7601, picture (a)). At $t = 480.75\,ms$ (frame 7615) the melt surface breaks up, picture (b). At frame 7660 at $t = 483.00\,ms$ (picture (c)) the recorded force signal in 4.3 (a) is maximum. Some ash particles leave the system around the injection tube. The attached video shows the complete process (see appendix E).

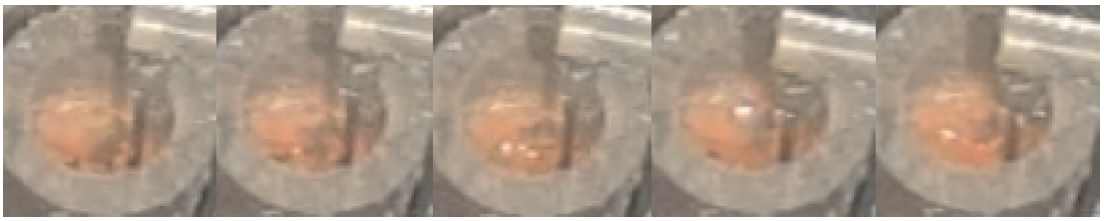

Figure 4.5: States during the injection of water. The different bright spots in the images show the locations, where agitated melt reflects light. The melt temperature in this run was 900 $^{\circ}C$, the crucible was filled with 70 ml of tin.

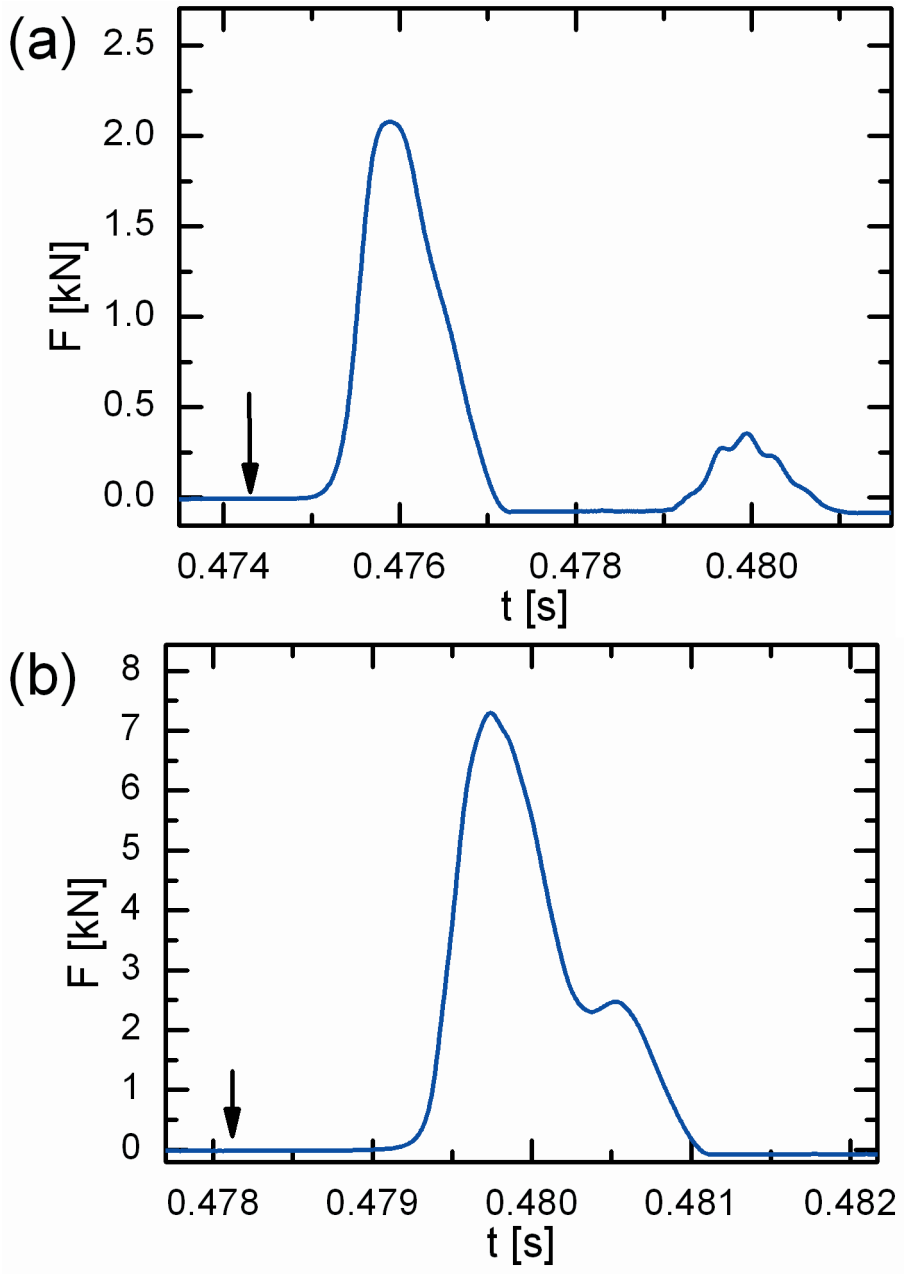

Figure 4.6: Effect on propagation of the force signal. The arrows show the moment of projectile impact obtained by the video analysis. (a) Single triggered explosion. The time between impact and beginning of expansion is $700\,\mu s$ seen in the video ($70\,ml$ of tin at $900\,^{\circ}C$). (b) Double explosion ($70\,ml$ of tin at $900\,^{\circ}C$). The time between impact and beginning of the force peak is longer, although the time according to the video is only $250\,\mu s$. This delay can be explained by the fact that the seismic signal has to pass several melt-water interfaces, before being detected by the force sensor.

Chapter 5

General acquisition

As described above the main aim of the investigations, the influence of melt temperature on MFCI is hardly directly visible from the recorded data. Thus a complex procedure of analysis was developed. It is not possible to reproduce exactly the same premix of melt and water in each run - which effects always a slight, yet detectable variation of results even by using identical experimental parameters. Nevertheless, these variations can be filtered in a subsequent data analysis (see Figure 5.1).

The procedure is based on the following considerations:

- The area of the initial surface between melt and water depends on the individual geometry of premixture. The area for vapor film collapse and **initial direct contact surface** is pretended. This area has dominant influence on the **interactive melt mass** and the **interactive water mass**, which are responsible for heat transfer.
- It is useful to normalize the data of each run to the interactive mass before comparing serveral runs.
- The easiest way to acquire the interactive melt mass is collecting the particles after each run. The fragments were fractioned by their diameter size. The two fractions with the lowest diameters ($63\,\mu m$ and $125\,\mu m$) were analysed with an optical microscope. But hydrodynamically fragmentated particles were also collected. By shape analysis (ZIMANOWSKI, BÜTTNER, LORENZ, and HÄFELE, 1997) it was possible to discriminate interactive particles (i.e. particles generated by brittle fragmentation) from dry or non-interactive (hydrodynamically fragmented) ash particles. The mass of each fraction is determined by a scale.
- But not all particles can be sampled and weighed after the experiments. Some particles are lost in the setup or remelt with blown-out hot coarse melt. If the blowout is weak, additionally not all particles will be ejected from the crucible; most of the particles will rest within the crucible and will re-melt immediately with the rest of hot tin. As this makes a quantitative analysis and the fixing of interactive mass complicated, the following procedure was chosen: In order to reconstruct the particle mass, an effective mass m_{eff} has to be calculated by the measured change of momentum

and the particle velocity detected in the video films:

$$m_{\text{eff}} = \frac{p}{v_{\text{mean}}} , \tag{5.1}$$

where p is the pulse which is calculated by

$$p = \int F\,dt . \tag{5.2}$$

F is the repulsion force on the crucible that results from the acceleration of the fragments. The difference between effective mass and the weighed mass is low at strong explosions and high at low explosions. In all cases the weighed mass of blown-out fragments was lower than the calculated effective mass, which shows that the approach of calculating the effective mass is at least not in conflict to the measured results. As a result one obtains the effective interactive mass $m_{\text{eff,i}}$. But in both cases, concerning the scaled mass values and the calculated effective mass, there is also no explicit direct trend recognizable for the influence of temperature, a reason are the variations in premix, too. It should be noted that the value for the pulse p is lower by absorption between the crucible and the force sensor in the setup. The detected particle velocities are slower than the velocities of the particles directly after their acceleration in the crucible. Furthermore, the part of interactive particles from the collected samples is taken as basis for part of the interactive particles in the effective masses. It is to note that there are some errors in the estimation of the particle velocities, because in the video recordings only a particle front and not single particles can be observed. For high velocities, which mostly occur at strong explosions, the estimation is tendencially too high, for slow velocities it is too low. As a consequence the calculated effective masses are a little bit too low for strong explosions and too high for weak explosions.

In this way the influence of premix can be largely filtered. For the following analysis of the influence of melt temperature a maximum and a minimum estimation for the transferred energy was performed, because it is difficult to access the real values of some energy forms. The following procedures allow to discover and describe some trends for the influence of melt temperature on an MFCI-process.

The maximum estimation is based on a high value for the transferred thermal energy. After that the values for the output energy are calculated based on the recorded data. At least the law of conservation of energy is applied to get rough values for energies, which could not be directly detected.

- Estimation of transferred thermal energy
  The total output energy must be provided by transferred thermal energy of the interactive melt. It is assumed that the interactive melt cools down from its initial temperature to 350 $^{\circ}C$. This assumed end temperature is close to the critical temperature of liquid water. The released energy can by

calculated by

$$\Delta E_{\mathrm{i}} = c \cdot m_{\mathrm{eff,i}} \cdot \Delta T \ , \tag{5.3}$$

where c is the specific heat capacity of the melt material and $m_{\mathrm{eff,i}}$ is the interactive melt mass, which transfers heat. According to BÜTTNER, ZIMANOWSKI, MOHRHOLZ, et al., 2005, not all interactive fragments cool down to the end temperature as a consequence of the very short time for the cooling process. This is an issue for magmatic melts, for tin melt it is negligible because of the high thermal conductivity and the low heat capacity of tin. Calculations demonstrate that most of the small tin particles can cool down to the end temperature even in this short time. Because of the assumed exponential decay for the cooling of the particles even big fragments can nearly cool down to the end temperature in a very short time of direct contact. By use of the effective interactive mass and an estimated end temperature the maximum value for transferred heat is calculated.

- Fragmentation energy for new surface
  The fine particles have a big surface compared to their mass. During the fragmentation process a lot of new surface has to be created. Therefore energy is needed. For the fragmentation energy the energy for brittle fragmentation has to be separated from the energy for hydrodynamic fragmentation. The possibility should be mentioned that tin glass or metallic glass is developed because of high cooling rates of interactive melt during this process (FAUPEL et al., 2010).

  The energy is calculated by the determined mass and the specific surface. The surface tension is a value for the necessary energy to create a certain area of new surface. All in all the fragmentation energy for new surface $E_{\mathrm{frag,i}}$ by brittle fragmentation can be calculated by

$$E_{\mathrm{frag,i}} = \sigma_{\mathrm{i}} \cdot S \cdot m_{\mathrm{eff,i}} \ , \tag{5.4}$$

  where σ is the specific surface tension and S is the specific surface per mass. The fragemnatation energy for hydrodynamic fragmentation is calculated by

$$E_{\mathrm{frag,h}} = \sigma_{\mathrm{h}} \cdot S \cdot \left(m_{\mathrm{eff}} - m_{\mathrm{eff,i}} \right) \ . \tag{5.5}$$

- Shock wave energy
  Shock waves are emitted during brittle fragmentation. This energy was determined in package with fragmentation energy for new surface for tin melt. For tin melt both energies in correlation to brittle fragmentation are handled in package for tin experiments. For magmatic melts they can be handled separately after detailed investigations (BÜTTNER and ZIMANOWSKI, 1998; DÜRIG, 2011; E. SHARON et al., 1996). It can be assumed that the shock wave energy E_{shock} is proportional to

surface energy for brittle fragmentation $E_{\mathrm{frag,i}}$.

$$E_{\mathrm{shock}} = c_{\mathrm{shock}} \cdot E_{\mathrm{frag,i}} \,, \tag{5.6}$$

where c_{shock} is the proportionality factor. The total energy to create new surface by brittle fragmentation is the sum of the energy for brittle fragmentation and the shock wave energy: $E_{\mathrm{surf}} = E_{\mathrm{frag,i}} + E_{\mathrm{shock}}$.

- Kinetic energy for mass blowout
  Kinetic energy E_{kin} is needed to blowout mass. The major part of this energy is obtained by the fine particles, because their velocity is higher than that of the rough blowout, that mainly consist of liquid melt. For the calculation the weighed mass is used. The velocities are taken from the high-cam videos. The velocity of single particles is not detectable. Therefore the average velocities of four values for each of three particle fronts are measured. It is assumed that most of the small particles are in the front with high velocity, middle size fragments in the front with middle velocity and rough fragments in the front with low velocity. The velocity of liquid tin is also detected. This is an approximation for the kinetic energy. E_{kin} is calculated by

$$E_{\mathrm{kin}} = \frac{1}{2} m v^2 \,. \tag{5.7}$$

- Enthalpie of evaporation
  The enthalphie of evaporation E_{V} dissipates a big part of total energy because of the high supply r that water can change from liquid to gas phase, although the evaporating water volume is small. It cannot be directly measured. Former investigations have shown that this volume is not exceeding 10 % of the injected water volume (MOHRHOLZ, 2002). This is really a maximum estimation. In the runs of this work the conservation of energy would be outraged if the vaporized water volume was 10 % of the injected volume, i.e. about 0.7 ml. For an estimation of the vaporizing water volume it is obvious that it depends on the interactive melt mass. According to conservation of energy the water volume is estimated directly proportional to the interactive melt mass. The energy is mostly from residual energy, which is not yet supplied for other energies. The onset of this estimation is done at low melt temperatures, where the avaiable energy and the vaporizing water volume are lowest. An increase of vapor is to be expected according to STENZEL et al., 1958. The thickness of a fully developed vapor film is proportional to $T^{\frac{1}{4}}$, but it would be to challenge, whether this is applicable to short time experiments. E_{V} is calculated by

$$E_{\mathrm{V}} = c_{\mathrm{V}} \cdot r \cdot m_{\mathrm{eff,i}} \,, \tag{5.8}$$

where c_{V} is a temperature dependent factor. For low temepratures of 400 $^{\circ}C$ it is 0.005, for 500 $^{\circ}C$ it is 0.01, and for all higher melt temperatures with tin melt it is 0.03, for magmatic melt at about

1300 $^{\circ}C$ it is 0.08.

- Other energies
  Beyond the presented energies there are still other energies, for example acoustic or seismic energy. Their part is low and negligible (BÜTTNER, DELLINO, et al., 2006; EX et al., 2000).

Concluding all, there is the residual energy, which is the part of the transferred energy that is not converted into an outcoming energy:

$$E_{\text{res}} = \Delta E_{\text{i}} - E_{\text{frag,i}} - E_{\text{frag,h}} - E_{\text{shock}} - E_{\text{kin}} - E_{\text{v}} \; . \tag{5.9}$$

The efficiency η is calculated by

$$\eta = 1 - \frac{E_{\text{res}}}{E_{\text{i}}} \; . \tag{5.10}$$

The approach of the minimal estimation is the sum of all outcoming energies, which are calculated from the recorded data. The enthalphie of evaporation has to be added. The value for the energy for volume expansion $p\Delta V$ in the term $\Delta H = \Delta U + p\Delta V$ is based on kinetic energy of blowout. The according value for ΔU is calculated. The results are in agreement to the recorded data in each run. The sum of all energies is the minimum value of the involved energy for each run. The real transferred energy of a run is between the minimum estimated and the maximum estimated value:

$$E_{\text{out}} = E_{\text{frag,i}} + E_{\text{frag,h}} + E_{\text{shock}} + E_{\text{kin}} + \Delta U \; . \tag{5.11}$$

With the transferred energy E_{out} the assumed end temperature difference for the interactive effective mass $\Delta T_{\text{out,eff}}$ for this case is calculated by

$$\Delta T_{\text{out,eff}} = \frac{E_{\text{out}}}{c \cdot m_{\text{eff,i}}} \; . \tag{5.12}$$

The end temperature T_{end} of the effective interactive mass is calculated by

$$T_{\text{end}} = T - \Delta T_{\text{out,eff}} \cdot \tag{5.13}$$

This procedure can also be done for some checks by using the weighed interactive mass m_{i}, where the calculation of the output energy $E_{\text{out,w}}$ has to be based on outcoming energy forms, which are calculated with the weighed masses:

$$\Delta T_{\text{out}} = \frac{E_{\text{out,w}}}{c \cdot m_{\text{i}}} \; . \tag{5.14}$$

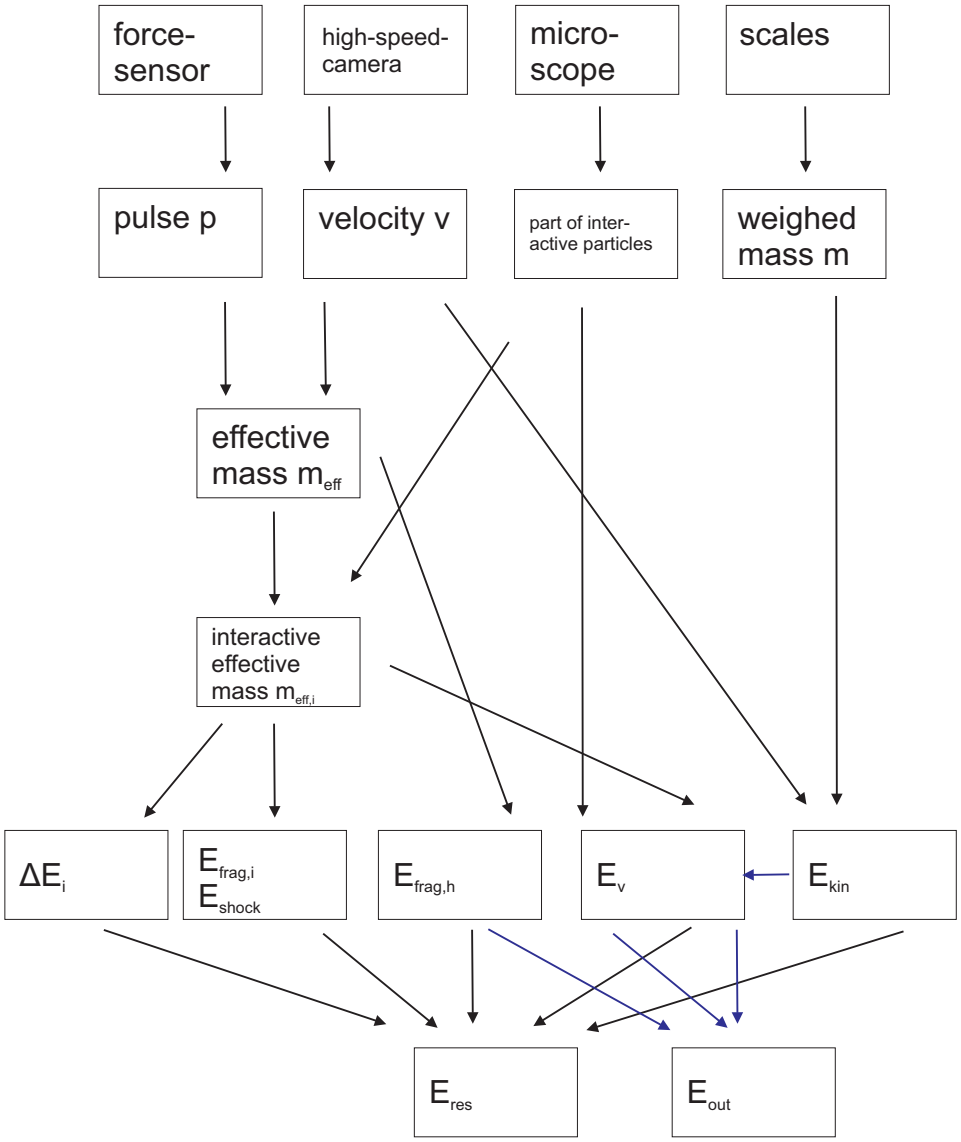

Figure 5.1: General acquisition procedure. The black arrows show the way for the maximum estimation of transferred energy, the blue arrows the way for the minimum estimation.

Chapter 6

Significant results from MFCI-experiments

6.1 Lower limiting temperature for vapor film stability

The first phenomena for measurements with several melt temperatures was a lower limiting temperature for vapor film stability in this kind of tin experiments. This limit is about 600 $^{\circ}C$. For lower temperatures almost all experiments were self-triggered, which means that the vapor film collapsed and the third stage of the process (energy transfer) had started before the trigger bullet arrived in the crucible. For higher temperatures the vapor film collapse had to be mechanically triggered by the bullet impact.

Reasons for the self-collapse at low temperatures are instabilities in the vapor film. If the melt temperature is only a little higher than the HNT of water, the vapor film is thin (STENZEL et al., 1958), it can be easily destroyed by movement of water bubbles in the melt.

6.2 Correlation of melt temperature and repulsion force

As expected there is an increase in average of the repulsion force to higher melt temperatures. This is caused by a higher energy transfer at higher temperatures. In the range of high temperatures of 900 to 1040 $^{\circ}C$ this increase is lower than in the range of lower temperatures. The later behaviour of the repulsion force for temperatures over 1040 $^{\circ}C$ cannot be discovered with tin melt.

A reason for the lower increases at high temperatures or an eventual constant level for the repulsion force is probably due to the fact that the end temperature of melt increases with higher initial melt temperatures and this again limits the transferred thermal energy. It is to note that the temperature is not the only factor for the repulsion force. An overlap of several explosions in a multiple triggered experiment leads to higher repulsion force. Strong and weak explosions occur at high temperatures. These variations are a consequence of different premixtures, because the material parameters should be the same at the same temperature. Furthermore, if there are disturbing influences on a run, such as tin oxide in the melt, the explosion is weak. Complex analysis is required to eliminate the influence of premixture and to get rare influence of melt temperature. To get a first easy separation of weak and strong explosions, the

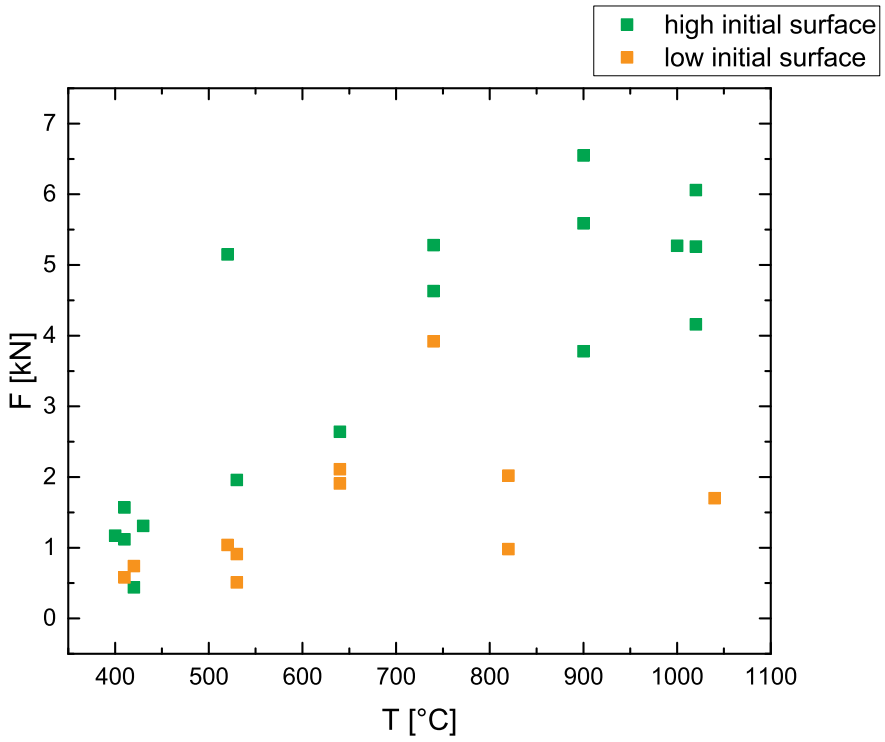

Figure 6.1: Repulsion force versus melt temperature. In all runs a water volume of about $(7.2 \pm 0.7ml)$ at an injection time of $440ms$ and $100ms$ valve delay was injected. The trigger was started after $440ms$ at the end of the injection time and arrived on the melt surface at about 370 to $375ms$. Run with a low initial contact surface caused by the individual premix are marked in orange, runs with a high initial surface in green.
With this separation the correlation of repulsion force and melt temperature is more clearly visible, especially for strong explosions. For strong explosions the *Pearson* correlation coefficient for a linear dependence is 0.824 and its p-value is 0.00009. For weak explosions the correlation coefficient is less, only 0.482 and a p-value of 0.13. This is a first result, that melt temperature has influence on explosions remarkably for strong explosion with a high initial direct contact surface caused by the individual premix.

explosions are divided into a weak and a strong group for each temperature. It is justified to assume that the difference between weak and strong explosions is caused by the premix and initial direct contact surface. This is checked by runs with a different injected water volume at the same temperature. The runs with a lower water volume result in a generally lower initial direct contact surface and a weaker explosion. This relation is significant. But it is also to remark that there are even differences under weak and strong explosions with the same experimental parameters.

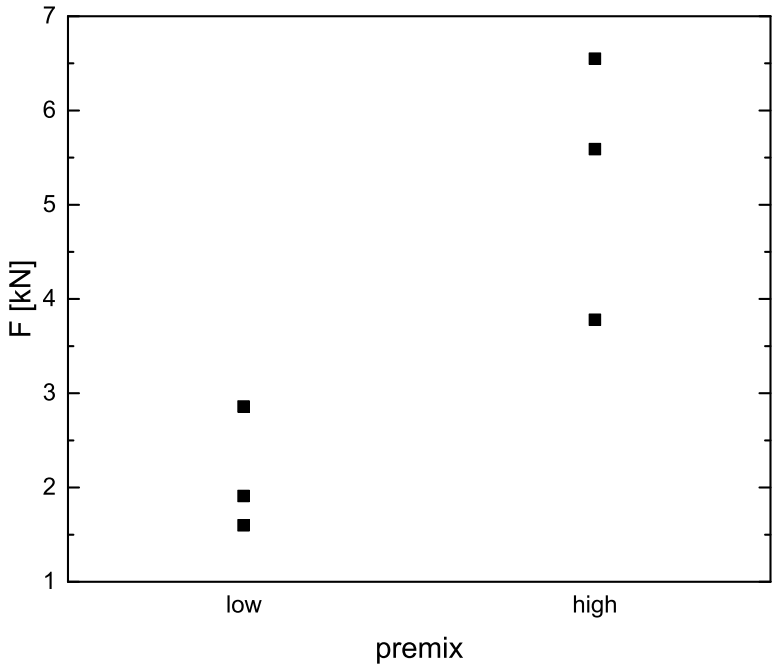

Figure 6.2: Repulsion force for premixes with low and high injected water volume. The high volume was $7.2\,ml$ at an injection time of $440\,ms$ and $100\,ms$ valve delay as in all other standard runs. The low volume was $(5.5 \pm 1.6)\,ml$. At an injection time of $400\,ms$ and $100\,ms$ valve delay. The trigger bullet was started at the end of the injection time in all runs.

6.3 Correlation of melt temperature and pulse

The repulsion force is not the only parameter to describe the magnitude of an explosion. It is also important how long the force acts. This time variates in a range from 0.5 to $4.2\,ms$; it does not correlate to the temperature. It is to check, whether the integer of force and time, the pulse, is correlated to temperature.

This value is also dominated by the individual premix. Naturally the total pulse in multiple triggered runs is higher. A rough relationship between pulse and temperature is visible, but it is ambiguous by premixture, multiple triggers or self-triggered runs at low temperatures. The *Pearson* correlation coefficient is 0.39 with a p-value of 3 %. An indicator for this correlation is the interactive mass. The interactive mass is higher in multiple triggered runs, where the total pulse is higher, too. In the run with three triggers at $520\,^{\circ}C$ the interactive mass and the pulse is the highest of all runs. Besides it can be remarked that both pulse p and weighed interactive mass m_{i} and the calculated effective interactive mass $m_{\mathrm{eff,i}}$ increase at higher temperatures.

It is to note for strong explosions at high temperatures that the falling slope of the force signal is significantly longer than the rising slope. In some cases a small peak after the main peak is visible,

which might be caused by expanding steam (SPITZNAGEL et al., 2013). This can be interesting for the estimation of the vaporizing water volume. It is also remarkable for the values of the pulse that they are influenced by premix and initial direct contact surface, even if this relation is not so significant as for the values of the respulsion force.

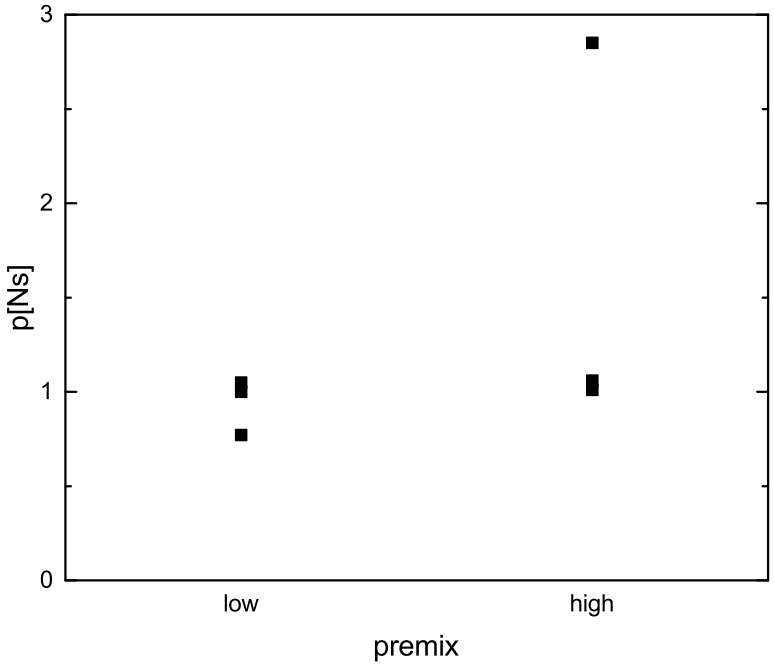

Figure 6.3: Transferred pulse for premixes with low and high injected water volume. The high volume was $7.2\,ml$ at an injection time of $440\,ms$ and $100\,ms$ valve delay as in all other standard runs. The low volume was $(5{,}5 \pm 1{,}6)\ ml$ at an injection time of $400\,ms$ and $100\,ms$ valve delay. The trigger bullet was started at the end of the injection time in all runs.

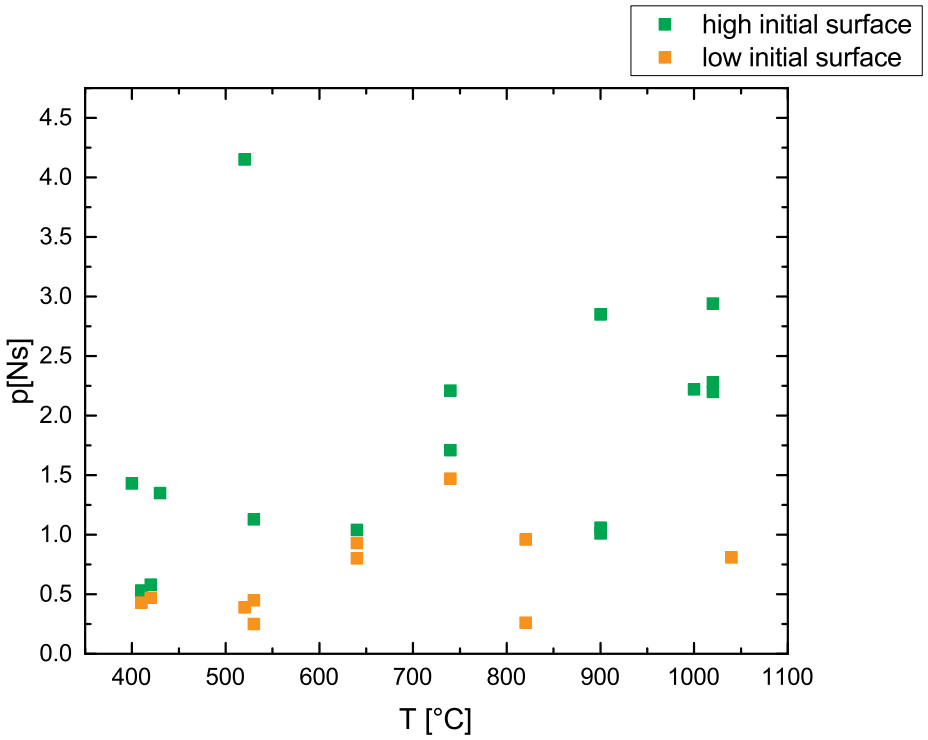

Figure 6.4: Pulse versus melt temperature. In all runs a water volume of about 7.2 *ml* at an injection time of 440 *ms* and 100 *ms* valve delay was injected. The trigger was started after 440 *ms* at the end of the injection time and arrived on the melt surface at about 370 to 375 *ms*. Runs with a low initial contact surface caused by the individual premix are marked in orange, runs with a high initial surface in green.

6.4 Correlation of melt temperature and multiple trigger

As mentioned in chapter 4 and SPITZNAGEL et al., 2013, multiple trigger often occurs at a tremor in the premix (Figure 4.5). It might be the main reason for multiple trigger.

It can be observed in runs with an adjusted mirror with view on the top of the surface that tremor is rare at lower temperatures. The cases with tremor increase with temperature. At a low temperature of 650 $^{\circ}C$ a motion of the melt surface, which indicates a tremor, only in 25 % of the runs is detected, but at 900 $^{\circ}C$ in 71 %.

Multiple trigger appears to be correlated to tremor at low temperatures (650 $^{\circ}C$) and only takes place in union with tremor. At high temperature (900 $^{\circ}C$) this union is obliterated. Indeed, there was multiple trigger in four of seven cases, but in three cases the runs were only single triggered in spite of tremor. For these studies single triggered runs are most appropriate. Multiple trigger at high temperatures is more rare due to more stable vapor films. There was not any multiple trigger in a “quiet“ premix without tremor. At high temperatures it would be more complicated to build more water domains in the melt because of the lower viscosity of melt. More water domains in the premix cause multiple trigger (SPITZNAGEL et al.,

2013). At higher temperatures a bigger domain can develop for a higher initial contact surface.

All in all multiple trigger took place in two of 19 cases at all runs with tin melt at a low temperature of 650 $^{\circ}C$, at high temperature above 890 $^{\circ}C$ in three of 19 cases. For all runs it is to conclude that there is no relationship between melt temperature and multiple trigger.

6.5 Influence of temperature on the interactive melt mass

For the amount of transferred energy the involved interactive melt mass has important influence. There might be a relation between the interactive mass and the pulse as a proportion for the intensity of an explosion. But there is neither a relation between melt temperature and effective interactive mass nor the weighed interactive mass directly detectable. On the first view, the amount of interactive mass depends on the transferred energy, which is not only influenced by temperature. As discussed, other effects such as premixture and initial contact surface have influence on the intensity of an explosion and also on the involved interactive mass.

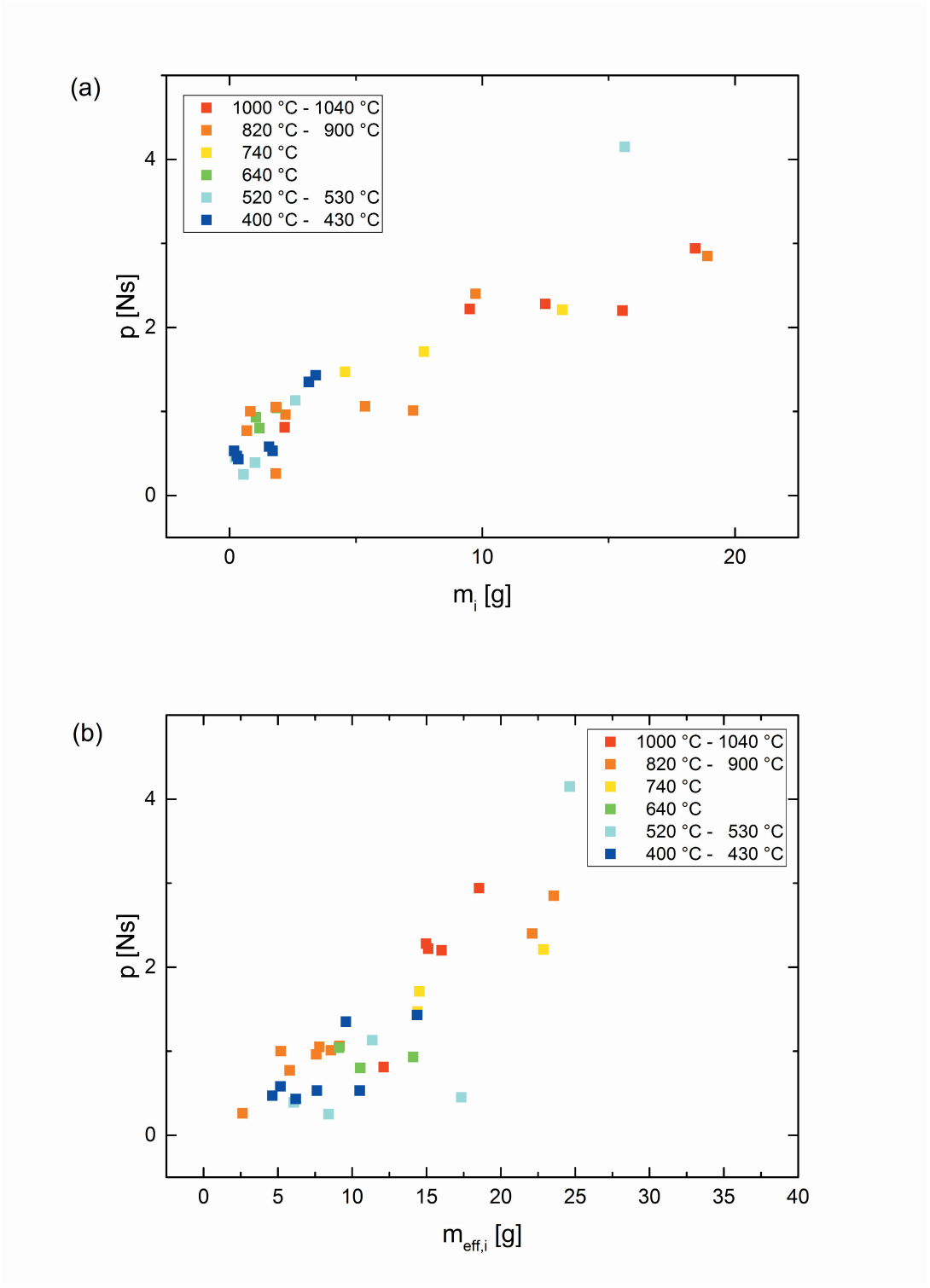

Figure 6.5: Pulse versus (a) weighed interactive mass and (b) effective interactive mass.

6.6 Influence of temperature on the normalized pulse

The normalized pulse on the effective interactive mass weakly increases with melt temperature. For normalizing to the weighed mass the relationship is reverted. This is mainly caused by the low weighed masses at low temperatures. At high temperature the variation of the normalized pulse values is clearly smaller than at low temperatures. It is to assume for low temperatures that a big part of the interactive particles remelts in the crucible before blowout, and the remelted part has big variations.

Chapter 7

Shape analysis

Conclusions about brittle fragmentation cannot only be won by the mass and number of interactive particles, but also by analysis of the shapes. According to DÜRIG, MELE, et al., 2011, size and form of a shape are controlled by the individual fracture process and by the available energy. The form of a particle is a fingerprint of its creation procedure (ZIMANOWSKI, BÜTTNER, LORENZ, and HÄFELE, 1997).

For this shape analysis the software "MacShapeII" was used. It analyses vector graphics of the fragments and discovers the following form parameters:

- Relation of area to circumference
- Maximum diameter
- Feret diameter, that is edge length of the circumscribing rectangular parallel to the coordinates
- Parts of concave and convex curvature and plain parts of the circumference

The investigation of curvature is most interesting. It is made in raw mode (first order, $C1$, $V1$, $P1$) and a smooth mode (second order, $C2$, $V2$, $P2$).

Interactive particles have a high part of convex curvature, because their surface is rough. A rough surface is bigger than a plane surface of a body with the same volume. More energy for surface creation is needed to build a body with a rough surface.

For several melt temperatures the following trend can be observed: At high temperatures a higher proportion of the particles is more convexly curvatured. At low temperatures there is a big part of particles which has nearly no convex curvature. Additionally the part of convex curvature is highest for interactive particles from runs at high temperature:

1. highly significant positive correlation of temperature to $P1$ (Correlation coefficient 0.559)
2. highly significant negative correlation of temperature to $V1$ (Correlation coefficient -0.468)

3. significant positive correlation of temperature to $C1$ (Correlation coefficient 0.170 $\rightarrow$ i.e. not distinctive)
4. highly significant positive correlation of temperature to $P2$ (Correlation coefficient 0.516)
5. highly significant negative correlation of temperature to $V2$ (Correlation coefficient -0.507)
6. highly significant positive correlation of temperature to $C2$ (Correlation coefficient 0.393)

The most clear positive correlation of temperature to $P1$ and the most clear negative correlation of temperature to $V2$ are detected.

The dependencies on the fracture processes allow the assumption that the premix also influences the shape form. It is to note that in a premix, which leads to a weak explosion, the shapes have a high plane part and a low concave part at high temperatures as well as at low temperatures. But there is no correlation of temperature and particle form at low temperatures. It is indicative that high fragmentation is only possible if there is enough energy provided. This result is in good accordance with the values of interactive mass for the appropriate runs. This accords to the results in section 6.3 that there is a significant correlation between repulsion force, transferred pulse and temperature for strong explosions. This correlation is not so explicit for weak explosions.

The most fragmentation energy is needed for small particles. At high temperature there are on the one hand more particles in the finest fraction and on the other hand particles with rougher surface. Fragmentation is stronger at high temperatures. One explanation is the higher thermal energy, but it might also be the lower surface tension at high temperatures. For hydrodynamic fragmentation the surface tension is about 10 % lower at 900 $^\circ C$ than in temperature range of 500 $^\circ C$ (BIRCUMSHAW, 1926). The surface tension for brittle fragmentation of pure tin was discovered in seperate blowout experiments (see appendix C), because they are not provided in any literature. Only values for tin alloys could be found (see e.g. RIEM, 1999; ROUABHI et al., 2005). For brittle fragmentation it could also be noted that the surface tension is lower at high temperatures.

For the second least fraction with diameter from 63 μm to 125 μm a trend for strong explosions is visible. But the correlation between temperature and shape parameters is inverted to correlations for the lowest fraction. This accords to the classification of hydrodynamic and brittle fragmented particles with the optical microscope. For the more rough fragmentation it is to ask, whether temperature or premix is more relevant for fragmentation and shape form.

To conclude, there is a relationship between explosion intensity and fine fragmentation. For stronger explosions temperature dominates fine fragmentation.

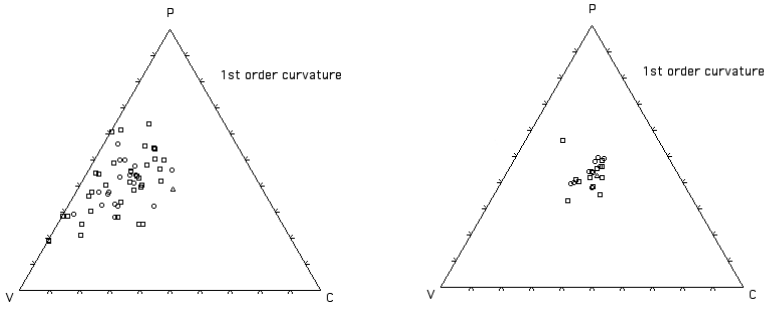

Figure 7.1: Ternary for particle classification for a strong explosion at 1020 $^{\circ}C$. Left ternary shows the classification of particles with a diameter smaller than 63 μm, right ternary shows the classification of particles with a diameter between 63 and 125 μm.

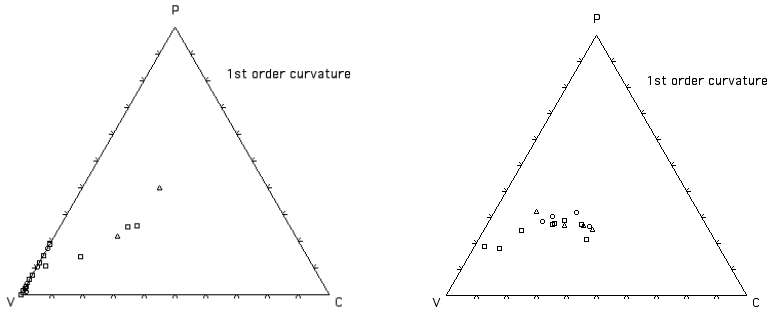

Figure 7.2: Ternary for particle classification for a strong explosion at 520 $^{\circ}C$. Left ternary shows the classification of particles with a diameter smaller than 63 μm, right ternary shows the classification of particles with a diameter between 63 and 125 μm.

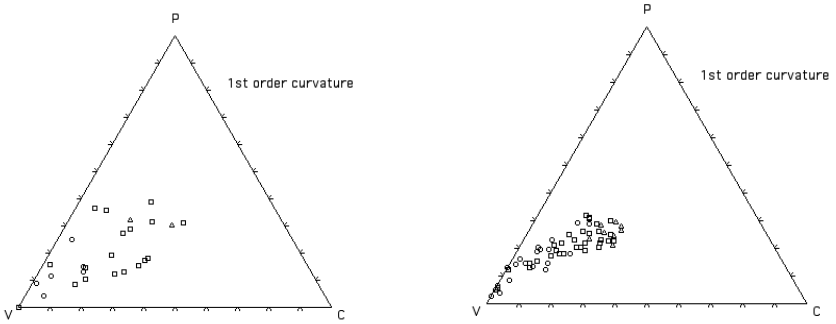

Figure 7.3: Ternary for particle classification for a weak explosion at 900 $^{\circ}C$. Left ternary shows the classification of particles with a diameter smaller than 63 μm, right ternary shows the classification of particles with a diameter between 63 and 125 μm.

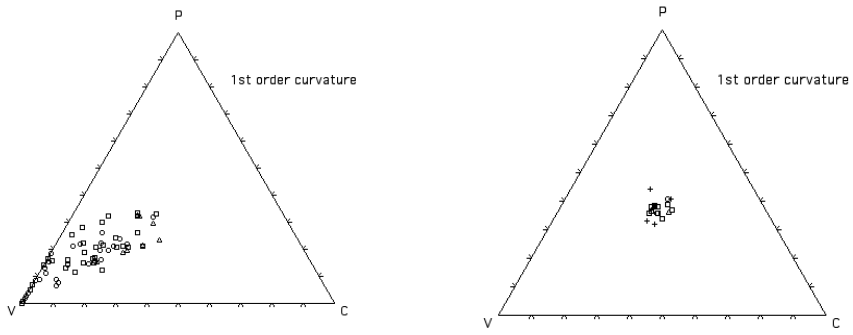

Figure 7.4: Ternary for particle classification for a weak explosion at 420 $^{\circ}C$. Left ternary shows the classification of particles with a diameter smaller than 63 μm, right ternary shows the classification of particles with a diameter between 63 and 125 μm.

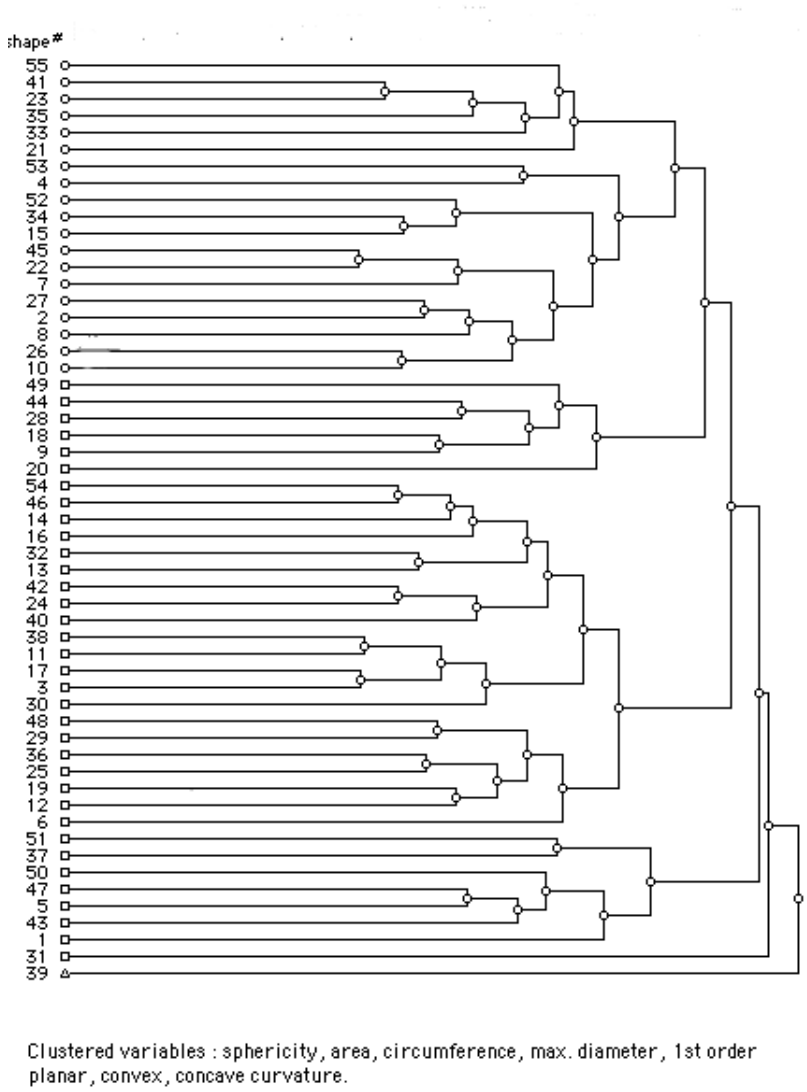

Figure 7.5: Flow sheet for particle classification of small particles with a diameter lower than $63\,\mu m$ for a strong explosion at $1020\,^{\circ}C$.

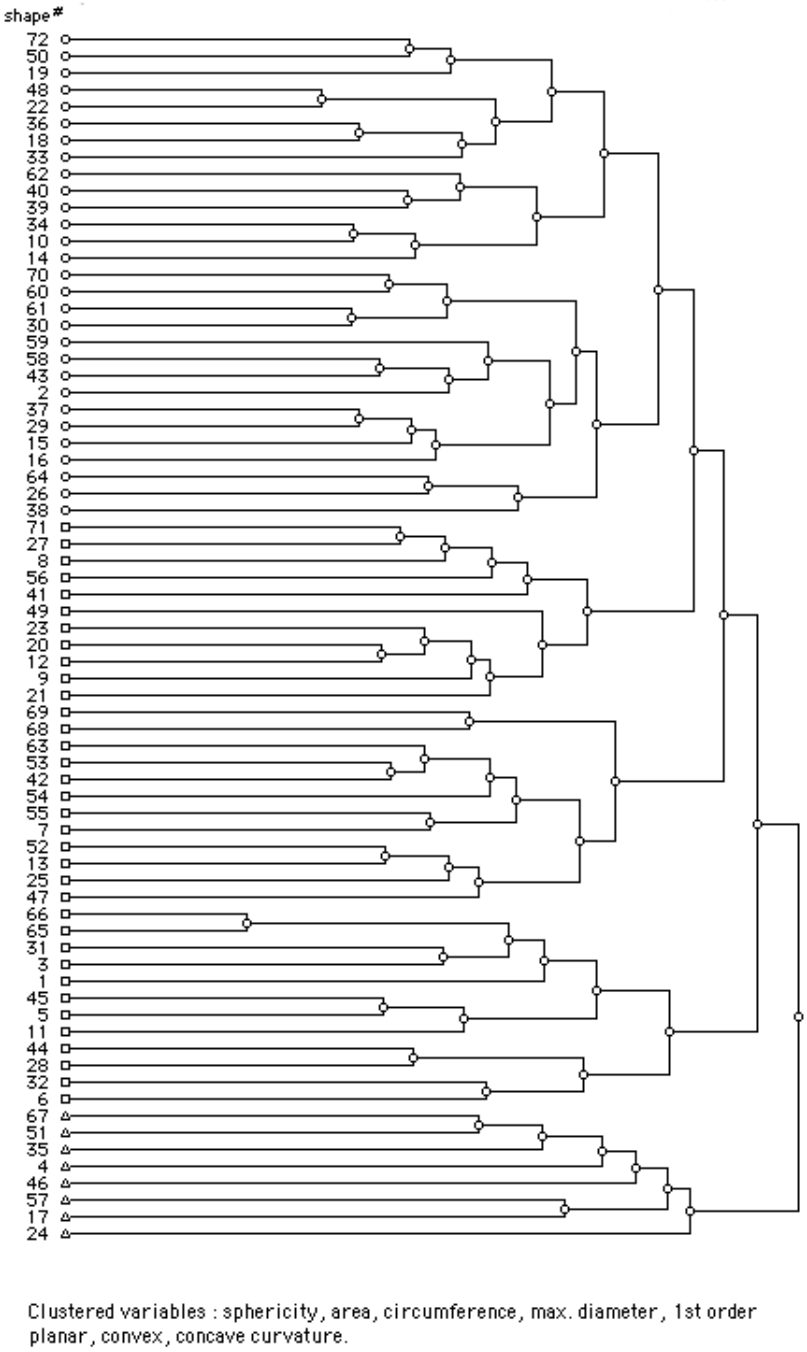

Figure 7.6: Flow sheet for particle classification of small particles with a diameter lower than $63\,\mu m$ for a weak explosion at $410\,^{\circ}C$.

Chapter 8

Influence of the duration of direct contact

The very short time of direct contact between melt and liquid water limits the possible time for energy transfer. Although this timespan is very short, according to SPITZNAGEL et al., 2013, only about 500 ms; it is to check, whether there are variations in this time, which could have a major influence on energy transfer and the whole explosion, because the cooling rate of interactive melt is very high and a high transfer can already be existent in the timescale of milliseconds. Furthermore it will be interesting if there is a relation between this duration and melt temperature.

It should be mentioned again that the time for direct contact cannot be directly measured from the video recordings. Only the total time for bullet impact, vapor film collapse and direct contact (t_{opt}) can be observed. It is significant that this time is shorter for higher pulses. A correlation analysis shows a *Pearson* coefficient for tin melt of -0.855. This correlation is significant on the 0.01-level. The assumption can not be confirmed that the time of direct contact is longer at strong explosions for higher energy transfer. It is to assume that for short "optical times" the time for vapor film collapse is shorter, otherwise there would not be any time for energy transfer in two cases. A time of 50 ms would be too short to transfer enough energy despite high cooling rates of the melt. The relation between time and pulse also suggests that particles might not cool down to the suggested end temperatures. For tin melts it is not possible to acquire all data for time and energy acquisition in the same run, because the modification with the mirror for time measurement excludes the acquisition of all necessary data for energy analysis. It is also not possible to get more information of the durations from the recorded force signals, because the transmission times through the crucible to the force sensor are individual for each run.

It is to suppose that in cases of quick vapor film collapse a big initial surface for high energy transfer is built simultaneously. In cases of slow collapses it may be that the system opens after a weak explosion before the initial vapor film has completely collapsed. The condition and the destructibilty of a vapor film depend on the premix.

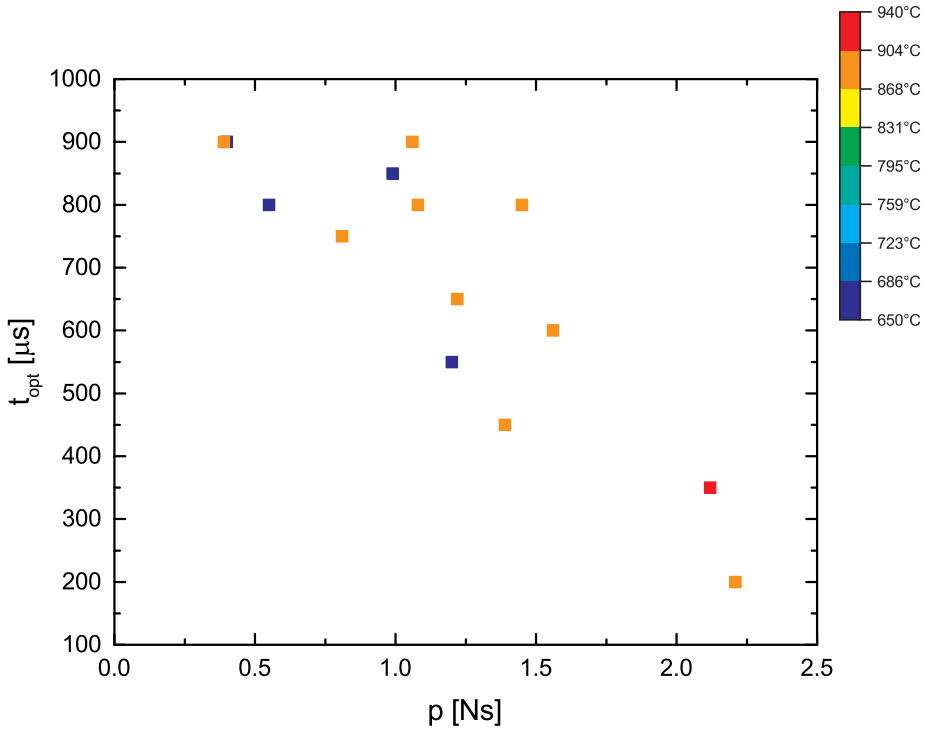

Figure 8.1: Optical time t_{opt} versus pulse. It gives a hint for the time of direct contact. It can be remarked that the optical time decreases with higher pulse. The shown values are from the runs with the optional mirror for a view on the melt surface.

A comparison of optical time and melt temperature does not show any significant correlation. It is only to recognize that for temperatures of 650 $^{\circ}C$ the optical times are in the range from 500 to 900 ms and at high temperatures of 900 $^{\circ}C$, respectively 940 $^{\circ}C$ in the range of 200 to 900 ms. At high temperatures short times are more probable, although there are also long times as at low temperatures. A precise conclusion for the end temperature or the water temperature at the end of direct contact is not possible. It can only be suggested that under advantageous conditions at high melt temperature water becomes earlier supercritical and finishes the phase of direct contact. In cases of very short optical periods of times it would be an aspect that the phase of direct contact might be too short for complete cooling of all fragments. This means that eventually fragments of the first generation, that are broken at the beginning of direct contact, can cool down on the suggested temperature of 350 $^{\circ}C$. Fragments of later generations can only cool down less. It can be further assumed that water becomes supercritical and finishes this process.

All in all the influence of the pure fragmentation time on explosions cannot be investigated in this experimental series and also dependences of this time cannot be discovered. Melt temperature has no or only little influence on the time of direct contact.

Chapter 9

Correlation of melt temperature and energy transfer

After the execution of the analysis from the recorded data and videos more concrete results about the correlation of melt temperature and energy transfer can be provided.

9.1 Results of the maximum estimation

9.1.1 Transferred thermal energy ΔE_i

In the maximum estimation for the thermal energy delivered by the melt it depends on the interactive melt mass and the temperature difference, in which the interactive melt cools down. For very low melt temperatures of 410 and 430 $^\circ C$ the transferred thermal energy for weak explosions is about $0.8 \cdot 10^2 J$ to $1.7 \cdot 10^2 J$, for strong explosions at these temperatures about $1.2 \cdot 10^2 J$ to $2.0 \cdot 10^2 J$. All values are listed in appendix D. The self-triggered single explosions or explosions with a mechanical trigger have the lowest energy transfer. Explosions with more than one trigger are in the middle and upper range of this interval. For temperatures from 520 to 530 $^\circ C$ the values are already higher in the range from $2.6 \cdot 10^2 J$ to $8.1 \cdot 10^2 J$ for simple triggered weak explosions, a simple triggered strong explosion has $5.3 \cdot 10^2 J$. A triple triggered strong explosion has a calculated energy transfer of $1.1 \cdot 10^3 J$. This is the result of a very favorable premix. The interactive mass of this run is very high, it is all in all about $24\,g$ and almost all rough material was blown out of the crucible. The weighed interactive mass is about $15\,g$. This difference can mostly be explained by the loss during the particle collection. But it shows that a strong blowout is necessary to eject a high part of the fine particles. At the other explosions at this temperature the interactive mass is only 1 to $4\,g$. $0.6 \cdot 10^3 J$ to $1.1 \cdot 10^3 J$ of energy were transferred at a temperature of 640 $^\circ C$. A difference for weak and strong explosions is not detectable for the transferred energy. For the next higher temperature of 740 $^\circ C$ the transferred energy for weak explosions is calculated to $1.4 \cdot 10^3 J$, and for strong explosions it is in the range from $1.5 \cdot 10^3 J$ to $2.3 \cdot 10^3 J$. For 820 $^\circ C$ two values of $3.2 \cdot 10^2 J$ and $9.2 \cdot 10^2 J$ are discovered for weak explosions. For the high temperature these both energy values stand out, because there was a lot of tin oxide in the crucible, which prevented a good premix. Also the weighed interactive mass for these runs is low, they are only 1 and $3\,g$, while they should be about 5 to $20\,g$ under normal conditions. For standard runs at 900 $^\circ C$ the values are 1.2 to $3.4\,kJ$. At a

lower injected water volume of about $6\,ml$ a smaller initial surface is to be expected. Only $7.3 \cdot 10^2\,J$ to $1.2 \cdot 10^3\,J$ are transferred at this temperature. At a triple trigger the transferred energy is $3.1 \cdot 10^3\,J$. For the highest melt temperatures from 1000 to 1040 $^\circ C$ the energy is $2.1 \cdot 10^3\,J$ to $3.2 \cdot 10^3\,J$. The low value of $2.2\,kJ$ is caused by tin oxide. The interactive mass is only $3\,g$, at strong explosions it is up to $14\,g$. As expected the transferred thermal energy increases with melt temperature, because the interactive mass can provide more energy. At high temperatures variations in the interactive mass have more affect on the transferred energy, the variations in transferred energy are more expanded than at low temperatures.

If the roughly estimated contact temperature (see equation 11.5) between melt at its particular initial temperature and water at its injection temperature (room temperature) is used as the end temperature of the cooled particles, all values are lower in the range from $1.9 \cdot 10^2\,J$ to $2.4\,kJ$. Because of the lower difference between melt temperature and contact temperature at high melt temperatures the calculated transferred energy is lower for high initial temperatures.

For the maximum estimation it is to conclude that the temperature difference ΔT is very high for high initial melt temperatures. This is the reason, why most of the values for the transferred energy are much higher for high melt temperatures than for low melt temperatures. Only extreme low or high values for the interactive mass can exclude some runs from this framework. But for these runs it might be sure that the calculated values are higher than the real values.

Now it is to check, how much transferred thermal energy is converted into each other energy.

9.1.2 Fragmentation energy $E_{\mathrm{frag,i}}$ for brittle fragmentation

First fragmentation energy $E_{\mathrm{frag,i}}$ for the creation of new surface by brittle fragmentation during the direct contact of melt and water is needed. It is proportional to the new created surface S and the specific surface tension σ. The values for tin in the relevant temperature range for brittle fragmentation had to be discovered by blowout experiments (see appendix C). The specific surface was measured by BET gas adsorption method (*Braunauer-Emmett-Teller*) for the relevant particle fractions at temperatures of 520 and 1020 $^\circ C$. The values are $0.078\,\frac{m^2}{g}$ for 1020 $^\circ C$ and a diameter from 63 to $125\,\mu m$, for a diameter smaller than $63\,\mu m$ $0.105\,\frac{m^2}{g}$. For 520 $^\circ C$ and 63 to $125\,\mu m$ the value is $0.062\,\frac{m^2}{g}$ and for less than $63\,\mu m$ $0.051\,\frac{m^2}{g}$. For the remaining temperatures the values are linearly extrapolated. The pictures of particles from a run at a temperature of 1000 $^\circ C$ are shown in Figure 9.1. A view on the new created surface in several runs is interesting. The most new surface was created at strong explosions. Generally the created surface at multiple triggers is higher than at single triggers caused by the higher contact surface. The values are in the range from 0.19 to $1.92\,m^2$. The part of particles in the finest fraction with diameters lower than $63\,\mu m$ is higher at strong explosions. The fragmentation grade is defined as the ratio finest and second finest particle fraction. For strong explosions it is between 0.46 and 0.69, for middle strong

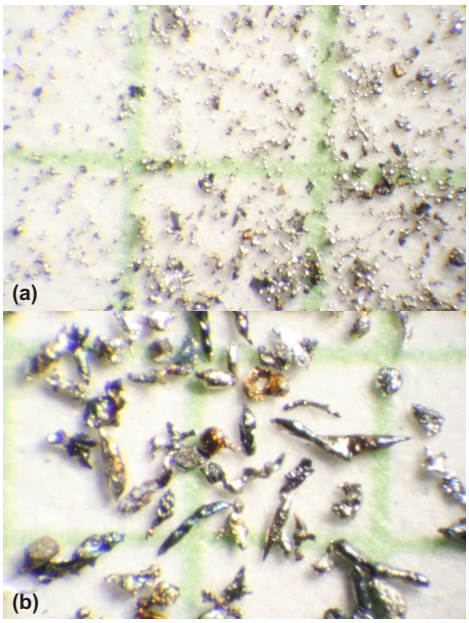

Figure 9.1: Particles of an MFCI-run at 1000 $^{\circ}C$ (a) Smallest fraction woth a particle diameter amaller than 63 μm. The small spheres are hydrodynamically fragmented particles, the rough shapes are mostly interactive particles. (b) Fraction with particle diameters between 63 and 125 μm. The long small particles are hydrodynamically fragmented, the more compact particles are interactive particles. The space between two green lines is 1 mm.

explosions 0.20 to 0.35. The only exception is a middle explosion at 900 $^{\circ}C$ with a fragmentation grade of 0.54. At weak explosions with low interactive mass it is only 0.16 to 0.32.

There is not any direct relation of temperature and new created surface, just a relation between thermal energy and new surface exists. Only a secondary correlation of temperature and created surface exists derived from the dependence of temperature and transferred energy. It is to note that at low energy transfer the fragmentation grade is low, the creation of new surface is limited and there are only few particles in the finest fraction. Obviously the pressure increase in water and tension in the melt is not high enough to crack a lot of fine particles. The particle analysis by “MacShape“ shows the same trend. Two form parameters strongly depend on the explosion intensity. There is no trend discovered for particles of weak explosions, and this is independent on temperature. Premix has significant influence on fragmentation. The triple triggered run at 520 $^{\circ}C$ shows that “good“ fragmentation is possible in case of a big contact surface and a huge energy transfer even if the melt temperature and the thermal energy provided by mass are low. At a triple trigger at 900 $^{\circ}C$ the fragmentation grade is higher than at simple triggers at the same temperature. It might be that there will be an interaction between the several triggers in a multiple trigger, if they are close enough together in place and time. In general there is more interactive mass and more created surface in multiple triggered explosions, but a direct proportionality to the number of triggers and the interactive mass and the created surface is not directly detectable.

The comparison to simple triggers at high temperatures shows that the fragmentation grade is lower and the interactive mass is slightly lower, but not as low as they can be at simple triggered explosions at low temperatures. Here the fragmentation grade is the lowest. It allows the conclusion that the melt temperature has influence on fragmentation, even if it is not the only factor. Reasons are the higher thermal energy and the lower surface tension at higher temperatures. This again can more strongly pressurize the interactive water and cause higher tensions in the interactive melt. A better feedback mechanism for magnification of the contact surface of melt and liquid water is possible. The analysis by "MacShape" in chapter 7 should be mentioned. The results of this analysis agree to these results. It has to be considered, whether the lower viscosity of tin at higher temperatures is the reason for a general better premix and higher fragmentation as one consequence. But with a lower injected water volume and reduced initial surface at high temperatures the fragmentation grade is still higher in average than at low temperatures. The highest fragmentation grade is 0.54 at high temperatures. This maximum value is never reached at low temperatures. Very high fragmentation grades over 0.5 occur only at high temperatures and cannot be reached at low temperatures with very good premix. At last metals tend less to brittle fragmentation at increasing temperatures. This is also a hint for higher water pressure and melt tension at higher temperatures. It is interesting to see, whether there is a correlation between the new created surface and the fragmentation grade. But there is only a lower correlation. It could depend on some non-visible influences, whether a higher interactive mass is fragmented following a bigger new surface with more rough particles or whether the newly created surface is lower and more fine fragments are created.

Correlation analyses show that there is a small correlation between melt temperature and total interactive mass. A light increase of the interactive mass with melt temperature is detectable, but there is big variation in several runs. The *Pearson* coefficient for correlation of melt temperature T and effective interactive mass $m_{\mathrm{eff,i}}$ is 0.24, the p-value 0.18. If only simple triggers are incorporated, the correlation coefficient is only 0.11. A correlation between melt temperature and newly created surface in the fraction for diameters between 63 μm and 125 μm of 0.43 is significant on the 0.05-level. The correlation for the smallest fraction for particles with a diameter less than 63 μm is 0.58 and this is highly significant with a significance less than 0.001. A correlation between melt temperature and fragmentation grade is detected (correlation coefficient 0.65, significance less than 0.001). A correlation between melt temperature T and fragmentation energy is not detected (correlation coefficient -0.1). An explanation can be that the specific surface tension is lower for higher temperatures and this compensates the increase of created surface with higher temperature. The correlation coefficient between the total of the created surface and the fragmentation grade is only 0.63. But high fragmentation grades only occur if the created surface is not at its lower limit.

Furthermore, not only the melt temperature but also the total energy transfer has influence on brittle fragmentation. There are correlations of the pulse to the total generated surface and to the generated

surface in the two smallest particle fractions with correlation coefficients between 0.8 and 0.85 on a very high significance. But the correlation coefficient between pulse and fragmentation grade is only 0.64, although it is highly significant, whereas there are higher correlations to the kinetic energy of blowout. The correlation coefficient to the total created surface is 0.77 and to the fragmentation grade it is 0.71. Both correlations are very highly significant. This also suggests that fragmentation influences the explosions. At least the correlation of repulsion force F and fragmentation grade is high at a coefficient of 0.77.

The surface tension of tin is low. Thus the fragmentation energy is only a small part of the totally transferred energy. It cannot be checked, whether the necessary energy for fragmentation influences or limits the fragmentation and the MFCI-process, because there was no more energy available for more fragmentation. Eventually it can be that for the finest fragments there is no more energy in themselves, that is sufficient for further fragmentation of the smallest particles. All in all there should be enough energy that can allow more fragmentation in the energetical view than it occurred in the experiments. It stands to result that fragmentation is stopped by another influence as the outcropping of energy. For other materials with higher surface tension it could be that fragmentation is limited, because there is too little energy available.

During fragmentation shocks are emitted, which transport energy E_{shock}. For tin melt it is not separately itemized, it is listed within the fragmentation energy.

9.1.3 Blowout energy E_{blow}

For the blowout of rough tin and fine particle blowout energy E_{blow} is needed. To this energy for the opening of the melt surface E_{open} and the kinetic energy of the blown-out material E_{kin} are corrsponding. E_{open} cannot be detected, but for tin melt it can be neglected in the cases of no tin oxide cover over the melt.

The values for the kinetic energy E_{kin} have a big variation in the range from less than $1\,J$ up to $118\,J$, because it depends on the force of the explosions. At first view there is no direct relation between the kinetic energy and the totally transferred energy. The part of kinetic energy variates from less than 1 % up to 5 %. Only in the cases with tin oxide in the crucible the part of kinetic energy is very low, perhaps more energy for the opening of the cover is used. There is also no correlation of melt temperature and kinetic energy. It seems that the kinetic energy depends much on secondary influence, such as water pressure and expansion of vapor. Also for the separation in weak and/or strong explosions no correlation between E_{blow} is found. All in all kinetic energy is only a small part of the total energy in a MFCI-explosion, although it is the most recognizable part of such an explosion. But it does not show the amount of totally transferred energy. As proposed in BÜTTNER and ZIMANOWSKI, 1998, the expression thermohydraulic

explosion is more appropriate than the formerly used expression steam explosion.

9.1.4 Vaporization energy E_V

The calculated values for the vaporization energy E_V are in the range from $0.5 \cdot 10^2 J$ to $1.6 kJ$. Low values mostly occur at low melt temperatures and high values at high melt temperatures due to the higher interactive masses at most runs with high melt temperature and to the way of estimation according to equation 5.8.

But a comparison of kinetic energy of the blown-out material and the expansion work of vapor shows agreement in magnitude of both energies within the limits of measurement inaccuracy. That confirms that the blowout is mostly accelerated by expanding steam. The values for the steam expansion energy based on the kinetic energy of the blowout can be the basic for the calculation of the thermal energy needed for the change of water from liquid to gas. Generally the enthalpie of evaporation is calculated by

$$\Delta H = \Delta U + V\Delta p + p\Delta V, \tag{9.1}$$

where ΔU is the change of thermal energy by the change from liquid to gas phase, $V\Delta p$ the additional energy for pressurizing and $p\Delta V$ the energy for volume expansion. It is to assume that the vapor is at about $100\ ^\circ C$ under atmospheric condition at the end, wherever the way of pressurizing, vaporizing and volume expansion and the several values for the evaporation enthalpie (WAGNER, 2011; WAGNER and KRETZSCHMAR, 2008) are unknown. For the specific enthalpie of vaporization H the standard value of $2256 \frac{kJ}{kg}$ is used.

This delivers more exact values of the vaporization energy than the estimation only based on the interactive mass. The vaporizing water volume quite surely depends on the interactive melt mass, because the more interactive mass the more interactive water can get energy from the interactive mass. It might also depend on the melt temperature or the transferred energy, because the more thermal energy can be provided by the melt, the more water it can accept. There is a strong correlation between the interactive melt mass and the kinetic energy of blowout respectively the work for volume expansion. There is also a strong correlation for the fragmentation grade. This means that the vaporizing water volume depends on the interactive melt mass, because more mass can heat more water. But it is shown that there is no strong correlation between interactive melt mass and fragmentation grade in this runs, so it is rare that both factors increase the vaporizing water volume together. However it depends also on the fragmentation grade, because finer particles can transfer more heat from the same mass. The vaporized water volumes m_v are in the range from less than 0.01 to $0.63 g$. These values confirm the experience that 10 % of the injected water vaporize at maximum. In many cases the vaporizing volume is much lower yet. The values for the change of thermal energy ΔU are from $4 J$ to $1.3 kJ$.

9.1.5 Fragmentation energy $E_{\mathrm{frag,h}}$ for hydrodynamic fragmentation

During blowout more fine particles are generated by hydrodynamic fragmentation. The part of hydrodynamic particles is analogue detected to the part of interactive particles. The created surface and the fragmentation energy $E_{\mathrm{frag,h}}$ can be calculated with the specific surface and the specific surface tension. The specific surface tension depends on temperature, the variation in the interesting temperature range is about 20 % (BIRCUMSHAW, 1926; BLOMEYER, 1962; DRATH, 1927). The specific surface tension for tin is low compared to many other materials. As for brittle fragmentation also for hydrodynamic fragmentation little energy is necessary and many small particles can develop. In the smallest particle fraction there are many particles with a diameter of about $30\,\mu m$, which must be hydrodynamic particles due to their smooth surface and spherical form. They are smaller than the smallest interactive particles. The newly created surface by hydrodynamic fragmentation is in the range from 0.4 to $14\,m^2$. Principally the newly created surface increases with the force of explosions. A correlation to melt temperature is not visible. The values for $E_{\mathrm{frag,h}}$ are between 0.3 and $3.0\,J$.

The acoustic energy E_{son} is the most important part of the several energies. According to EX et al., 2000, this part cannot be more than 5 % by air surrounding and can be neglected in our cases. But in more complex surroundings of volcanoes, e.g. under water, the part of acoustic energy is higher caused by the incompressibility of water and the low acoustic impedance of melt and water is not negligible.

9.1.6 Residual energy E_{res}

The residual energy E_{res}, which is not converted or converted in unknown energies, is in the range from 0.01 to $1.9\,kJ$. It is interesting that E_{res} is low for low temperatures and high for high temperatures. The normalized residual energy per effective interactive mass is in the range from less than $1\,\frac{J}{g}$ to $1.1 \cdot 10^2\,\frac{J}{g}$. For the relation to temperature the same trend as for E_{res} is discovered. The efficiency η of the explosions ranges from 38 % to 98 %. Premixture seems also ti have influence on efficiency at all temperatures. The residual energy for high melt temperatures is higher than for low temperatures. Otherwise the efficiency is lower for high melt temperatures. The reason is that in the assumption for the end temperature of the interactive mass of 350 $^\circ C$ for all melt temperatures the calculated transferred thermal energy E_{i} is higher for high melt temperatures and this results in a higher residual energy E_{res}.

9.1.7 Conclusion for maximum estimation

To draw a conclusion of the maximum estimation of transferred energy first all results are in accordance with the conservation of energy. In average the residual energy increases with melt temperature. It might be that the end temperature of melt is higher for higher initial melt temperatures. The assumption that the interactive melt cools down to the same end temperature for all initial temperature should be corrected.

9.2 Results of the minimum estimation

For the transferred energy (see Figure 9.2) the lowest values are between 5 and 20 J at the lowest melt temperatures of 400 and 500 $^\circ C$. The values increase with melt temperature and the maximum value is about 1.4 kJ at 1000 $^\circ C$. The normalized values for the effective interactive mass are in the range from 1 to $8 \cdot 10 \frac{J}{g}$. These values increase with melt temperature. To be able to make these energy amounts available, the interactive melt must cool about 3 to 10 K at low temperatures from 400 $^\circ C$ and nearly 300 K at high temperatures of 900 $^\circ C$ or 1000 $^\circ C$. The lowest final temperature of the melt lies at 350 $^\circ C$, on this occasion the initial temperatures were 400 $^\circ C$ and 500 $^\circ C$. However, it appears that the cooling depends not only on the beginning temperature, but also on the premixture and the involved mass in each case. At low temperatures with relatively big interactive mass the cooling is strengthened, too. Also the cooling is lower with high temperatures and small mass. It appears that the cooling depends on the temperature as well as on the interactive mass.

The interactive mass is influenced by the premixture. But it also increases with the melt temperature. Nevertheless for the correlation between temperature and interactive mass because of the big dispersions with the given experiments no more exact proportionality is recognizable, a linear connection is recognizable to some extent (see Figure 9.3). This temperature dependence can be explained by a higher offer of the hot melt, decreasing viscosity of the tin melt at rising temperature, and the higher pressure in the interactive water at higher temperature, by which more melt can be fragmented. The increase for the scaled mass is stronger, because there is the additional effect of more blown out and not remelted particles.

$$m_{\mathrm{eff,i}} \propto T. \tag{9.2}$$

The relationship between melt temperature T and temperature difference $\Delta T_{\mathrm{out,eff}}$ the melt is cooling more obviously as shown in Figure 9.4. For polynomial fits the proportionality is linear to square:

$$\Delta T_{\mathrm{out,eff}} \propto T \text{ or} \tag{9.3}$$

$$\Delta T_{\mathrm{out,eff}} \propto T^2. \tag{9.4}$$

For the transferred energy generally counts:

$$\Delta E_{\mathrm{i}} = c m_{\mathrm{eff,i}} \Delta T. \tag{9.5}$$

For ΔE_{out} it is:

$$\Delta E_{\text{out}} = cm_{\text{eff,i}} \Delta T_{\text{out,eff}} \quad . \tag{9.6}$$

For the transferred energy the following relationship between melt temperature T and temperature difference $\Delta T_{\text{out,eff}}$ results:

$$\Delta E_{\text{out}} \propto \Delta T_{\text{out,eff}}^2 \quad \text{up to} \tag{9.7}$$

$$\Delta E_{\text{out}} \propto \Delta T_{\text{out,eff}}^3 \quad . \tag{9.8}$$

Fit functions for these relations both have nearly the same correlation, the indices R^2 are 0.52 for the correlation to T^2 und 0.54 for T^3. The results are in accordance with the dependence of fragmentation (see fragmentation grade) on melt temperature and the premix.

An exponential fit for all explosions shows no clear result. But if only single triggered explosion are included in the fit, the exponential growth function has a R^2 of 0.73. For a parabolic or cubic fit for the simple triggered explosions the R^2 is about 0.73 and 0.72, too. It has to be discussed and investigated in more detail, what kind of relation exists between melt temperature and transferred energy.

At low temperatures of 400 and 500 $^\circ C$ some explosions are stronger against the just described trend. This can be explained by the instable vapor film at low temperatures and by the occurence of many self-triggers. After that the regular mechanical trigger followed and the whole energy transfer was higher.

There are some variations from this general trend that should be especially mentioned. At strong multiple triggered explosions at low temperatures the outcoming energy, the interactive mass, and the temperature difference of interactive melt are higher than in normal explosions at the same temperature. At high temperatures there are weak explosions with little energy transfer, low interactive mass and comparably low cooling of the interactive mass. Premix is a reason for these low values. For strong explosions a good premix must generally exist to get enough initial direct contact surface so that good energy transfer can start and trigger the positive feedback mechanism. From the results of interactive mass and the vaporizing water volume in the several runs a good initial energy transfer seems to be necessary so that a high interactive mass and a high interactive water volume are involved for a strong explosion. The conditions therefore are better the higher the initial direct contact surface and the temperature difference are. The explosions will be medium strong if one of the two conditions is weak. If both conditions are weak only a weak explosion will occur.

There is a trend that for strong explosions the calculated end temperature T_{end} of the interactive mass is lower than for strong explosions. This shows that for strong explosion with a high energy transfer a higher cooling of interactive particles can be possible. Also the end temperatures of strong explosions are in the area of the contact temperatures T_C (see equation 11.5). The end temperature are higher for higher melt temperatures, which confirms the result in section . This shows a principal good accordance of both estimations and it confirms the energy considerations. The differences in the interactive weighed and effective mass can be explained by the unavoidable loss during collection. All in all the two estimations are more close for strong explosions. It seems to be that for weak explosions there are some in the saving of the results, which enlarge the measurement errors respectively the ratio of the values and their errors. It should be noted that the described relations are only valid for tin melt in the investigated temperature range. It is possible that in another temperature range or with other melt material other effects become more important, which lead to other results.

Nevertheless there are many hints that supercritical water finishes the phase of direct contact between melt and liquid water and limits the energy transfer. For high temperatures a higher thermal power is possible. There are some hints that the direct contact may be shorter at high temperatures, because water becomes supercritical earlier. A clearer indication is the end temperature of interactive melt at higher melt temperatures. If supercritical water would not stop energy transfer, the cooling would be higher. It should be theoretically considered that at higher temperatures there will be a maximum for energy transfer.

The minimum estimation was also made without the change of thermal energy ΔU for the vaporizing water. A comparison to the maximum transferred energy based on the weighed interactive mass shows that in some cases the calculated energy is a little bit higher than the energy from the minimum estimation without vapor. But in some cases for weak explosions, it is still lower and this is a hint that the weighed mass is lower than the real interactive mass especially at weak explosions. For strong explosions, the thermal energy based on the weighed mass, is only sufficient if the steam generation is (nearly totally) excluded. But for MFCI-experiments with injected water it cannot be neglected. The energy would not be enough even for a very low estimated volume of vaporizing water. All in all the calculation of the effective interactive mass for the energy consideration is justified.

To draw a conclusion, it is confirmed that melt temperature has influence on the energy transfer of an MFCI-explosion. The cooling of interactive melt depends on the initial melt temperature respectively the initial temperature difference between melt and water. Furthermore energy transfer is influenced by other factors, such as premix and the resulting vapor film. Premix and vapor film are partially dependent on temperature, too.

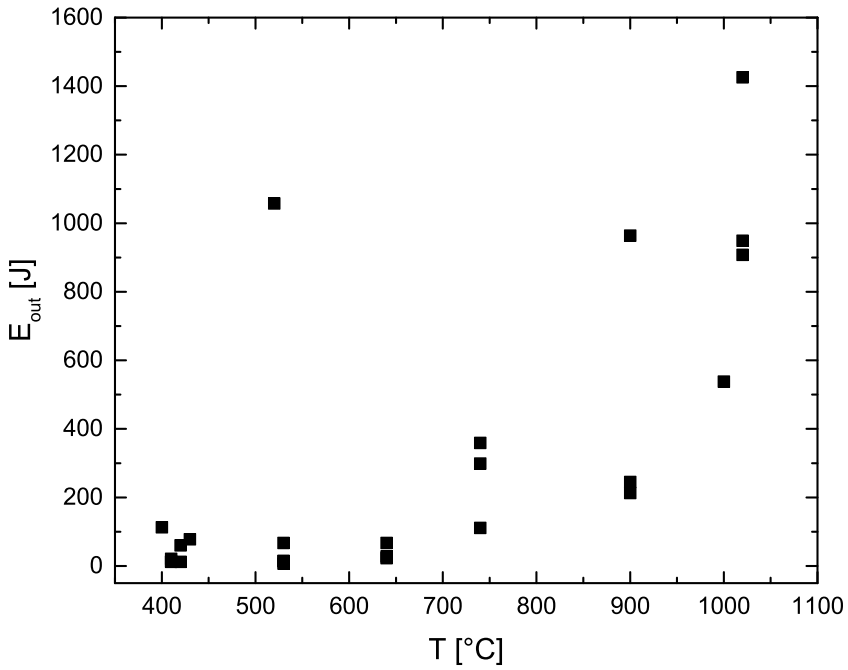

Figure 9.2: Output energy versus melt temperature. The trend shows a correlation between melt temperature and output energy.

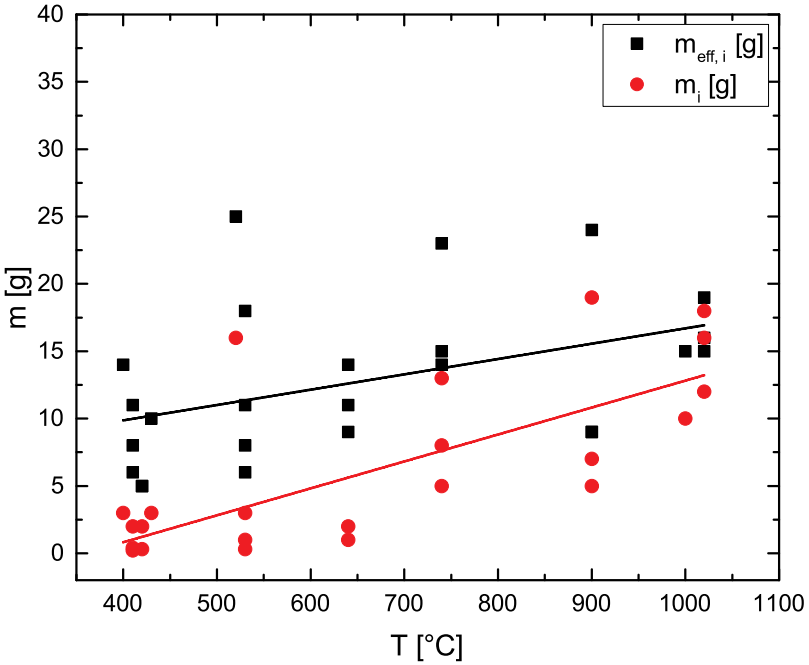

Figure 9.3: Effective and measured interactive melt masses versus melt temperature. In both cases there is an increase of interactive melt mass with higher melt temperatures detectable. The two lines show a linear fit for the weighed and effective interactive mass.

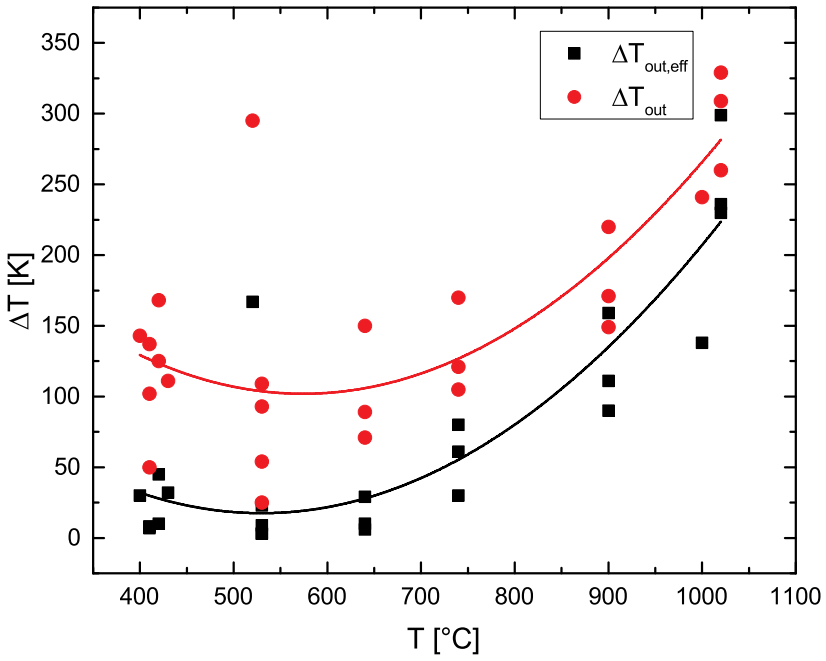

Figure 9.4: Temperature difference ΔT versus melt temperature T. The temperature difference $\Delta T_{\text{out,eff}}$ is calculated with the effective interactive mass and for each run also ΔT_{out} with the measured interactive mass. The increase of ΔT with melt temperature T is visible. The increase might be stronger than a linear increase. The two lines show a polynomial fit to T^2 for the values based on the weighed and the effective interactive mass.

Chapter 10

Draught for energy transfer

10.1 Process of energy transfer

From all results of the investigations of this work the following draught can be concluded:

1. At initial direct contact of melt and liquid water energy is transferred from hot melt into colder water. This energy transfer can be maximized by high melt temperature and a big simultaneously created initial contact surface.
2. The pressure of interactive water increase with input of thermal energy. The pressurized water expands and breaks up the melt surface.
3. Liquid pressurized water flows into the melt crack. The direct contact surface is enlarged. As a consequence (positive feedback) the thermal energy transfer from melt to water increases (BÜTTNER and ZIMANOWSKI, 1998; BÜTTNER, ZIMANOWSKI, MOHRHOLZ, et al., 2005; FREUNDT et al., 1998; FRÖHLICH et al., 1992; ZIMANOWSKI, BÜTTNER, LORENZ, and HÄFELE, 1997).
4. Thermal tensions occur in the cooled melt. This leads to a breakout of particles in the melt cracks (BÜTTNER and ZIMANOWSKI, 1998). During brittle fragmentation energy dissipates into new surface of the cracks and particles and for emitted shock waves (cf. DÜRIG, SONDER, et al., 2012; DÜRIG and ZIMANOWSKI, 2012). It depends on the initial conditions, how much energy can be transferred at all, and how much melt is how finely fragmented.
5. The amount of involved interactive water depends on heat flux. After a while the interactive water becomes supercritical.
6. The high pressure opens the cover of the system and expanding steam also blows melt material.

Especially the variation of melt temperature has the following influences:

- At high melt temperature more interactive water can be heated. The water pressure can become higher.
- The thermal gradient and the thermal tension in the interactive melt are higher.

- The positive feedback is higher. The interactive melt can be fragmented more finely or a higher mass of interactive melt can be fragmented.
- More interactive water vaporizes and the kinetic energy is higher.

10.2 Comprehension of influences on explosions

At this place the multiple influences on explosions should be concluded. Although it was the main intention of this study to investigate the influence of melt temperature on explosions, it was shown that melt temperature and influences depending on melt temperature are not the only influence that significantly affect such explosions.

As known from previous works (SPITZNAGEL et al., 2013; ZIMANOWSKI, BÜTTNER, and LORENZ, 1997) premix has an important influence. Interesting additional facts for stability and collapse of the isolating vapor film before triggering have been found. First there is a temperature limit of about 640 $^{\circ}C$, below which the vapor collapsed by instabilities before the mechanical trigger in our experimental configuration with our chosen parameters. Secondly in experiment with thinner vapor film the time between bullet impact and opening of the system is longer in average. These explosions are rather weak, because only a small initial contact surface of melt and liquid water is established **simultaneously**. A stronger mechanical collapse is necessary for stronger vapor films, but in these cases a bigger initial surface is mostly built up for a stronger explosion with higher energy transfer. The pressure increase in the interactive water is faster and water becomes earlier supercritical. A significant negative correlation of pulse of the explosion and optical time between bullet impact and the onset of blowout was detected. According to FRÖHLICH, 1978, a vapor film generally can be rebuilt in a shorter time during an MFCI-process if it was more stable before its collapse.

After the initial direct contact surface is built, melt must be fragmented for the positive feedback mechanism. Therefore a minimum initial surface of 1 $\frac{m^2}{m^3}$ of interactive melt (FREUNDT et al., 1998) is needed. Particle analyses show that if this value is only reached at its minimum, overall fragmentation is less fine. In these cases pressure increase in the interactive water and/or thermal tension in the interactive melt is not yet high enough to cause efficient fragmentation. For tin melt the thermal energy itself would be sufficient, but the energy transfer is lacking.

The enthalphie for vaporization of water is hard to estimate. On the one hand, the vaporizing water volume cannot be exactly detected, on the other hand it is still unknown, at which temperature and pressure the vaporization takes place and whether this is dependent on temperature or premix. From all experiments it can be concluded that the estimation of vaporizing volume from previous works (BÜTTNER, ZIMANOWSKI, MOHRHOLZ, et al., 2005; FRÖHLICH et al., 1992) with 10 % of the injected water volume is the ultimate maximum. It is shown that the volume of interactive water depends on the

fragmentation process. For a high interactive mass or a high fragmentation grade the energy transfer from the interactive melt is enlarged. As a consequence, a higher volume of interactive water can be heated, respectively more water can vaporize.

The result of the minimum estimation for transferred energy shows that for a efficient fragmentation there must be enough energy that is possible to be transferred. Only under this condition enough fine fragments can be produced. Therefore a big initial surface must exist so that a good positive feedback can be initiated. More fine fragments can be generated under a high cooling rate. For the cooling of interactive melt it can be said that it is lower for strong explosions at low initial temperature and also for weak explosions at high temperature. For weak explosions at low temperature cooling is the lowest and it is the highest for strong explosions at high temperature.

Although the premix has influence on explosions, there are proved influences of the melt temperature. The obvious aspect is surely that the interactive mass can deliver more thermal energy at higher temperatures. But this is not the only influence. The premix can be influenced by different material properties at different temperatures. However there is not only this indirect influence, but also a direct influence on the vapor film and the resulting initial direct contact surface. First there is the lower limit for a stable vapor film. If the film collapses before the mechanical trigger, the initial surface is low and mostly weak explosions occur. But also for triggered explosions stable vapor films are necessary to create a big initial surface simultaneously. The conditions therefore are better at higher melt temperatures. At last the higher thermal energy transfer causes higher pressure in the interactive water and higher stress in the interactive melt due to a possible higher cooling. This enforces the positive feedback mechanism and more fragmentation of melt. As a consequence, more interactive water is involved and a stronger blowout of material can occur. All in all the quantitative relation of melt temperature respectively the temperature difference between melt and water temperature and energy transfer is higher than linear. For the reproduction of explosions it is to mention that an explosion cannot be predicted by the tunable parameters in the laboratory. There are a lot of chance effects, which cannot be controlled and result in different premixes.

For energy analyses in future it has shown that estimation with cooling interactive mass delivers upper limits for transferred heat. The sum of detectable outcoming energies is the lower limit. It is to notice for the maximum estimation that the values for the end temperature of interactive melt and of interactive water have to be estimated. It is not yet possible to measure these values. All in all more experimental series, also with different melt materials and in a greater temperature range have to be done to get more precise information about the transferred energy and to bring the two estimations more closely together.

Chapter 11

Investigations with magmatic melt

For a better comparison to natural volcanism and to get a better quantitative analysis of fragmentation energy, experiments with magmatic melt are necessary. The used melt material was from Grimsvötn and Hohenstoffeln. Because of the high dependence on relevant material values, such as heat capacity and thermal conductivity, it was not necessary to perform measurement for the influence of melt temperature. Therefore heat transfer is lower due to the lower thermal conductivity and higher heat capacity than for tin melt. It is also usable to check the model for heat transfer (BÜTTNER, ZIMANOWSKI, MOHRHOLZ, et al., 2005).

11.1 Melt production

The melt is made out of stone granulate from above mentioned materials, which is melted in a crucible in the laboratory. Magmatic melt in nature is inhomogeneous. Often there are solid parts and gas bubbles in it next to molten liquid material. These inhomogeneties bring additional disturbing variations in several runs. To get a comparable melt in several runs, it is important to get an as far as possible homogeneous melt for experiments in the laboratory (ZIMANOWSKI, BÜTTNER, and LORENZ, 1997). The melting procedure is not achieved to get a preferably natural melt but an idealized melt, which consists only of liquid material, however the properties of this should be similar to nature. In a long procedure gas bubbles are stirred out and solid parts are molten. Before a run is started, it is checked whether the melt satisfies these conditions.

For this series about $300\,g$ idealized melt were used and the crucible was filled to its maximum. The temperature for the runs was about $1320\,^{\circ}C$, and it was paid attention for a mostly equal temperature in the whole crucible.

11.2 Experimental runs

As for tin melt entrapment experiments were performed. The parameters were $500\,ms$ water injection time without valve delay and trigger delays of $300\,ms$. The bullet impact on the melt surface took place

about 330 ms after the onset of water injection, but at a time when it was still running. The voltage of the injection pump and the resulting injection velocities were variated to get different premixes.

11.3 Data acquisition

11.3.1 Experimental data aquisition

The data acquisition occurred with the same procedure as for tin melt, required material parameter are taken from BÜTTNER, ZIMANOWSKI, BLUMM, et al., 1998; ZIMANOWSKI, BÜTTNER, LORENZ, and HÄFELE, 1997. The analyzed materials have a similar composition and similar properties to Grimsvötn and Hohenstoffeln melt. For energy consideration, the influence of different premixes in several runs could be mostly eliminated. For the calculation of the transferred thermal energy the model of cooling fragments according to section 11.3.2 (BÜTTNER, ZIMANOWSKI, MOHRHOLZ, et al., 2005; MOHRHOLZ, 2002) was exercised, because of the slower cooling of magmatic melt the particles could not cool down to a favorised end temperature in the short time spans of direct contact. For the average values of the particle diameters in the three finest fractions 50 μm for the fraction with particle diameters of less than 63 μm , 100 μm for the fraction with particles of diameters between 63 and 125 μm and 175 μm for the fraction with particle diameters between 125 and 250 μm are assumed. The estimation of time for cooling was made by the high-speed videos. It was not necessary to install the mirror, because the crucible was always filled at its maximum so that the melt surface was visible in the direct view. For the calculation from the visible optical time to the time of direct contact, in a first step 100 μs were subtrahated from the optical times for all runs. This results in a maximum value for the cooling time of interactive particles and the transferred thermal energy from these particles. It is to assume that particles, which are first broken out at the end of the direct contact phase, cannot transfer energy during the full time. But it might be that their interactive mass already transfers energy before the final particle is broken out. The calculated end temperatures are average values from the results for cubes with constant surface temperature and spheres with constant surface temperature. The values for spheres at constant heat flux are only minimally different, only in decimal places, from the values of sphere at constant surface temperature. The transferred energy of a fraction of particles is calculated by the interactive mass in this fraction and the average temperature difference for the particles of the associated size. The calculated transferred thermal energy is the sum of the transferred energy of all particles.

For the specific heat capacity and thermal conductivity of basaltic melts the dependency on temperature is generally to include (BÜTTNER, ZIMANOWSKI, BLUMM, et al., 1998; EBERT et al., 2003; MOHRHOLZ, 2002). But it is to be assumed that a change in properties can be neglected in the short time of direct contact. Thus for the material parameters average values over the temperature range they can cool down is calculated and used. For the specific heat capacity the value is 1.1 $\frac{kJ}{kg \cdot K}$ and for the thermal conductivity it is 1.35 $\frac{W}{m \cdot K}$ and for the thermal diffusivity it follows 0.46 $\frac{mm^2}{s}$.

11.3.2 Model of cooling fragments

The model of cooling fragments (according to BAEHR et al., 2010; BÜTTNER, ZIMANOWSKI, MOHRHOLZ, et al., 2005; MOHRHOLZ, 2002) is based on the following assumptions:

- There is no interaction between several particles.
- Each particle begins to cool down from the initial melt temperature after it is broken out of the melt.
- The surface temperature of the particle is the temperature of the surrounding water. A warming of the water is not included, the water temperature stays constant during the cooling of the particle.

The general approach of the model is the heat conduction equation. It is solved for a cube at constant surface temperature and a sphere at constant surface temperature and constant heat flux. After the solution of the temperature in the particle at place and time the mean temperature dependent on time is calculated. This again can be used for the calculation of the transferred heat of a particle.

The equations for the temperature of the cooling particles are (the detailed way of solution is shown in BÜTTNER, ZIMANOWSKI, MOHRHOLZ, et al., 2005; MOHRHOLZ, 2002) for a cube of thickness $2d$ with initial temperature T_0 and surface temperature T_M:

$$T_\mathrm{mean}(t) = \left[\frac{8}{\pi^2}\sum_{n=1}^{5000}\frac{1}{(2n-1)^2}\exp\left(-\frac{(2n-1)^2\pi^2}{4}\frac{at}{d^2}\right)\right]^3 (T_0 - T_M) + T_\mathrm{M} \tag{11.1}$$

For a sphere of diameter $d = 2r$:

$$T_\mathrm{mean}(t) = \left[\frac{6}{\pi^2}\sum_{n=1}^{5000}\frac{1}{n^2}\exp\left(-n^2\pi^2\frac{at}{r^2}\right)\right](T_0 - T_\mathrm{M}) + T_\mathrm{M} \tag{11.2}$$

For a sphere at constant heat flux in a sourounding with temeprature T_U:

$$T_\mathrm{mean}(t) = 3\left[\sum_{n=1}^{5000}\frac{2}{n\pi}\frac{\sin(n\pi) - n\pi\cos(n\pi)}{n\pi - \sin(n\pi)\cos(n\pi)}\left(\frac{\sin(n\pi)}{n^2\pi^2} - \frac{\cos(n\pi)}{n\pi}\right)\exp\left(-n^2\pi^2\frac{at}{r^2}\right)\right](T_0 - T_\mathrm{U}) + T_\mathrm{U} \tag{11.3}$$

11.4 Results

11.4.1 Transferred thermal energy ΔE_i

A comparison of weak and strong explosions shows interesting results for the transferred energy (see tables D.6, D.7, and D.8). First the optical time from the video recordings is clearly longer for weak explosions (about $1.0\,ms$) than for strong explosions of about 400 to $600\,\mu s$ (see Figures 11.1 and 11.2). The estimation cannot be correct that the time for energy transfer in weak explosions would be about $900\,\mu s$ and that more energy would be transferred over the longer time, as the energy transfer would be

maximum possible for strong explosions in the shorter times of 400 to 600 μs. It can be concluded that vapor film collapse takes more time for weak explosions than for strong ones or a much greater initial surface can be created for strong explosions, which is already suggested in BÜTTNER and ZIMANOWSKI, 1998. For estimations of multiple triggers there is the problem that the interactive mass, which is not involved in the first trigger, participates a shorter time at energy transfer. How much mass is in the first and the later triggers and how long the direct contact phases for the several triggers are, cannot be measured. But even by excluding multiple triggers from the analyses it is to note that at weak explosions with a long estimated time for energy transfer more energy would be transferred than at explosions with shorter transfer times, which are to be declared as stronger by other measurement data. An important aspect for the high heat transfer during short times is that for this strong explosion the interactive mass is extremely high. For the experiments of magmatic melt it can be ruled out that different melt viscosities at different temperatures caused different premixes for the initial contact surface. Additionally it is shown again that a big initial contact surface follows on a fast vapor film collapse. With this new knowledge, the times for direct contact are corrected downward. For weak explosions where the first estimation would be too long, the times of direct contact are so much shortened that transferred heat is smaller than at strong explosions. Additionally it was taken to ensure that the new calculated values for transferred energy are in accordance with values of the outcoming energy by comparing several runs. The results for the transferred thermal energy are in the range from 0.25 to 1.29 kJ (see table D.6).

11.4.2 Transferred thermal power

A further aspect is the thermal power. For the thermal power only average values over the time of heat transfer are calculated:

$$P_{\mathrm{th}} = \frac{\Delta E_{\mathrm{i}}}{t_{\mathrm{frag}}} \,. \tag{11.4}$$

A detailed illustration of thermal power during the phase of heat transfer is too difficult, because it would be necessary to know the involved interactive mass and the temperature of all particles for a certain point in time. The maximum power in average for one run is 4.3 MW. This is a strong explosion with a high energy transfer of 1.3 kJ within a time of 300 μs. For the calculation of the lower limit the estimation of the time for heat transfer is difficult just for weak explosions. Too high variations in time cause too high variations for the calculated thermal power. If the time was too long, the minimum power would be at $4.1 \cdot 10^5\, W$. Under the assumption that the time of variation is shorter, the minimum thermal power is up to $6.2 \cdot 10^5\, W$. It is to remember that in the model for the cooling fragments (BÜTTNER, ZIMANOWSKI, MOHRHOLZ, et al., 2005) the cooling rates become lower the longer the cooling time is. In the last period of a long heat transfer the transfer and the power are lower than at its beginning. On the other hand in the calculations following this model, the thermal power for explosions with short times of direct contact is automatically higher. The experience for the time measurements with the mirror and experiences from former experiments show that time of direct contact is not longer than 0.5 ms (see also chapter 4 and

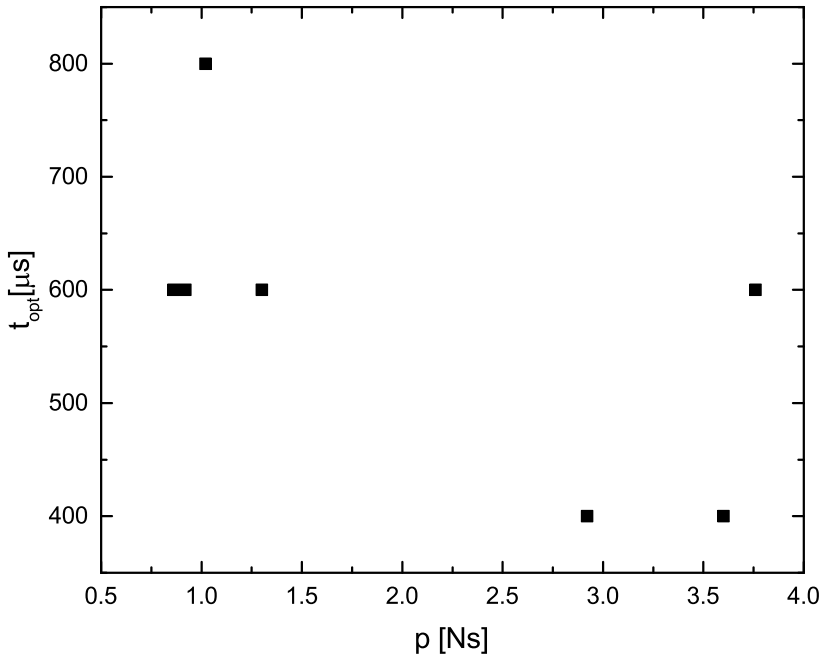

Figure 11.1: Correlation between optical time t_{opt} as a measure for the duration of energy transfer and pulse for Hohenstoffeln melt. Weak explosions have long optical times and strong explosions have shorter times. Two additional values are shown, which are not listed in the data acquisition.

SPITZNAGEL et al., 2013). The times up to $0.9\,ms$ do not accord to this. As already mentioned there is a negative correlation of optical time t_{opt} and pulse. This enforces the result that the thermal power is much higher for strong explosions performed by a big initial surface. It is also interesting to compare the transferred thermal energy to the thermal power. It is to note that the thermal power P_{th} increases with transferred thermal energy E_i, as shown in Figure 11.3. The correlation coefficient is 0.95 with a p-value of $5 \cdot 10^{-6}$.

11.4.3 Particle analysis and fragmentation energy

It is generally to remark that for basaltic melts the differences between the weighed and effective masses of particles is lower than for tin particles, because basaltic material cannot remelt so easily as tin particles. As described in the work with metallic melts, an important part of the transferred energy is used for fragmentation of particles. Despite of tin melt in the case of basaltic melt it is possible to determine the surface energy E_{surf} separately from the fragmentation energy $E_{frag,i}$ for brittle fragmenation. For the generation of new surface the specific surface of brittle fragmented particles, in the case of magmatic melt which we can call “phreatomagmatic fragmentation“, has to be regarded more detailed. You can see from the values of specific surface and from the pictures of such particles that the surface is not the theoretically lowest for each particle size. Altogether these particles have no optimum form as a cube

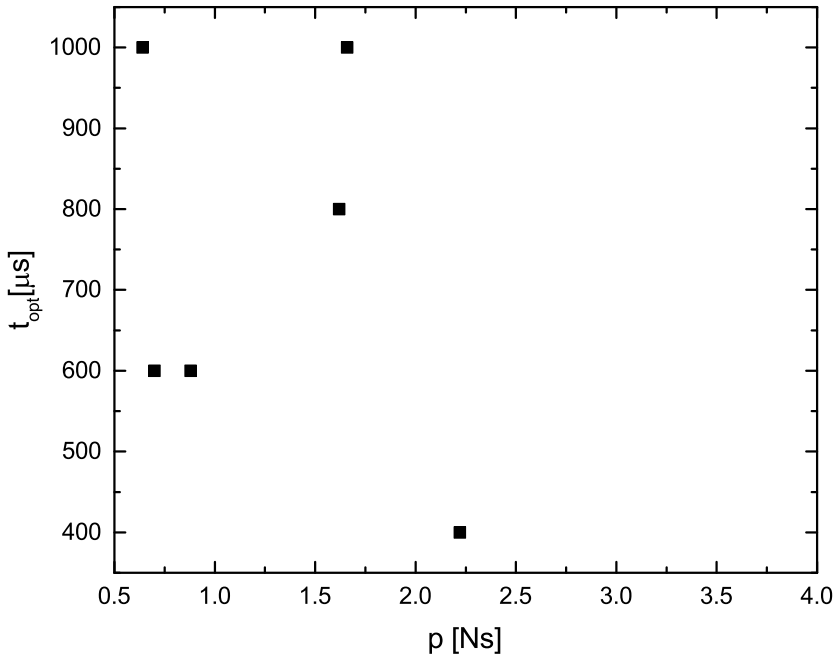

Figure 11.2: Correlation between optical time t_{opt} as a measure for the duration of energy transfer and pulse for Grimsvötn melt. Weak explosions have long optical times and strong explosions have shorter times.

or ball, and in fine consideration they have even many points (see Figure 11.4). First as much energy for fragmentation as necessary is taken, the fragmentation process is faster than the heat transfer and an energy conversion into other energies. Only afterwards the rest of thermal energy is converted into other forms of energy. The break process is defeated not by the minimisation of the fragmentation energy, but particle crack and form is influenced dominantly by areas of weakness and heterogeneities in the material that does not lead to optimum forms (see e.g. RÄTZKE et al., 1999; SÄHN et al., 1987). A comparison of ideal Figures with real ones shows: With bigger particles the specific surface is around factor 20, with small particles up to factor 50 and higher. Calculations for the ratio of transferred thermal energy, following BÜTTNER, ZIMANOWSKI, MOHRHOLZ, et al., 2005, to surface energy shows that there would be a minimum for ideal particles with diameters from 1 to 2 mm. The optimized particles would be much greater than the real ones. In this view it is to input, whether a higher surface improves heat transfer. The results of transferred thermal energy in 11.4.1 show that the values are not much higher than for ideal cubes and spheres. The particles have a form close to cubes and spheres in the "macroscopic" view and the rough surface structure cannot enlarge the heat transfer from the inner particle to the environment. Therefore the whole particles should be elongated and thinner. For a better understanding of the fracture, complex simulations e.g. according to ATTARD et al., 2005, should be made. In the runs with magmatic melt the created surface area is in the range from 0.08 to 0.44 m^2. The according energy needed for it is

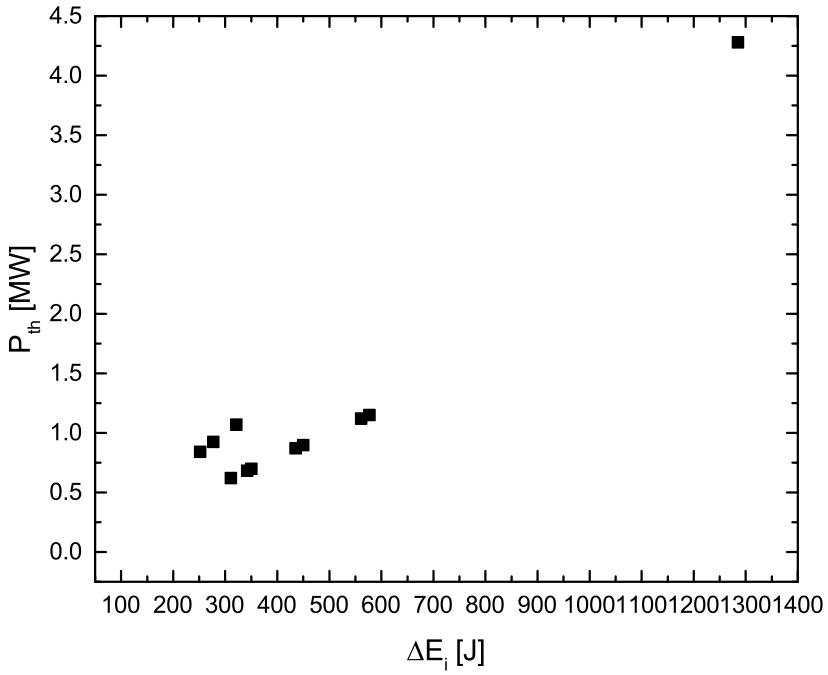

Figure 11.3: Thermal energy versus thermal power.

between $2 \cdot 10^1 J$ and $1.1 \cdot 10^2 J$. The percentage from the totally transferred energy is from 7 % to 8 %. The energy for shock waves E_{shock} is calculated by the values presented in the example in BÜTTNER and ZIMANOWSKI, 1998. In our experiments the results for E_{shock} are $0.2 \cdot 10^2 J$ to $1.4 \cdot 10^2 J$. It is 9 % to 11 % of the totally transferred energy. As the energy for generation of new surface E_{surf} is the sum of fragmentation energy $E_{\text{frag,i}}$ and shock wave energy E_{shock}, the values of E_{surf} are in the range of $0.3 \cdot 10^2 J$ to $2.6 \cdot 10^2 J$ and a percentage from 16 % to 19 % of the totally transferred energy ΔE_{i}. All in all $E_{\text{frag,i}}$ and ΔE_{i} are in correlation, there is a trend that the more thermal energy ΔE_{i} is available the more energy is used for $E_{\text{frag,i}}$.

During the expansion stage melt is hydrodynamically fragmented. The newly created surface therefrom is from 0.08 to $1.1 m^2$ and the energies are from $0.4 \cdot 10^2 J$ to $2.5 \cdot 10^2 J$. The parts of the totally transferred energy ΔE_{i} are in the range from 13 to 26 %. This energy does not correlate to the pulse p or the totally transferred energy ΔE_{i}. A rough relation to the energy for brittle energy exists for some runs, but not for all.

11.4.4 Kinetic energy

The kinetic energy E_{kin} is only a small part of the totally transferred energy ΔE_{i} in the range from 1 to $12 J$. These are only at maximum one count percent of ΔE_{i}. The velocity of the finest particles was high,

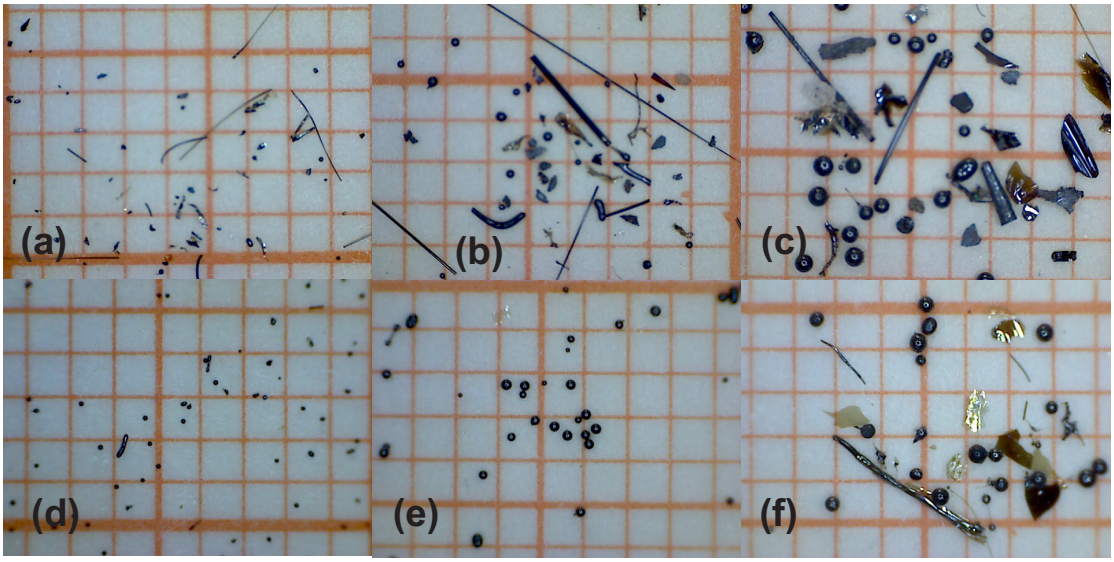

Figure 11.4: Particles produced during MFCI-experiments with melt from Grimsvötn. (a) Run TGR 10, fraction smaller than 63 μm, (b) Run TGR 10, fraction from 63 μm to 125 μm, (c) Run TGR 10, fraction from 125 μm to 250 μm, (d) Run TGR 11, fraction smaller than 63 μm, (e) Run TGR 11, fraction from 63 μm to 125 μm, (f) Run TGR 11, fraction from 125 μm to 250 μm. The paper in the background is mm-scaled.

it was in the range of 20 to 100 $\frac{m}{s}$. But the mass of the finest fragments is low compared to tin experiments. More rough particles have lower velocities and also the blowout of liquid melt is slow. This causes a low total kinetic energy.

11.4.5 Evaporation energy for steam

After all relevant energies are discovered, the energy for evaporation of water can now be estimated. It is assumed that 10 % of the totally transferred energy ΔE_{i} are used for neglected energies, such as acoustic energy. For each run with magmatic melt it is possible that 0.08 g water per gram interactive melt can vaporize at least. For explosions with high thermal energy transfer it would moreover be possible that still more water can evaporate. But more detailed calculations are difficult, for instance which effects have influence on the evaporation of water and under which temperature and pressure evaporation takes place. Above all, the process of evaporation and steam expansion can be different in the laboratory experiments with only a little cover of the system and natural scenarios. For the analyzed runs E_{V} is in the range of $0.7 \cdot 10^2\,J$ to $4.1 \cdot 10^2\,J$.

11.4.6 Residual energy

The values for the residual energy for the runs with magmatic melt are in the range from $0.7 \cdot 10^2\,J$ to $3.8 \cdot 10^2\,J$, the values for the residual energy per effective interactive mass in the range from $1.3 \cdot 10^2\,\frac{J}{g}$ to $3.9 \cdot 10^2\,\frac{J}{g}$. Although the highest value for the residual energy correlates to the run with the highest thermal energy transfer and the highest thermal power, there is no general trend detectable for correlations of the transferred thermal energy and the thermal power to the residual energy and the residual energy per

interactive mass.

11.4.7 Minimum estimation of thermal energy

For the minimum estimation the values for the totally transferred energy E_{out} are between $1.0 \cdot 10^2 J$ and $5.4 \cdot 10^2 J$. As expected, these values are lower than the values from the maximum estimation with regard on the model according to BÜTTNER, ZIMANOWSKI, MOHRHOLZ, et al., 2005, which is relevant for magmatic melts. The difference between the two estimations is smaller for strong explosions than for weak explosions. In one case, both values are almost identic. In this case the time for vapor film collapse might be shorter than $100 ms$ and the time for direct contact longer than the optical time t_{opt}. The cooling of fragments in average determined in this way is not in contradiction to the calculated end temperatures of the particles according to the model. The values from the minimum estimation for the end temperature in average are always higher than in the model calculations. Even for the highest cooling of almost 400 K the end temperature is still higher than the calculated end temperature of the biggest particle fraction, that cools down lowest. It is to recognize that the differences between minimum and maximum estimation is high for weak explosions. One reason is the longer contact time and the following higher energy transfer. But another important reason is the large calculated values for the effective mass (see equation 5.1). It might be that the calculations result in large values for weak explosions, because the determination of the particle velocity is difficult. For weak explosion the estimations are lower than the real values and this causes a large result for the interactive mass. It also shows again that the minimum estimation without vapor is higher than the thermal energy transfer based on the weighed interactive mass. But all in all the loss of particles during blowout is not so high as for tin experiments. This does still not accord to BÜTTNER and ZIMANOWSKI, 1998; ZIMANOWSKI, BÜTTNER, LORENZ, and HÄFELE, 1997, where it is suggested that almost all interactive particles are blown out. The reason for this contradiction might be found in the fact that large numbers of analyzed explosions in the present study were weak, while the former mentioned findings apply to strong explosions. It is also shown that the difference between effective mass and weighed mass is lower for strong explosions, and that the blowout was stronger there.

The thermal power based on the minimum estimation is naturally lower, it is in the range from $2.1 \cdot 10^5 W$ up to $1.8 \cdot 10^6 W$. Again the power is higher for strong explosions. There is also a strong correlation between output energy and the corresponding thermal power, the correlation coefficient is even 0.96 with a p-value of $3 \cdot 10^{-6}$.

All in all the runs with Hohenstoffeln melt are stronger in energy transfer and thermal power as the runs with Grimsvötn melt.

To adapt the model from section 11.3.2 (BÜTTNER, ZIMANOWSKI, MOHRHOLZ, et al., 2005) closer to the minimal estimation of heat transfer, one step could be to change surface temperature T_{M} of the

fragments from the critical temperature of water drifting to the contact temperature T_C between melt material and water at its critical temperature. The contact temperature T_C of two media 1 and 2 in contact is calculated by

$$T_C = \frac{b_1 \cdot T_1 + b_2 \cdot T_2}{b_1 + T_1} , \tag{11.5}$$

where $b = \sqrt{c \cdot \lambda \cdot \rho}$ with the specific heat capacity c, the heat conductivity λ and the density ρ is the heat intrusion coefficient for each medium (SCHWEIZER, 2015). This temperature is higher and this effects a higher end temperature limit for the particles and a lower cooling down. In this way it can also be respected that the interactive water is not yet at the critical temperature during the complete energy transfer phase, because the contact temperature is higher anyway. The contact temperature for the used melt at $1600\,K$ melt temperature and a water temperature of $650\,K$ at the critical point is about $1290\,K$ and much higher than $650\,K$. Even for a lower water temperature at $300\,K$ room temperature, the contact temperature is still about $1170\,K$. Further discussion is required as to whether these contact temperatures calculated for a stable environment can appear in the short time process. Furthermore, temperature dependencies of material parameters can influence contact temperatures. The heat transfer of small fragments would be much lower and the total thermal energy transfer is too low compared to the minimum estimation. For strong explosions, the surface temperature might be close to $650\,K$, because the difference between maximum and minimum estimation is small. Strong explosions also have shorter times of direct contact, so it would be more difficult for the melt particles to cool down and for the water to heat up. All in all there is a contradiction for the assumption that cooling is higher for strong explosions. But this enforces the supposition of more involved interactive water in strong explosions, which can receive more heat. This again can cause a lower contact temperature in average for strong explosions and a better heat transfer.

Chapter 12

Final discussion and outlook

In the framework of the executed investigations some important questions to describe thermohydraulic explosions, especially during the fine fragmentation phase and energy transfer at different melt temperatures, could be answered.

In this chapter an outlook on still lacking and new questions is announced, which came out during this work.

12.1 Separation of vapor film collapse and direct contact phase

One of the most important problems is the separation of the optical time into time for vapor film collapse and time of direct contact of melt and liquid water. This problem is not caused by errors of measurement but by opacity of melt and crucible. The time for energy transfer, the cooling rates of interactive melt, and the thermal expansion could be localized in more detail. A solution would be to use transparent melt, e.g. carbonate melt in a glass crucible. But therefor modifications in the setup would be necessary, which do not allow an accurate control of melt temperature.

Furthermore it could be possible to to analyze in more detail the relation of vapor film stability and collapse. The resulting initial direct contact surface has much influence on the following explosion.

12.2 Additional influences of melt temperature

Variations in melt temperature can cause other effects on explosions, that are not yet investigated in the frame of these studies.

Is the minimum initial contact surface smaller for high temperatures, because more energy per surface area is available? A further question is whether an absolute minimum for the initial direct contact surface exists, because otherwise there could not be enough interactive melt and water involved anyway. An analogue would be a hammer impact and a rock fall of a small stone with high energy, that can cause a

small hole into glass but not break it.

There are many hints that the interactive water warms up during premix and also during the influx into the melt cracks. How does this warming eventually reduce the energy transfer and how could this be placed into a model of heat transfer? An answer could be a good correction of the maximum estimation for transferred energy toward the real values. How dominant is this not yet proofed indirect effect for the explosion compared to other effects?

12.3 Influence of the temperature of injected water

As often mentioned the temperature of the injected water has influence on melt water interaction, vapor film stability, and energy transfer. To check this, experiments are necessary, where heated or cooled water on several temperatures is injected into melt. It is a complex task to realize such a water injection system, which allows an accurate control of the injected water temperature.

With such experiments and analyses it should be possible to see how much a variated temperature difference between melt and water on waterside affects the process. Can warmer water accept less energy, before it becomes supercritical or vaporizes? Is the development and stability of vapor film similar or different? These are important aspects for thermohydraulic explosions, where answers are absolutely important in the view of risk management.

12.4 Detailed exploration of multiple triggered explosions

Multiple triggered explosions are not rare, so the cooperation of several triggers in one explosion has to be checked. There are following questions: Can the explosions in the several water domains trigger each other? Which time difference is between the triggers? Is there a maximum distance between the water domains for interdependent triggering? How long is the direct contact in the several domains and their contribution to the total energy transfer? Does direct contact for all domains end at the same time or at different times?

For a better separation of single triggers in a multiple triggered explosion the crucible in the laboratory is too small. A larger setup is needed. This would allow to inject more water domains, which are not close together, into melt. In this way a better examination of each trigger would be possible.

Appendix A

Estimation of delay times of the triggers for high-speed camera and data logger

The trigger signals for the data logger and the high-speed camera are produced by an electrical pulse, which is produced by the switching of relais. These switchings have several delays so that all the devices start with delay and these delays are different for each device. Reasons therefor are that the data logger is usually triggered on the falling slope of the trigger pulse and the high-speed camera on the rising slope. Additionally on the rising slope there is a chatter of the relais, which can delay the start of the device. The last problem is important if the recording of several devices have to be compared. Therefore the time values of the devices have to be corrected about the difference of the time values of the involved devices.

For a good calibration test experiments with aluminium stripes were made. An electrical current flows through the stripe until it is cut by a trigger bullet. This cut is filmed by the HiCam and the slope of the current is recorded by the data logger. This delivers an accurate comparison of both devices. Furthermore the impact of the bullet on the base plate is filmed and can be compared with the force signal. This way the time for the signal transmission from the plate to the force sensor can be estimated. This knowledge is important for the signal transmission of the repulsion force for MFCI-experiments.

For this test run the frame rate of the camera was 20000 pictures per second. In Figure A.1 frames 7580 and 7581 are shown, when the alu stripe is cut and the bullet has arrived on the plate. The plot in Figure A.2 shows the recording from the data logger of the current and the force signal. The video recordings show that the cut of the alu stripe is at $t = 478.85\,ms$ in camera time. Frame 7577 is $378.85\,ms$ after the trigger of the camera recorded, and the trigger for the camera was $100\,ms$ later than the trigger for the logger. In the logger data, the offset of the current begins at $t = 474.81\,ms$ in logger time. In this case, there is a difference of $4.04\,ms$ in the time scales of both devices.

For a comparision of video recordings to a force signal it is additionally to respect that the force signal needs a certain time to be transmitted from the crucible or the top of the plate through the coolant coil

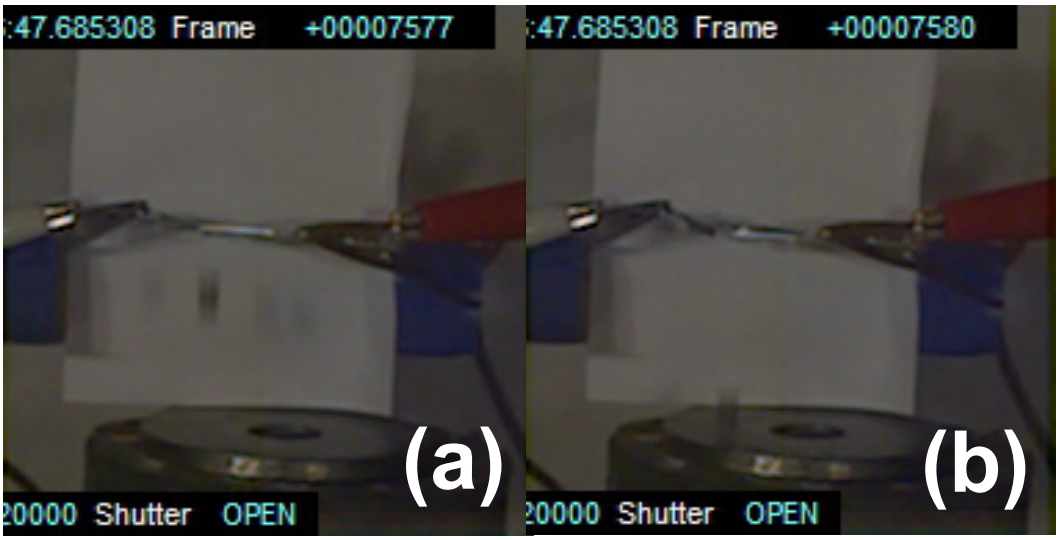

Figure A.1: Video recordings of the calibration tests with an alu stripe. (a) Cut of the alu stripe by a trigger bullet. (b) Impact of the trigger bullet on the plate.

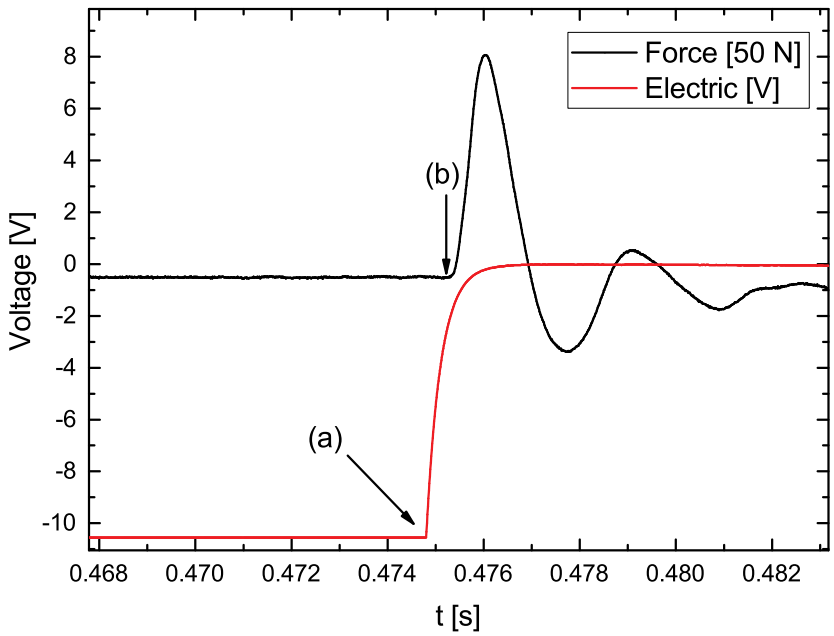

Figure A.2: Force and electric signals of the calibration tests with an alu stripe. (a) Cut of the alu stripe by a trigger bullet. (b) Impact of the trigger bullet on the plate.

between the plate and the force sensor. For short time experiments, even the signal propagation with speed of sound cannot be neglected. Following the video HiCam recording, the force peak of the bullet impact on the plate should have its onset at $t = 479.00\,ms$ in camera time. The logger data show that this onset is at $t = 475.29\,ms$ in logger time. For the force signal and the video recording the time difference is only $3.71\,ms$, because bullet impact is recorded without a delay (signal propagation with speed of light) by the camera, but the data logger runs on until the force signal arrives at the force sensor. Other test runs show time differences between video and offset of the current through the alu stripe of $4.00\,ms$, $3.91\,ms$ and $3.96\,ms$. For the bullet impact on the plate and onset of the force peak there are time differences of $3.58\,ms$, $3.57\,ms$ and $3.64\,ms$. It might be that the last times are shortened, because the force sensor is so delicate that it can detect the pulse of the bullet already before its arrival on the plate.

For the MFCI-experiments a more precise estimation for the time difference with a crucible makes sense. Also it is to consider that a mixture of liquid melt and water has to be in the crucible, which does not start an explosion. But this is impossible. The only way is to use a crucible only filled with some water or only filled with some liquid tin. For MFCI-experiments a test with liquid tin makes more sense, because during the experiments the melt volume is about ten times higher than the water volume. In the test run the bullet impact on the top of the melt surface is observed at frame 7655 at $482.75\,ms$ in camera time (see Figure A.3). The onset of the corresponding force peak is at $479.05\,ms$ in logger time (see Figure A.4). The time difference is $3.70\,ms$. This time difference is used for the comparison of video recordings and the recorded force signals.

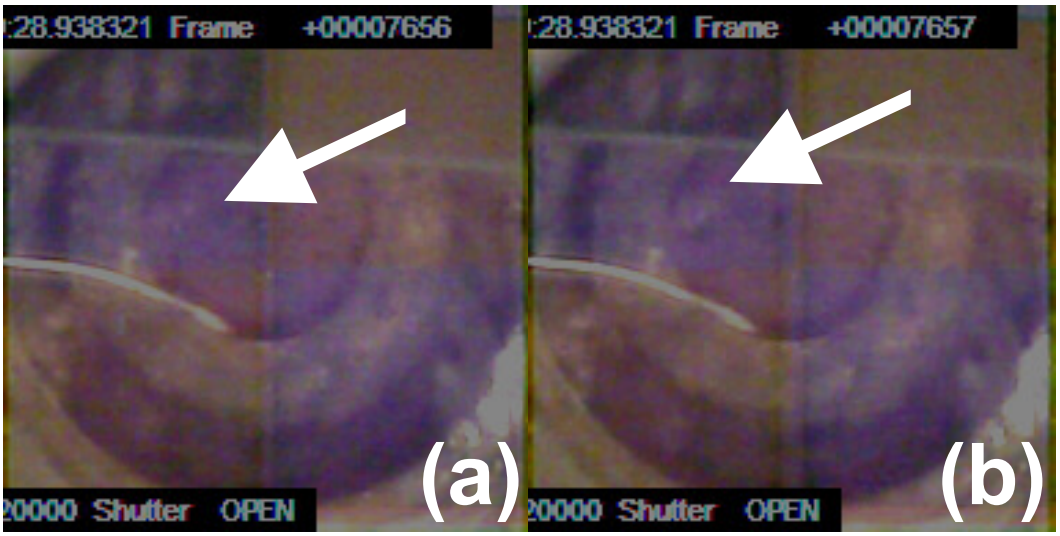

Figure A.3: Impact of the trigger bullet on the surface of pure tin, marked by the white arrow. Because of the high framerate and the short exposure time the frame pictures are dark in its original. The two pictures are enlightened by an image editing software. The left picture (a) shows the frame with the bullet impact on the melt surface, the right picture (b) shows the impact crater.

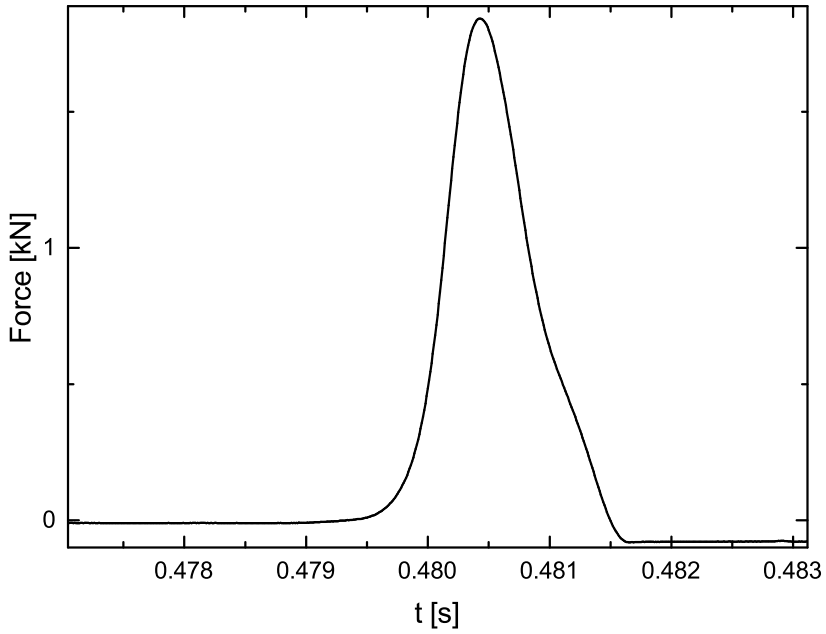

Figure A.4: Force signal of the bullet impact from Figure A.3.

Appendix B

Calibration of the water injection

The table shows the values of water injection volumes for several injection times at a pump voltage of $6.0V$ and an associated injection velocity of $1.3\,\frac{m}{s}$ into water. The diagram B.1 shows the recorded voltage at the potentiometer for the position of the piston pump. The pictures B.2 show a sequence of water injection procedures with the impact of a trigger bullet.

Table B.1: Injection volumes for several injection times at a voltage of $6.0V$ and a valve delay of $100ms$.

t/ms	m/g
380	$6{,}3 \pm 2{,}0$
390	$5{,}3 \pm 1{,}1$
400	$5{,}5 \pm 1{,}6$
420	$6{,}6 \pm 0{,}9$
440	$7{,}2 \pm 0{,}7$

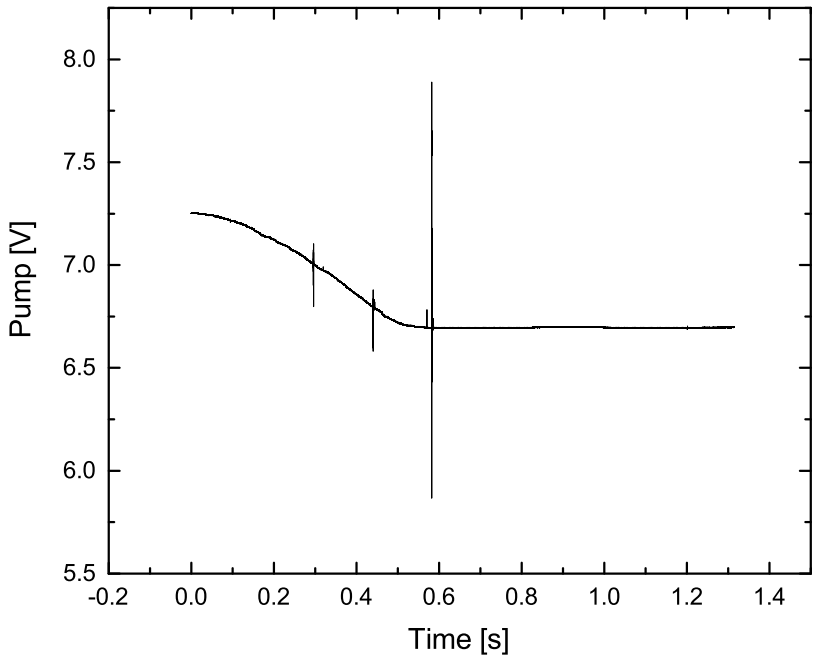

Figure B.1: Signal of the potentiometer voltage, which controls the piston pump position and the injection time and the injected water volume. Excluding the short onset and offset of the movement, a linear drive of the piston is visible, which confirms a constant injection velocity. The single peaks are caused by perturbations of other devices in the setup. In the presented plot the piston pump was driven from $t = 0$ to $t = 440\,ms$. The artefact peaks are caused by perturbations of other devices in the setup.

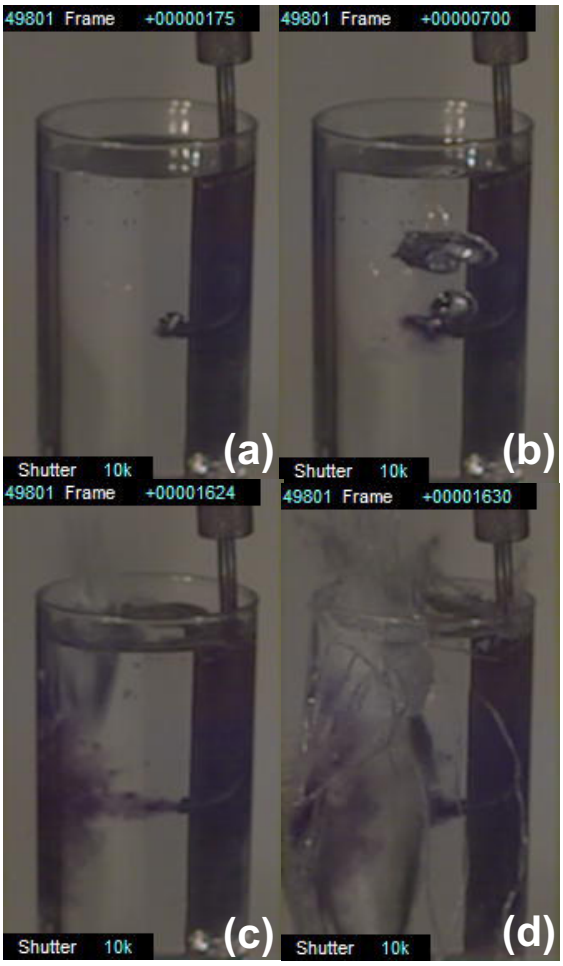

Figure B.2: Some snapshoots of a test run for the water injection with trigger bullet impact. In the presented run the pump voltage is $6.0V$. The injection time is $270ms$ with a valve delay of $100ms$. The recording framerate is 5000 pictures per second. The record is started after $100ms$ at the opening of the valve at frame 0. (a) At frame 175 $35ms$ after the opening of the valve the blow out of rest air in the injection tube starts. (b) Onset of the water jet after $140ms$ at frame 700. (c) Impact of the trigger bullet on the water surface at frame 1624 after $325ms$. (d) The bullet crossed the injected water and reaches the bottom of the vessel after $326ms$ at frame 1630.

Appendix C

Blow-out experiments for the determination of the surface tension of tin during brittle fragmentation

For the surface tension of tin during brittle fragmentation, where interactive particles are developed, no values for the relevant temperature range could be found in literature sources. For an approximation to these values blow-out experiments were made according to DÜRIG, DIOGUARDI, et al., 2011. The experimental setup and the procedure is analogue to BÜTTNER, DELLINO, et al., 2006. Measurements for tin melt were made at temperatures of 500 $^{\circ}C$ and 850 $^{\circ}C$, to check, whether the surface tension depends on melt temperature. The values for all other melt temperatures are extrapolated.

The difference to the analyses in DÜRIG, DIOGUARDI, et al., 2011, is that not the kinetic energy of particles, but the surface tension was detected. This can be calculated using the recorded data from the experiments:

The transmitted pulse to the force sensor is integrated over time:

$$p = \int F dt \tag{C.1}$$

As the mass is known, the general relation between pulse and energy exists:

$$E = \frac{p^2}{2m} \tag{C.2}$$

For the calculation of pulse the integration limits have to be suitably chosen. For this analysis the values for energy for brittle fragmentation $E_{\text{frag,i}}$ and shock waves E_{shock} are interesting. The conversion of the initial mechanical energy into these both forms takes place in the time span from $[t_0;t_2]$ (DÜRIG, DIOGUARDI, et al., 2011). Time t_0 is at onset of the force peak and time t_2 taken from the onset of blowout in the video recordings.

For the surface tension the specific surface has additionally to be detected. The generated fragments are collected and sieved. Almost all interactive fragments are in the two smallest sieve fraction with diameter lower than $63\,\mu m$ and $125\,\mu m$. The part of interactive particles is detected by shape analyses with an optical microscope. Using the specific surface for these fractions the surface tension can be calculated now.

The results achieved in this way are values for the surface tension during brittle fragmentation of $8.1\,\frac{J}{m^2}$ for a temperature of $500\,^{\circ}C$ and $4.9\,\frac{J}{m^2}$ for $850\,^{\circ}C$. The other extrapolated values are listed in table C.1. During this blowout experiments additional recordings with a FLIR® camera were made to

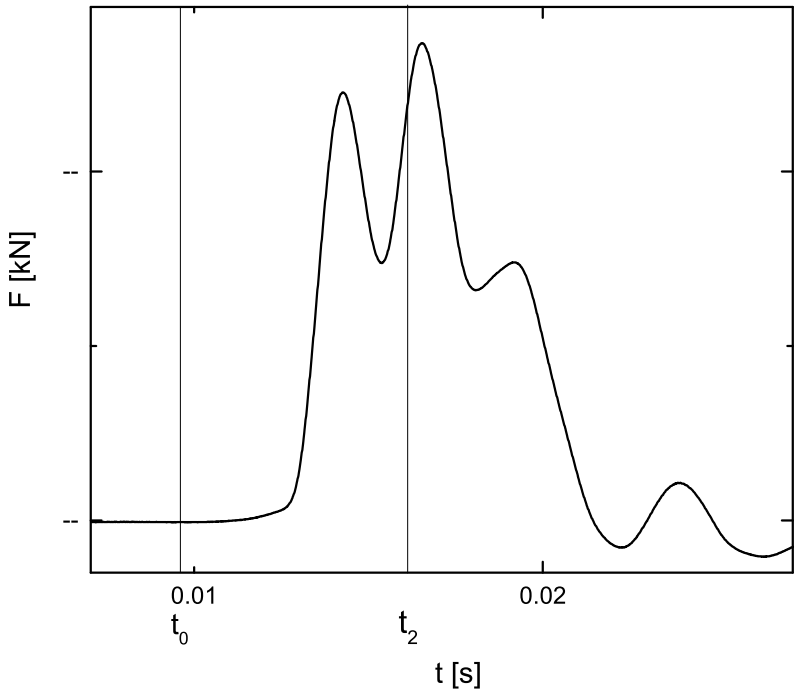

Figure C.1: Force signal of a tin blowout experiment. The relevant times t_0 and t_2 are marked. The melt temperature for this run was $500\,^{\circ}C$.

watch the temperature and the cooling of fragments.

First it is to determine that the fine fragments cool down faster than the rough blown-out melt. The fine fragments reach approximately room temperature already during the flight in air. Thus the rough material is significantly warmer after its crash on the containment. The reason is the higher surface-mass-ratio for fine particles and the lower thermal energy in the particles. The low amount of energy can be delivered in a short time. It is to add that this is in accordance to the model BÜTTNER, ZIMANOWSKI, MOHRHOLZ, et al., 2005, and to the calculations in chapter 11. Also the longer cooling times for higher initial temperature are confirmed.

Table C.1: Extrapolated surface tensions for brittle fragmentation of tin melt at relevant temperatures.

$T/^\circ C$	$\sigma/\frac{J}{m^2}$
400	9.0
410	8.9
420	8.8
430	8.7
500	8.1
510	8.0
520	7.9
530	7.8
640	6.8
740	5.9
800	5.4
820	5.2
890	4.6
900	4.5
1000	3.6
1020	3.4
1040	3.2

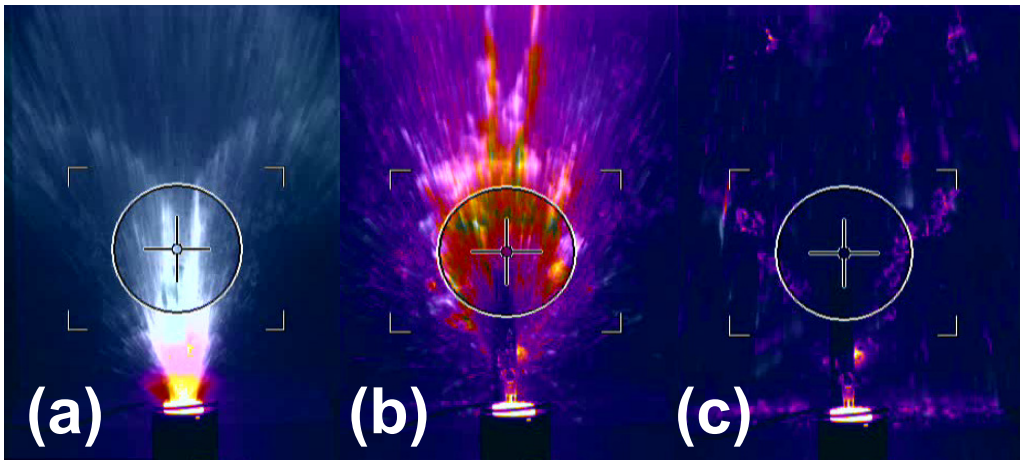

Figure C.2: Some snapshots of a FLIR® thermo camera. (a) The fine fragments leave the crucible and still have high temperature. (b) The fine fragments have already larger distance to the crucible and are no longer visible in the thermo picture. It shows that they are already cooled down. Some rough blowout leaves the crucible and is still hot in larger distance to the crucible. (c) The rough blowout is down on the containment and has still high temperature.

Appendix D

Tables of experimental data

D.1 MFCl-experiments with tin

Table D.1: Repulsion force and transferred pulse versus melt temperature. Remarks: 1) Unfavorable premix causing a weak explosion. 2) Multiple triggered explosion. 3) Self-triggered explosion. 4) Two self-triggered explosions. 5) First self-triggered explosion, afterwards mechanically triggered explosion.

Run	T/ ° C	F/kN	p/Ns	Remarks
Tin-1000-1	1020	5.26	2.28	
Tin-1000-2	1020	4.16	2.20	
Tin-1000-3	1020	6.06	2.94	
Tin-1000-4	1040	1.70	0.81	1
Tin-1000-5	1000	5.27	2.22	
Tin-900-1	900	3.78	1.06	
Tin-900-2	900	6.55	2.85	
Tin-900-3	900	5.59	1.01	
Tin-900-4	890	1.60	0.77	1
Tin-900-5	900	2.86	1.00	1
Tin-900-6	900	1.91	1.05	1
Tin-900-7	900	2.27	2.40	1, 2
Tin-800-1	820	0.98	0.26	1
Tin-800-2	820	2.02	0.96	1
Tin-700-1	740	5.28	2.21	
Tin-700-2	740	3.92	1.47	
Tin-700-3	740	4.64	1.71	
Tin-600-1	640	2.64	1.04	
Tin-600-2	640	1.91	0.80	
Tin-600-3	640	2.11	0.93	
Tin-500-1	530	1.96	1.13	
Tin-500-2	530	0.91	0.45	
Tin-500-3	520	5.15	4.15	2
Tin-500-4	530	0.51	0.25	
Tin-500-5	520	1.04	0.39	
Tin-400-1	410	1.12	0.53	
Tin-400-2	420	0.74	0.47	3
Tin-400-3	410	0.58	0.43	3
Tin-400-4	400	1.17	1.43	4
Tin-400-5	420	0.44	0.58	5
Tin-400-6	410	1.57	0.53	5
Tin-400-7	430	1.31	1.35	5

Table D.2: Values for new created surface of tin experiments.

Run	$A_{i,125}/m^2$	$A_{i,63}/m^2$	$A_{i,tot}/m^2$	$A_{i,63}/A_{i,125}$	E_{surf}/J	A_h/m^2	$E_{frag,h}/J$
Tin-1000-1	0.77	0.53	1.30	0.69	4.5	3.95	2.0
Tin-1000-2	0.91	0.46	1.37	0.50	4.7	2.95	1.5
Tin-1000-3	1.02	0.57	1.59	0.55	5.4	3.67	1.8
Tin-1000-4	0.75	0.26	1.01	0.35	3.3	2.88	1.4
Tin-1000-5	0.85	0.44	1.29	0.52	4.7	3.88	1.9
Tin-900-1	0.54	0.18	0.72	0.34	3.3	1.79	0.9
Tin-900-2	1.18	0.75	1.92	0.64	8.6	5.94	3.0
Tin-900-3	0.42	0.28	0.70	0.68	3.2	2.86	1.4
Tin-900-4	0.37	0.08	0.45	0.22	2.1	1.95	1.1
Tin-900-5	0.27	0.15	0.42	0.54	1.9	2.00	1.1
Tin-900-6	0.47	0.15	0.62	0.32	2.8	2.72	1.5
Tin-900-7	1.16	0.63	1.79	0.55	8.0	5.07	2.8
Tin-800-1	0.15	0.04	0.19	0.29	1.0	0.46	0.2
Tin-800-2	0.43	0.12	0.55	0.28	2.9	3.30	1.7
Tin-700-1	1.17	0.39	1.56	0.33	9.3	7.36	3.8
Tin-700-2	0.74	0.25	0.99	0.34	5.8	4.02	2.1
Tin-700-3	0.69	0.31	1.00	0.44	5.9	3.62	1.9
Tin-600-1	0.43	0.15	0.58	0.34	4.0	3.60	1.9
Tin-600-2	0.55	0.13	0.68	0.25	4.6	3.84	2.0
Tin-600-3	0.77	0.14	0.91	0.18	6.2	4.09	2.2
Tin-500-1	0.57	0.11	0.68	0.20	5.3	4.27	2.3
Tin-500-2	0.79	0.23	1.03	0.29	8.0	5.32	2.9
Tin-500-3	0.98	0.45	1.43	0.46	11.3	13.11	7.1
Tin-500-4	0.37	0.13	0.49	0.35	3.8	3.15	1.7
Tin-500-5	0.32	0.05	0.37	0.16	2.9	2.20	1.2
Tin-400-1	0.36	0.07	0.43	0.20	3.8	3.97	2.2
Tin-400-2	0.20	0.06	0.26	0.31	2.2	3.76	2.1
Tin-400-3	0.28	0.06	0.35	0.22	3.1	3.05	1.7
Tin-400-4	0.61	0.19	0.80	0.31	7.1	5.02	2.8
Tin-400-5	0.23	0.06	0.29	0.25	2.5	2.16	1.2
Tin-400-6	0.48	0.11	0.59	0.23	5.2	4.17	2.3
Tin-400-7	0.42	0.11	0.53	0.27	4.6	4.98	2.7

Table D.3: Kinetic and vaporation energy for tin MFCI-experiments.

Run	E_{kin}/J	m_V/g	$\Delta U_V/10^2\,J$	$E_V/10^2\,J$
Tin-1000-1	75	0.40	8.3	10.1
Tin-1000-2	78	0.41	8.7	10.9
Tin-1000-3	117	0.62	13.0	12.6
Tin-1000-4	2	0.01	0.2	8.2
Tin-1000-5	44	0.23	4.9	10.2
Tin-900-1	17	0.09	1.9	6.2
Tin-900-2	79	0.42	8.7	15.9
Tin-900-3	20	0.11	2.2	5.8
Tin-900-4	1	0.01	0.2	3.9
Tin-900-5	3	0.01	0.3	3.5
Tin-900-6	5	0.03	0.6	5.3
Tin-900-7	34	0.18	3.7	15.0
Tin-800-1	3	0.02	0.4	1.8
Tin-800-2	5	0.03	0.5	5.1
Tin-700-1	29	0.15	3.2	15.5
Tin-700-2	9	0.05	1.0	9.8
Tin-700-3	24	0.13	2.7	9.8
Tin-600-1	5	0.03	0.6	6.2
Tin-600-2	2	0.01	0.2	7.1
Tin-600-3	1	0.01	0.1	9.6
Tin-500-1	5	0.03	0.5	2.6
Tin-500-2	0	0.00	0.0	3.9
Tin-500-3	86	0.46	9.5	5.6
Tin-500-4	0	0.00	0.0	1.9
Tin-500-5	1	0.00	0.1	1.4
Tin-400-1	1	0.00	0.1	0.9
Tin-400-2	1	0.00	0.1	0.5
Tin-400-3	1	0.00	0.1	0.7
Tin-400-4	8	0.05	0.9	1.6
Tin-400-5	5	0.02	0.5	0.6
Tin-400-6	1	0.01	0.1	1.2
Tin-400-7	6	0.03	0.7	1.1

Table D.4: Energy conversion of the maximum estimation for tin MFCI-experiments.

Run	$\Delta E_i / 10^2$ J	$E_{res} / 10^2$ J	$\frac{E_{res}}{m_i} / \frac{10^2 J}{g}$	η
Tin-1000-1	25.9	14.9	1.0	0.42
Tin-1000-2	27.7	16.0	1.0	0.42
Tin-1000-3	32.0	18.2	1.0	0.43
Tin-1000-4	21.5	13.2	1.1	0.38
Tin-1000-5	25.3	14.6	1.0	0.42
Tin-900-1	13.0	6.6	0.7	0.49
Tin-900-2	33.3	16.6	0.7	0.50
Tin-900-3	12.1	6.1	0.7	0.50
Tin-900-4	8.1	4.1	0.7	0.49
Tin-900-5	7.4	3.8	0.7	0.49
Tin-900-6	11.1	5.7	0.7	0.49
Tin-900-7	31.3	16.0	0.7	0.49
Tin-800-1	3.2	1.4	0.5	0.57
Tin-800-2	9.2	4.0	0.5	0.57
Tin-700-1	23.0	7.1	0.3	0.69
Tin-700-2	14.5	4.6	0.3	0.69
Tin-700-3	14.6	4.4	0.3	0.70
Tin-600-1	6.8	0.5	0.1	0.92
Tin-600-2	7.8	0.7	0.1	0.92
Tin-600-3	10.5	0.9	0.1	0.92
Tin-500-1	5.3	2.6	0.2	0.51
Tin-500-2	8.0	4.0	0.2	0.50
Tin-500-3	10.8	4.2	0.2	0.61
Tin-500-4	3.9	2.0	0.2	0.50
Tin-500-5	2.7	1.2	0.2	0.53
Tin-400-1	1.2	0.3	0.0	0.79
Tin-400-2	0.8	0.3	0.1	0.68
Tin-400-3	1.0	0.2	0.0	0.79
Tin-400-4	1.9	0.1	0.0	0.98
Tin-400-5	0.9	0.3	0.1	0.72
Tin-400-6	1.6	0.4	0.0	0.78
Tin-400-7	2.0	0.8	0.1	0.61

Table D.5: Energy conversion of the minimum estimation for tin MFCI-experiments.

Run	$E_{out}/10^2\,J$	$\frac{E_{out}}{m_{eff,i}}/\frac{10^2\,J}{g}$	$\Delta T_{out,eff}/K$	$T_{end}/^\circ C$	$Tc/^\circ C$
Tin-1000-1	9.1	0.6	236	784	600
Tin-1000-2	9.5	0.6	230	790	600
Tin-1000-3	14.2	0.8	299	721	600
Tin-1000-4	0.3	0.0	8	1032	600
Tin-1000-5	5.4	0.4	138	862	600
Tin-900-1	2.1	0.2	90	810	520
Tin-900-2	9.6	0.4	159	741	520
Tin-900-3	2.5	0.3	111	789	520
Tin-900-4	0.2	0.0	14	876	520
Tin-900-5	0.4	0.1	27	873	520
Tin-900-6	0.7	0.1	34	866	520
Tin-900-7	4.2	0.2	74	826	520
Tin-800-1	0.4	0.2	60	760	480
Tin-800-2	0.6	0.1	32	788	480
Tin-700-1	3.6	0.2	61	679	430
Tin-700-2	1.1	0.1	30	710	430
Tin-700-3	3.0	0.2	80	660	430
Tin-600-1	0.7	0.1	29	611	380
Tin-600-2	0.3	0.0	10	630	380
Tin-600-3	0.2	0.0	6	634	380
Tin-500-1	0.7	0.1	23	507	320
Tin-500-2	0.2	0.0	3	527	320
Tin-500-3	10.1	0.4	167	353	320
Tin-500-4	0.1	0.0	3	527	320
Tin-500-5	0.1	0.0	9	511	320
Tin-400-1	0.1	0.0	7	403	260
Tin-400-2	0.1	0.0	10	410	260
Tin-400-3	0.1	0.0	8	402	260
Tin-400-4	1.1	0.1	30	370	260
Tin-400-5	0.6	0.1	45	375	260
Tin-400-6	0.2	0.0	8	402	260
Tin-400-7	0.8	0.1	32	398	260

D.2 MFCI-experiments with magmatic melt

Table D.6: Estimated fragmentation time, calculated average end temperatures U for the finest particle fractions, transferred thermal energy and thermal power for runs with magmatic melt.

Run	t_{frag}/ms	U63/ °C	U125/ °C	U250/ °C	$\Delta E_i/10^2$ J	P_{th}/MW
THS03	0.5	405	635	920	4.5	0.9
THS04	0.5	405	635	920	4.4	0.9
THS05	0.5	405	635	920	3.4	0.7
THS06	0.3	464	745	995	12.9	4.2
THS07	0.5	405	635	920	5.8	1.2
TGR03	0.5	405	635	920	3.5	0.7
TGR08	0.3	464	745	995	3.2	1.1
TGR10	0.3	464	745	995	2.5	0.8
TGR11	0.5	405	635	920	5.6	1.1
TGR18	0.5	405	635	920	3.1	0.6
TGR19	0.3	464	745	995	2.8	0.9

Table D.7: Output energies for runs with magmatic melt.

Run	E_{kin}/J	$E_{frag,h}/10^2\,J$	$E_{frag,i}/10^2\,J$	$E_{shock}/10^2\,J$	$E_v/10^2\,J$	$E_{res}/10^2\,J$	$\frac{E_{res}}{m_{eff,i}}/10^2\,\frac{J}{g}$
THS03	0.15	0.7	0.3	0.4	1.1	2.0	3.4
THS04	0.39	0.6	0.3	0.4	1.0	2.0	3.4
THS05	0.14	0.5	0.2	0.3	0.9	1.5	2.9
THS06	4.04	2.5	1.0	1.4	4.1	3.8	1.7
THS07	0.35	0.8	0.3	0.5	1.4	2.7	3.4
TGR03	0.74	0.4	0.2	0.3	0.9	1.9	3.9
TGR08	0.98	0.6	0.3	0.3	1.0	1.3	2.5
TGR10	0.91	0.4	0.2	0.3	0.7	1.1	2.7
TGR11	4.07	1.1	0.4	0.5	1.6	2.3	2.6
TGR18	12.1	0.6	0.2	0.3	0.9	1.2	2.5
TGR19	11.5	0.7	0.2	0.3	1.0	0.7	1.3

Table D.8: Total outcomimg energy, normalized outcoming energy and calculated cooling of fragments in average.

Run	$E_{out}/10^2\,J$	$\frac{E_{out}}{m_{eff,i}}/10^2\,\frac{J}{g}$	$\Delta T_{out,eff}/K$
THS03	1.4	2.3	166
THS04	1.4	2.3	167
THS05	1.1	2.1	153
THS06	5.4	2.4	170
THS07	1.8	2.2	159
TGR03	1.1	2.3	166
TGR08	1.3	2.4	170
TGR10	1.0	2.4	173
TGR11	2.5	2.8	200
TGR18	2.5	5.2	371
TGR19	2.6	4.8	342

Appendix E

Contents of the attached DVD

High speed video recording of a test run for calibration of the water injection (folder *waterinjection*)

High speed video recording of a test run for the water injection with an impact of a trigger bullet (folder *waterinjection-triggerbullet*)

High speed video recording of an MFCI-run with tin melt (folder *MFCI-run-tin*)

High speed video recording of an MFCI-run with Grimsvötn melt (folder *MFCI-run-Grimsvoetn*)

High speed video recording of a blowout-run with tin melt (folder *tin-blowout*)

Bibliography

Arte – Tschernobyl + Europa. May 2011. URL: http://antiatomowl.wordpress.com/2011/05/04/arte-tschernobyl-europa/ (visited on 8. Apr. 2014) (cit. on p. 5).

ATTARD, M. M. and F. TIN-LOI: „Numerical simulation of quasibrittle fracture in concrete“. *Engineering Fracture Mechanics*, vol. 72, (2005): pp. 387–411 (cit. on p. 80).

BAEHR, H. D. and K. STEPHAN: *Waerme- und Stoffuebertragung, 7. Auflage*. Ed. by BAEHR, H. D. and K. STEPHAN. Springer, 2010 (cit. on p. 77).

BIRCUMSHAW, L. L. B.: „The surface tension of liquid metals. Part I. Tin and lead“. *Philosophical Magazine Series*, vol. 7(2:8), (1926): pp. 341–350 (cit. on pp. 50, 63).

BLOMEYER, F.: *Bestimmung der Oberflächenspannung von Zinn und einiger Blei-Zinn- und Wismut-Blei-Zinn-Legierungen nach der Methode des ruhenden Tropfens*. Ed. by BLOMEYER, F. 1962 (cit. on p. 63).

BOARD, S. J., R. W. HALL, and R. S. HALL: „Detonations of fuel coolant explosions“. *Nature*, vol. 254, (1975): pp. 319–321 (cit. on p. 6).

BUCHANAN, D. J.: „A model for fuel-coolant interactions“. *J. Phys. D: Appl. Phys.* Vol. 7, (1974): pp. 1441–1457 (cit. on p. 6).

BÜRGER, M., C. CHARACHALIOS, D. S. KIN, and H. UNGER: „Theoretical Investiagation on the Fragmentation of Drop of Melt with Respect to the Description of thermal Detonations (Vapor Explosions) and their Application in the Code of FRADEMO“. IKE, Universität Stuttgart, 1985 (cit. on p. 6).

BÜTTNER, R., P. DELLINO, H. RAUE, I. SONDER, and B. ZIMANOWSKI: „Stress-induced brittle fragmentation of magmatic melts: Theory and experiments“. *Journal of geophysical research*, vol. 111, (2006): pp. 1–10 (cit. on pp. 39, 95).

BÜTTNER, R., H. RÖDER, and B. ZIMANOWSKI: „Electrical effects generated by experimental volcanic explosions“. *Appl. Phys. Lett.* Vol. 70(14), (1997): pp. 1903–1905 (cit. on p. 29).

BÜTTNER, R. and B. ZIMANOWSKI: „Physics of thermohydraulic explosions“. *Physical Review E*, vol. 57, (1998): pp. 5726–5729 (cit. on pp. 6, 14, 15, 37, 61, 71, 78, 81, 83).

BÜTTNER, R., B. ZIMANOWSKI, J. BLUMM, and L. HAGEMANN: „Thermal conductivity of a volcanic rock material (olivine-melilitite) in the temperature range between 288 and 1470 K“. *Journal of Volcanology and Geothermal Research*, vol. 80, (1998): pp. 293–302 (cit. on pp. 10, 76).

BÜTTNER, R., B. ZIMANOWSKI, C.-O. MOHRHOLZ, and R. KÜMMEL: „Analysis of thermohydraulic explosion energetics“. *Journal of Applied Physics*, vol. 98(043524), (2005): pp. 1–8 (cit. on pp. 7, 10, 30, 37, 71, 72, 75–78, 80, 83, 96).

COLGATE, S. A. and T. SIGURGEISSON: „Dynamic mixing of water and lava“. *Nature*, vol. 244, (1973): pp. 552–555 (cit. on p. 6).

CORRADINI, M. L.: „Analysis and modelling of steam explosion experiments“. *Sandia National Laboratories, Alberquerque, NM, NUREG/CR2072, SAND 80-2131*, vol., (1981) (cit. on p. 6).

DRATH, G.: *Die Oberflächenspannung von Zinn, Blei, Antimon, Kupfer, Wismut-Zinn-, Wismut-Blei-, Kupfer-Antimon-Legierungen und Gußeisen*. 1927 (cit. on p. 63).

DULLFORCE, T. A., D. J. BUCHANAN, and R. S. PECKOVER: „Self-triggering of small-scale fuel-coolant interactions“. *J. Phys. D: Appl. Phys.* Vol. 9, (1976): pp. 1295–1303 (cit. on p. 6).

DÜRIG, T.: „Fracture Dynamics in Silicate Glasses“. Diss. Universität Würzburg, 2011 (cit. on p. 37).

DÜRIG, T., F. DIOGUARDI, R. BÜTTNER, P. DELLINO, D. MELE, and B. ZIMANOWSKI: „A new method for the determination of the specific kinetic energy (SKE) released to pyroclastic particles at magmatic fragmentation: theory and first experimental results“. *Bull Volcanol*, vol., (2011) (cit. on p. 95).

DÜRIG, T., D. MELE, P. DELLINO, and B. ZIMANOWSKI: „Comparative analyses of glass fragments from brittle fracture experiments and volcanic ash particles“. *Bull Volcanol*, vol., (2011) (cit. on p. 49).

DÜRIG, T., I. SONDER, B. ZIMANOWSKI, H. BEYRICHEN, and R. BÜTTNER: „Generation of volcanic ash by basaltic volcanism“. *ournal of geophysical research*, vol. 117(B01204), (2012) (cit. on p. 71).

DÜRIG, T. and B. ZIMANOWSKI: „“Breaking news“ on the formation of volcanic ash: Fracture dynamics in silicate glass“. *Earth and Planetary Science Letters*, vol. 335 - 336, (2012): pp. 1–8 (cit. on p. 71).

EBERT, H.-P., F. HEMBERGER, J. FRICKE, R. BÜTTNER, S. BEZ, and B. ZIMANOWSKI: „Thermophysical Properties of a Volcanic Rock Material“. *Unpublished*, vol., (2003) (cit. on p. 76).

EDER, F. X.: *Arbeitsmethoden der Thermodynamik, Band I, Temperaturmessung*. Ed. by EDER, F. X. Springer-V, 1981 (cit. on p. 10).

EX, W. and G. A. SCHMÜCKER: „Neuerungen im Erschütterungs-Immissionsschutz“. *Spreng Info*, vol. 22(1), (2000): pp. 15–25 (cit. on pp. 39, 63).

FAGENTS, S. A., T. P. GREGG, and L. R. M. C., Hrsg.: *Modelling Volcanic Processes, The Physics and Mathematics of Volcanism*. Cambridge University Press, 2013 (cit. on p. 10).

FAUPEL, F., K. RÄTZKE, and B. GOJDKA: *Metallische Gläser - robust und extrem vielseitig*. German. Welt der Physik. Aug. 2010. URL: http://www.weltderphysik.de/gebiete/stoffe/metalle/metallische-glaeser/ (visited on 19. Nov. 2014) (cit. on p. 37).

FREUD, A., R. HARARI, and E. SHER: „Collapsing criteria for vapor film around solid spheres as a fundamental stage leading to vapor explosion“. *Nuclear Engineering and Design*, vol. 239 No. 4, (2009): pp. 722–727 (cit. on p. 6).

FREUNDT, A. and M. ROSI: *From magma to tephra, Modelling Physical Processes of Explosive Volcanic Eruptions*. Ed. by BURSIK, M., D. B. DINGWELL, A. FREUNDT, P. PAPALE, M. ROSI, G. VALENTINE, K. WOHLETZ, and B. ZIMANOWSKI. Elsevier, 1998 (cit. on pp. 71, 72).

FRÖHLICH, G.: „Dampfexplosionen durch Kontakt zwischen Wasser und heißen Schmelzen“. *Chem.-Ing.-Tech.* Vol. 50 No. 11, (1978): pp. 861–866 (cit. on pp. 6, 28, 72).

FRÖHLICH, G., B. ZIMANOWSKI, V. LORENZ, V. BAYER, E. von BERG, M. KHAN, and M. SCHINDLER: *Experimente zur Simulation phreatomagmatischer Explosionen und vergleichende Untersuchungen, Abschlussbericht*. unpublished, 1992 (cit. on pp. 11, 71, 72).

GLAZKOV, V. V., V. S. GRIGOR'EV, V. G. ZHILIN, Y. A. ZEIGARNIK, Y. P. IVOCHKIN, K. G. KUBRIKOV, N. V. MEDVETSKAYA, A. A. OKSMAN, and O. A. SINKEVICH: „A Possible Mechanism of Triggering a Vapor Explosion“. *High Temperature*, vol. 44, (2006): pp. 908–912 (cit. on p. 10).

GUDMUNDSSON, M. T. URL: https://c2.staticflickr.com/8/7020/6462574749_fd3a270212_b.jpg (visited on 8. Apr. 2014) (cit. on p. 5).

HALL, A.: „Outline of a new thermodynamic model of energetic fuel-coolant interactions“. *Nuclear Engineering and Design*, vol. 109, (1988): pp. 407–415 (cit. on p. 6).

HENRY, R. E. and H. K. FAUSKE: „Nucleation processes in large scale vapor explosions“. *J. Heat Transfer*, vol. 101, (1979): pp. 280–291 (cit. on p. 6).

HERION: *Beschreibung 2/2-wegeventile dn 6 und 10. Technical report*. Techn. Ber. Herion, 1994 (cit. on p. 23).

Hochwasser, Überschwemmungsgebiete & Anlagen am Gewässer, Historische Hochwasser: 1784 - das 300-jährliche Hochwasser. 2014. URL: http://www.wuerzburg.de/de/themen/umwelt-verkehr/wasser--abwasser/hochwasser--ueberschwemmungsgebiete/404971.Historische_Hochwasser__-_das_-_jaehrliche_Hochwasser.html (visited on 3. Dec. 2015) (cit. on p. 5).

Installation guide bnc-2110. National Instruments. 2007 (cit. on p. 15).

LI, T., Y. YANG, M. YUAN, and Z. HU: „Effects of molten material temperatures and coolant temperatures on vapor explosion“. *Nuclear Science and Techniques*, vol. 18 No. 5, (2007): pp. 311–315 (cit. on p. 28).

LORENZ, V.: „Phreatomagmatism and its relevance“. *Chem. Geol.* Vol. 62, (1987): pp. 149–156 (cit. on pp. 5, 6).

LYINSKAYA, E., G. LARSEN, and M. GUDMUNDSSON: *Catalogue of Icelandic Volcanoes*. URL: http://www.gso.uri.edu/lava/Laki%20Eruption/Lakierupt.html (visited on 9. Mar. 2016) (cit. on p. 5).

M series user manual. National Instruments. 2008 (cit. on p. 15).

MOHRHOLZ, C.-O.: „Betrachtungen zur thermohydraulischen Interaktion zwischen magmatischer Schmelze und Wasser: Thermodynamische Ansätze und Modellrechnungen“. Diplomarb. Universität Würzburg, 2002 (cit. on pp. 38, 76, 77).

NAC Image Technology. MEMRECAM GX-1 User's Manual ST-751. NAC Image Technology. Oct. 2008 (cit. on p. 17).

NEBEL, B.: *Das Hochwasser von 1784 in Würzburg*. last visited: 2015-06-17. URL: http://bernd-nebel.de/bruecken/index.html (visited on 9. Mar. 2016) (cit. on p. 6).

PANCENKOV, G. M.: „Viskosität geschmolzener Metalle". *Doklay. Akademija nauk SSSR. (Fiziceskaja chimijs)*, vol. 79(6), (1951): pp. 985–988 (cit. on p. 26).

PECKOVER, R. S., D. J. BUCHANAN, and D. E. T. F. ASHBY: „Fuel-coolant interactions in submarine volcanism". *Nature*, vol. 245, (1973): pp. 307–308 (cit. on p. 6).

PURVIS, E. E.: „The Chernobyl 4 accident sequence: update-April 1995". Vol., (1995) (cit. on p. 5).

RÄTZKE, K., P. KLUGKIST, and F. FAUPEL: „On The Role of Thermal Defects in Diffusion in Metallic Glasses". *Defect and Diffusion Forum Vols.* Vol. 165 - 166, (1999): pp. 43–52 (cit. on p. 80).

RIEM, W.-K. E. A.: „Noncontact technique for measuring surface tension and viscosity of molten materials using high temperature electrostatic levitation". *Review O Scientific Instruments*, vol. 70, 6, (June 1999): pp. 2796–2801 (cit. on p. 50).

ROUABHI, A., M. TIJANI, P. MOSER, and D. GOETZ: „Continuum modelling of dynamic behaviour and fragmentation of quasi-brittle materials: application to rock fragmentation by blasting". *Int. J. F. Numerical and analytical methods in Geomechanics*, vol. 29, (2005): pp. 729–749 (cit. on p. 50).

SÄHN, S., H. GÖLDNER, M. SCHAPER, E. KULLIG, R. FODHAIL, and S. P.: „Beanspruchungsparameter für Risse und Kerben bei statischer und zyklischer Belastung". *Technische Mechanik*, vol. 8, Heft 4, (1987): pp. 5–17 (cit. on p. 80).

SCHWEIZER, A.: *Formelsammlung und Berechnungsprogramme für Anlagenbau*. German. Apr. 2015. URL: http://www.schweizer-fn.de/waerme/sonstiges/sonstiges.php (visited on 23. Sept. 2015) (cit. on p. 84).

SEEHAUS, T.: „Umrüstung, Inbetriebnahme und Eichung eines Experimentaufbaus zur Untersuchung von MFCI-Reaktionen und Durchführung von Testversuchen". Diplomarb. Universität Würzburg, 2011 (cit. on p. 11).

SHARON, A. and S. G. BANKOFF: „On the existence of steady supercritical plane thermal detonations". *Ing. J. Mass Transfer*, vol. 24, (1981): pp. 1561–1972 (cit. on p. 6).

SHARON, E., S. GROSS, and J. FINEBERG: „Energy Dissipation in Dynamic Fracture". *Physical Review Letters*, vol. 76(12), (1996): pp. 2117–2120 (cit. on p. 37).

SPITZNAGEL, N., T. DÜRIG, and B. ZIMANOWSKI: „Trigger- and heat-transfer times measured during experimental molten-fuel-interactions". *AIP Advances*, vol. 3(102126), (2013) (cit. on pp. 44, 45, 55, 72, 79).

STENZEL, W. and R. SCHULTZE: „Verdampfungskuehlung, Teil II. Theorie der Verdampfungskuehlung und Messung des Waermeuebergangs bei Haerteionen und Salzloesungen". *Chemie-Ing.-Techn*, vol. 30 No. 18, (1958): pp. 720–728 (cit. on pp. 38, 41).

WAGNER, W.: *Wasser und Wasserdampf im Anlagenbau, 2., korrigierte und erw. Aufl.* Ed. by WAGNER, W. Vogel Fachbuch Würzburg, 2011 (cit. on p. 62).

WAGNER, W. and H.-J. KRETZSCHMAR: *International steam tables*. Springer, 2008 (cit. on pp. 9, 62).

WOHLETZ, K. H.: „Mechanismns of hydrovolcanic pyroclast formation: grain-size, scanning electron microscopy, and experimental studies“. *J. Volcanol. Geotherm. Res*, vol. 17, (1983): pp. 31–64 (cit. on p. 6).

WORLDWIDESCIENCE.ORG: *Sample records for steam explosion experiment*. URL: http://worldwidescience.org/topicpages/s/steam+explosion+experiment.html (visited on 16. July 2015) (cit. on p. 6).

ZIMANOWSKI, B., R. BÜTTNER, and V. LORENZ: „Premixing of magma and water in MFCI experiments“. *Bull Volcanol*, vol. 58, (1997): pp. 491–495 (cit. on pp. 7, 19, 72, 75).

ZIMANOWSKI, B., R. BÜTTNER, V. LORENZ, and H.-G. HÄFELE: „Fragmentation of basaltic melt in the course of explosive volcanism“. *Journal of Geophysical Research*, vol. 102, (1997): pp. 803–814 (cit. on pp. 7, 35, 49, 71, 76, 83).

ZIMANOWSKI, B., R. BÜTTNER, and J. NESTLER: „Britt[l!]e reaction of a high-temperature ion melt“. *Europhysics Letters*, vol. 38 (4), (1997): pp. 285–289 (cit. on p. 7).

ZIMANOWSKI, B., G. FRÖHLICH, and V. LORENZ: „Experiments on vapour explosions by interaction of water with silicate melts“. *Nucl. Engrg. Des.* Vol. 155, (1995): pp. 335–343 (cit. on p. 7).

ZIMANOWSKI, B., V. LORENZ, and G. FRÖHLICH: „Experiments on phreatomagmatic explosions with silicate and carbonatitic melts“. *J. Volcanol. Geotherm. Res.* Vol. 30, (1986): pp. 149–153 (cit. on p. 7).

– „Quantitative experiments on phreatomagmatic explosions“. *Journal of Volcanology and Geothermal Research*, vol. 48, (1991): pp. 341–358 (cit. on p. 7).

ZIMANOWSKI, B., K. WOHLETZ, P. DELLINO, and R. BÜTTNER: „The volcanic ash problem“. *Journal of Volcanology and Geothermal Research*, vol. 2557, (2002): pp. 1–5 (cit. on p. 7).

Danksagung

An dieser Stelle möchte ich mich bei den Personen bedanken, die zum Gelingen dieser Arbeit beigetragen haben.

Als erstes gilt mein Dank Herrn Prof. Dr. Bernd Zimanowski für die Ermöglichung der Arbeit im Physikalisch Vulkanologischen Labor der Universität Würzburg und der interessanten Themenstellung.

Des Weiteren danke ich Prof. Dr. Ralf Büttner, Dr. Tobias Dürig, Dr. Ingo Sonder, Sven Heyne, Kristina Drews, Thorsten Seehaus, Ewald Becker, Achim Ernst und Anton Uttinger für die kollegiale Zusammenarbeit im Physikalisch Vulkanologischen Labor.

Sodann bedanke ich mich bei Dr. Fabio Diugardi für die Oberflächenanlyse der Zinnfragmente und Prof. Dr. Magnus Gudmundsson für die Aufnahmen mit der Thermobildkamera.

Ganz besonderer Dank gilt meinen Eltern für alle Unterstützung während der Arbeit.